NASA CR-120883
GE R72AEG165

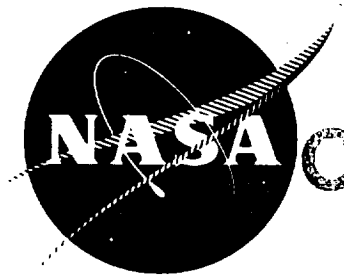

EXPERIMENTAL AND ANALYTICAL INVESTIGATION OF THE COOLANT FLOW CHARACTERISTICS IN COOLED TURBINE AIRFOILS

by

W. P. Damerow
J. P. Murtaugh
F. Burggraf

GENERAL ELECTRIC COMPANY
AIRCRAFT ENGINE GROUP
CINCINNATI, OHIO 45215

prepared for

NATIONAL AERONAUTICS AND SPACE ADMINISTRATION

NASA Lewis Research Center
Contract NAS 3-13499
John E. Rohde, Project Manager

1. Report No.	2. Government Accession No.	3. Recipient's Catalog No.
NASA CR 120883		

4. Title and Subtitle	5. Report Date
EXPERIMENTAL AND ANALYTICAL INVESTIGATION OF THE COOLANT FLOW CHARACTERISTICS IN COOLED TURBINE AIRFOILS	June 1972
	6. Performing Organization Code
7. Author(s)	8. Performing Organization Report No.
W.P. Damerow, J.C. Murtaugh, F. Burggraf	R72AEG165
	10. Work Unit No.
9. Performing Organization Name and Address	
General Electric Company Aircraft Engine Group Cincinnati, Ohio 45215	11. Contract or Grant No. NAS 3-13499
	13. Type of Report and Period Covered Contractor Report
12. Sponsoring Agency Name and Address	
National Aeronautics and Space Administration Washington, D.C. 20546	14. Sponsoring Agency Code

15. Supplementary Notes
Program Manager, John E. Rohde, Air Breathing Engine Division
NASA Lewis Research Center
Cleveland, Ohio 44135

16. Abstract

The flow characteristics of turbine airfoil cooling system components were experimentally investigated. Flow models representative of leading edge impingement, impingement with crossflow (midchord cooling), pin fins, feeder supply tube, and a composite model of a complete airfoil flow system were tested. Test conditions were set by varying pressure level to cover the Mach number and Reynolds number range of interest in advanced turbine applications. Selected geometrical variations were studied on each component model to determine these effects.

Results of these tests were correlated and compared with data available in the literature. Orifice flow was correlated in terms of discharge coefficients. For the leading edge model this was found to be a weak function of hole Mach number and orifice-to-impinged wall spacing. In the impingement with crossflow tests, the discharge coefficient was found to be constant and thus independent of orifice Mach number, Reynolds number, crossflow rate, and impingement geometry. Crossflow channel pressure drop showed reasonable agreement with a simple one-dimensional momentum balance. Feeder tube orifice discharge coefficients correlated as a function of orifice Mach number and the ratio of the orifice-to-approach velocity heads. Pin fin data was correlated in terms of equivalent friction factor, which was found to be a function of Reynolds number and pin spacing but independent of pin height in the range tested.

The coefficients obtained were incorporated into a compressible flow network analysis computer program, which was developed during this contract to predict the flow distribution in the complex turbine blade cooling configurations. Results using this program compared favorably with experimental results from the composite model, which simulated an actual turbine airfoil cooling system incorporating the individual components tested under this contract.

17. Key Words (Suggested by Author(s))	18. Distribution Statement
Turbine cooling Pressure drop Flow network Impingement Pin fins	Unclassified - Unlimited

19. Security Classif. (of this report)	20. Security Classif. (of this page)	21. No. of Pages	22. Price*
Unclassified	Unclassified	71	

* For sale by the National Technical Information Service, Springfield, Virginia 22151

ABSTRACT

Results of tests to determine flow characteristic of components of typical turbine cooling systems are presented. The components tested included models of leading edge impingement, impingement with crossflow, pin fins, and feeder supply tube. Empirical correlations of the data were obtained and these correlations were in turn incorporated into a compressible flow network analysis computer program, which was developed as part of this investigation. A composite model, which simulated an actual turbine blade and incorporated the above cooling components, was tested and the experimental results were compared to predictions using the computer program.

TABLE OF CONTENTS

LIST OF ILLUSTRATIONS

LIST OF ILLUSTRATIONS (Cont.)

SUMMARY

The flow characteristics of turbine airfoil cooling system components were experimentally investigated. Flow models representative of leading edge impingement, impingement with crossflow (midchord cooling), pin fins, feeder supply tube, and a composite model of a complete airfoil flow system were tested. Test conditions were set by varying pressure level to cover the Mach number and Reynolds number range of interest in advanced turbine applications. Selected geometrical variations were studied on each component model to determine these effects.

Results of these tests were correlated and compared with data available in the literature. Orifice flow was correlated in terms of discharge coefficients. For the leading edge model this was found to be a weak function of hole Mach number and orifice-to-impinged wall spacing. In the impingement with crossflow tests, the discharge coefficient was found to be constant and thus independent of orifice Mach number, Reynolds number, crossflow rate, and impingement geometry. Crossflow channel pressure drop showed reasonable agreement with a simple one-dimensional momentum balance. Feeder tube orifice discharge coefficients correlated as a function of orifice Mach number and the ratio of the orifice-to-approach velocity heads. Pin fin data was correlated in terms of equivalent friction factor, which was found to be a function of Reynolds number and pin spacing but independent of pin height in the range tested.

The coefficients obtained were incorporated into a compressible flow network analysis computer program, which was developed during this contract to predict the flow distribution in the complex turbine blade cooling configurations. Results using this program compared favorably with experimental results from the composite model, which simulated an actual turbine airfoil cooling system incorporating the individual components tested under this contract.

INTRODUCTION

Knowledge of the internal flow characteristics of turbine airfoil cooling system components and their interaction in the overall flow circuit are required to predict the performance of cooled airfoils. To improve aerodynamic performance and to maximize component life of advanced high temperature turbines, cooling air usage must be minimized while high heat transfer effectiveness is obtained. To achieve these goals, cooling system designs have become increasingly complex and the need for the capability of predicting their characteristics has become more critical. Typical passage configurations for which knowledge is lacking consist of impingement jets in leading edge and midchord regions, which are fed from supply passages with flow areas that impose a radial pressure gradient, and pin fin turbulence promoters in the trailing edge. In addition, the array of impingement jets utilized for the midchord region creates a spent impingement crossflow which interferes with downstream jets in the array and imposes a varying discharge pressure from row to row for the jets. To obtain the detailed data required to understand the flow characteristics of these components it is necessary to scale up engine hardware to permit adequate instrumentation. Model pressure levels and flow rates are then selected to simulate engine Mach number and Reynolds number conditions. Due to the complexity of these flow circuits, general computer programs capable of handling a wide variety of complex flow circuits are required.

The results of previous studies for flow through impingement orifices are available in a number of reports, including 1 and 2. A study of feeder tube effects is presented in Reference 3. Pressure drop investigations for flow through a tube bank are presented in References 4 to 8, while References 9 to 11 discuss the acoustical resonance problem associated with the flow. Calculated flow distributions in turbine airfoils are normally determined using results from these or similar references in conjunction with component tests. Development or production hardware is flow-checked to verify the calculated flow distribution and variation between blades.

The program herein reported considered leading edge impingement configurations where the jets impinge into a half-cylinder and the spent flow is split and bled off through holes simulating pressure and suction side film cooling holes. Effects of scaling, leading edge flow split and spacing between the jets and impinged surface were investigated over a range of jet Reynolds numbers and Mach numbers. The impingement with crossflow investigation considered a square impingement jet array with the effects of scaling, spacing between jets, spacing between the jets and the impinged surface and crossflow rate evaluated over a range of Reynolds and Mach numbers. An independent cross flow source was provided for the impingement with crossflow models. The leading edge impingement models and the crossflow impingement models were designed so that flow visualization studies could be conducted to help understand the complex flow fields. The pin fin turbulence promoter investigation considered a staggered pin fin array with two values of pin spacing and two values of passage height. The effects of passage convergence and scaling were also investigated. The pin fin models were tested over a range of Reynolds numbers and Mach numbers. The feeder tube model investigated typifies the supply system for an impingement cooled leading edge. Tests were run with the feeder tube supplying the flow for jets impinging into a leading edge cavity and also with the cavity replaced by plenums so the discharging flow could be measured along the tube and over a range of Reynolds numbers and Mach numbers. A composite model simulating an actual turbine airfoil cooling system was build incorporating the components previously tested. The composite model was tested over a range of Reynolds number and Mach

number with different suction, pressure and trailing edge discharge pressures. The results of the composite model tests were compared with the analytical results obtained from a flow network computer program.

A compressible one-dimensional flow network analysis computer program in Fortran IV was developed during this contract. This computer program determines the flow distribution through an arbitrarily connected network of one-dimensional flow passages with prescribed external temperature and pressure boundary conditions.

DESCRIPTION OF APPARATUS

Facility

Air at up to 125 psia (86.2 N/cm^2) was supplied through an air dryer, which lowered the dew point to below 0°F (-17.8°C), and a nominal 5 micron (0.0005 cm) filter to the supply plenum of the model. Throttling valves upstream and downstream of the models provided control for setting the test points. The vacuum downstream of the model was provided by a vacuum pump for the leading edge and feeder tube models and by a steam ejector for the models with higher flow (impingement, pin fin and composite). Flows were measured by calibrated Daniels flow orifices and air temperatures were measured by thermocouples located in the supply plenum of the models. Millivolt readings were taken directly with the use of a Leeds and Northrop potentiometer in conjunction with a recorded ice junction. Pressures were measured by either water or mercury manometers or Bourdon type gauges, depending on the magnitude of the measured pressures. Supply pressures were measured relative to the ambient pressure, while model pressures were measured relative to the supply pressure to improve accuracy of pressure differentials.

An error analysis was conducted prior to testing to determine the magnitude of the experimental error on both the full scale (1X) size and 5X size models used in this program. The method described in Reference 12 was used to calculate the error. Using the following assumed measurement errors:

Flow	1%
Temperature	1%
Area, 5X size model	±1.6%
Area, 1X size model	±4%
Pressure	0.1 inch mercury or water ± .25% Bourdon

The calculated experimental error in discharge coefficient for the 5X model ranged from ±2% at Mach numbers of 0.3 and 0.5 and ±7% at 0.1 Mach number. (The larger calculated error at the low Mach number was due to an error in measuring the small pressure drop across the model.) The experimental error calculated for the 1X size model was nearly constant at ±4.5% for all Mach numbers.

Description of the Models

Five basic models were tested in various configurations. The five models were:

1. Leading edge impingement
2. Impingement with crossflow
3. Pin fin
4. Feeder tube
5. Composite

The five models are shown schematically in Figures 1 to 5, which also provide a summary of the pertinent dimensions. The first three models simulated the three cooling regions of a blade or vane design; the leading edge, midchord and trailing edge. The fourth model, the feeder tube, was constructed identically to the leading edge model except that the flow was supplied perpendicular rather than parallel to the axis of the hole. The composite model represents the three cooling schemes combined into an airfoil cooling system.

Leading Edge Impingement Model

The leading edge impingement model was tested in two sizes; a full scale size (1X) representative of an engine application and a five times full scale size (5X) which permitted more instrumentation and greater testing accuracy. Figure 6 is a photograph of the 5X size model. The configuration of the leading edge models consisted of one row of equally spaced holes. Air was supplied through a rectangular passage with the supply velocity parallel to the axis of the hole. After passing through the holes in a concave surface, the air impinged upon another concave (half-cylinder) surface and then the flow split into two streams which were collected in plenums on either side of the model. The full scale or 1X size model contained 20 holes of 0.024-inch (0.0609 cm) diameter while the 5X size model contained 20 holes of 0.128-inch (0.325 cm) diameter. The wall thickness-to-hole diameter ratio was 0.66 for both models. The 1X size model had an orifice to impinged wall spacing-to-hole diameter ratio (Z/D) of 3, while the 5X size model was tested at Z/D ratios of 2, 3 and 5. The symbols are defined in Appendix A.

The pressure instrumentation was located in three planes parallel to the direction of the flow to detect any possible flow maldistribution. For the 5X size model, each plane contained pressure taps located in the supply plenums, in the duct just upstream of the holes, at the exit of the jet, and seven taps distributed around the concave surface on which the jet impinged as indicated on Figure 1. The 1X size model did not have the pressure taps located in the duct or at the exit of the jets due to space limitations. A flow visualization model of the 5X size leading edge model was constructed and consisted of a clear plastic casing with an opening for a hand held probe which could be moved within the impingement cavity to observe flow directions.

Crossflow Impingement Model

The impingement with crossflow models consisted of plates containing 10 rows of impingement holes with 5 holes per row and were tested in a 1X (engine scale) and 5X size. The air issuing from the holes impinged upon the opposite wall of a rectangular cross flow duct which collected the impinged air and provided self-generated crossflow past the downstream jets. Independent crossflow air was also supplied from a plenum upstream of the impingement holes. The impingement holes were arranged in a staggered array. Two hole spacing-to-diameter, S/D, ratios of 3.0 and 6.0 were tested. Each of the 5X size models were tested at orifice to impinged wall spacing-to-hole diameter ratios, Z/D, of 3.0 and 5.0 while the 1X size models were tested at a Z/D = 3.0. Nominal hole diameters were 0.015 inch (0.038 cm) and 0.075 inch (0.191 cm) for the 1X and 5X size models respectively. The details of the different model geometries are given in Figure 2. The 5X size models contained five impingement plenums with each plenum supplying two rows of holes (10 holes). The size of the 1X model prohibited the installation of individual plenums and, thus, all 50 holes were supplied from one plenum. Figure 7 shows the impingement plate for the 5X size model with an S/D of 3.0.

Pressure taps were located in all of the supply and collector plenums and on the four walls of the crossflow passage. The four walls of the crossflow passage are defined as: the impingement plate, the impinged wall, and the two side walls. The impingement plate was the

MODEL	1a FULL SIZE	1b 5 X SIZE
ORIFICE DIAMETER D	INCH (CM) .024 (.061)	INCH (CM) .128 (.325)
NUMBER OF ORIFICES	20	20
ORIFICE SPACING S	.05 (.127)	.25 (.635)
RADIUS B	.075 (.191)	.375 (.953)
RADIUS E	.045 (.114)	.225 (.571)
MODEL WIDTH L	1.0 (2.54)	5.0 (12.7)
FEEDER TUBE LENGTH H	.016 (.041)	.08 (.203)
FEEDER TUBE THICKNESS t	.56 (1.42)	2.80 (7.11)

NOTES:

1. ◆ DENOTES PRESSURE TAP
2. ✸ DENOTES PRESSURE TAP USED IN DATA CORRELATION

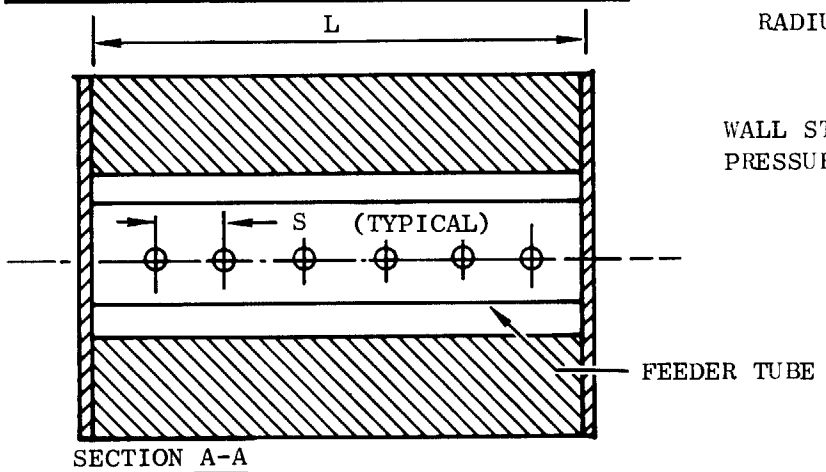

SECTION A-A

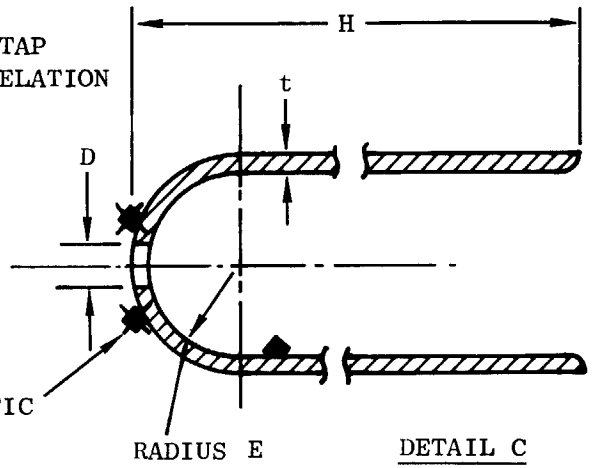

DETAIL C

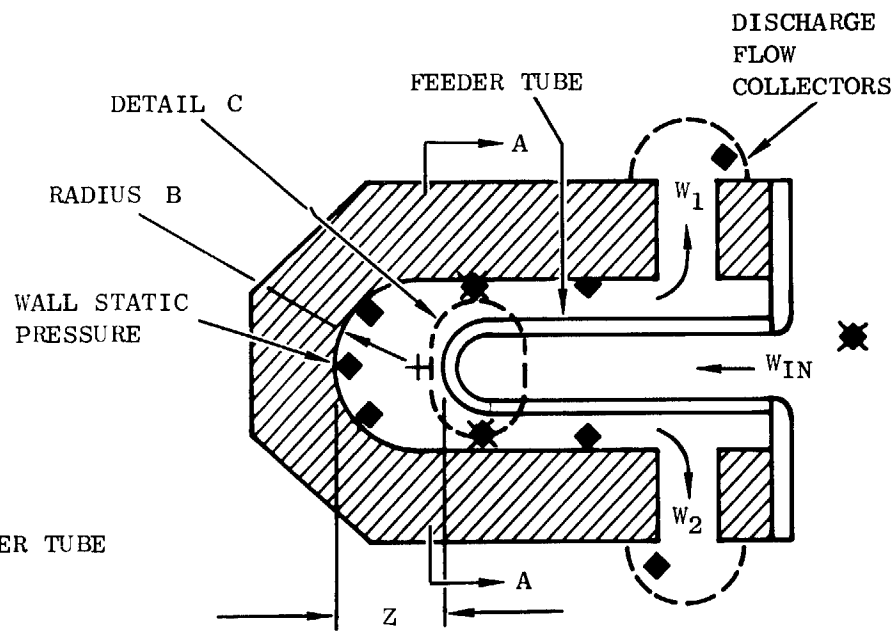

Figure 1 Schematic of Leading Edge Impingement Model

MODEL	FULL SIZE		5 X SIZE	
	2A	2B	2C	2D
ORIFICE DIA D	INCH (CM) .015 (.038)	INCH (CM) .015 (.038)	INCH (CM) .075 (.191)	INCH (CM) .075 (.191)
HOLE SPACING S	.045 (.114)	.090 (.229)	.225 (.572)	.45 (1.143)
NO. OF HOLES PER ROW	5	5	5	5
PLATE THICKNESS t	.015 (.038)	.015 (.038)	.075 (.191)	.075 (.191)

NOTES
1 ◆ DENOTES PRESSURE TAP
2 ✱ DENOTES PRESSURE TAP USED IN DATA CORRELATION
3 10 ROWS OF HOLES

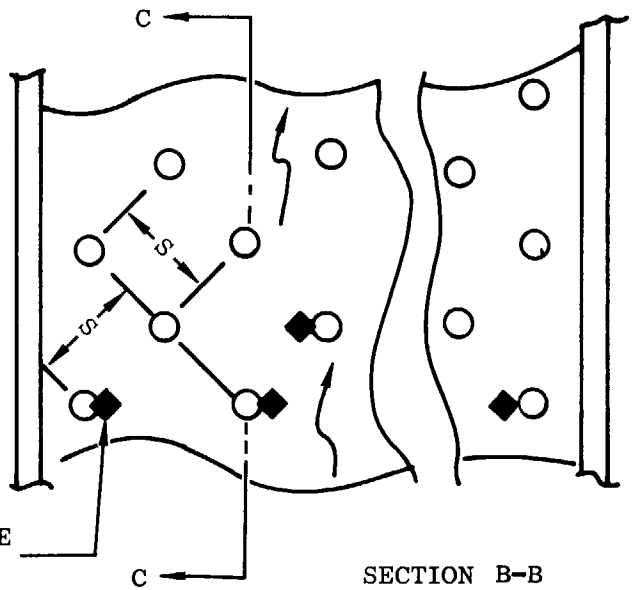

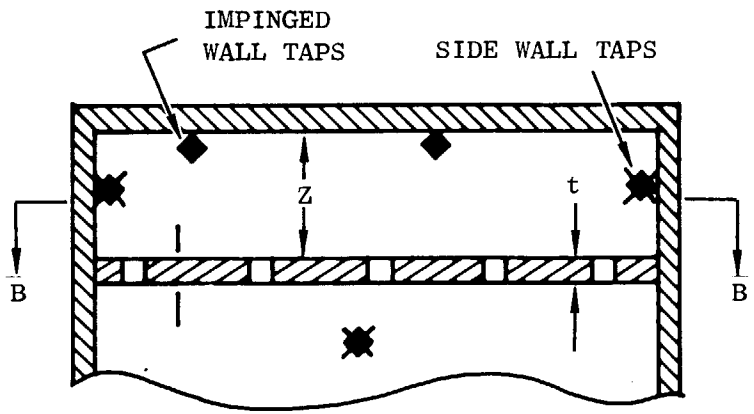

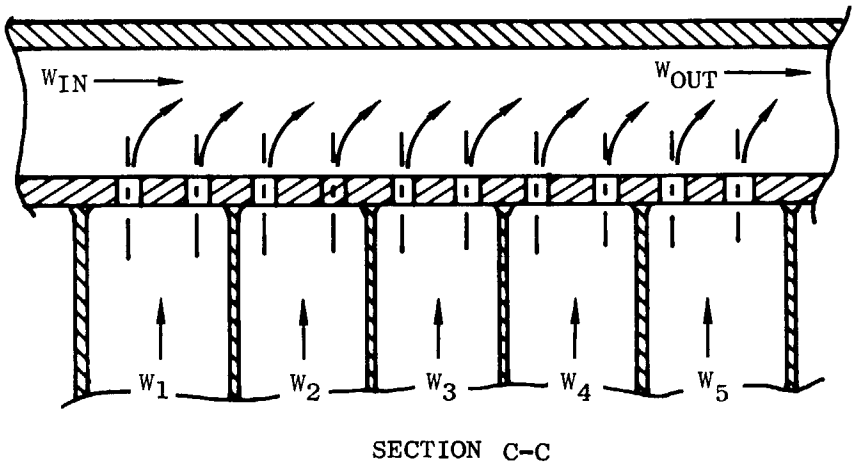

Figure 2 Schematic of Impingement with Crossflow Models

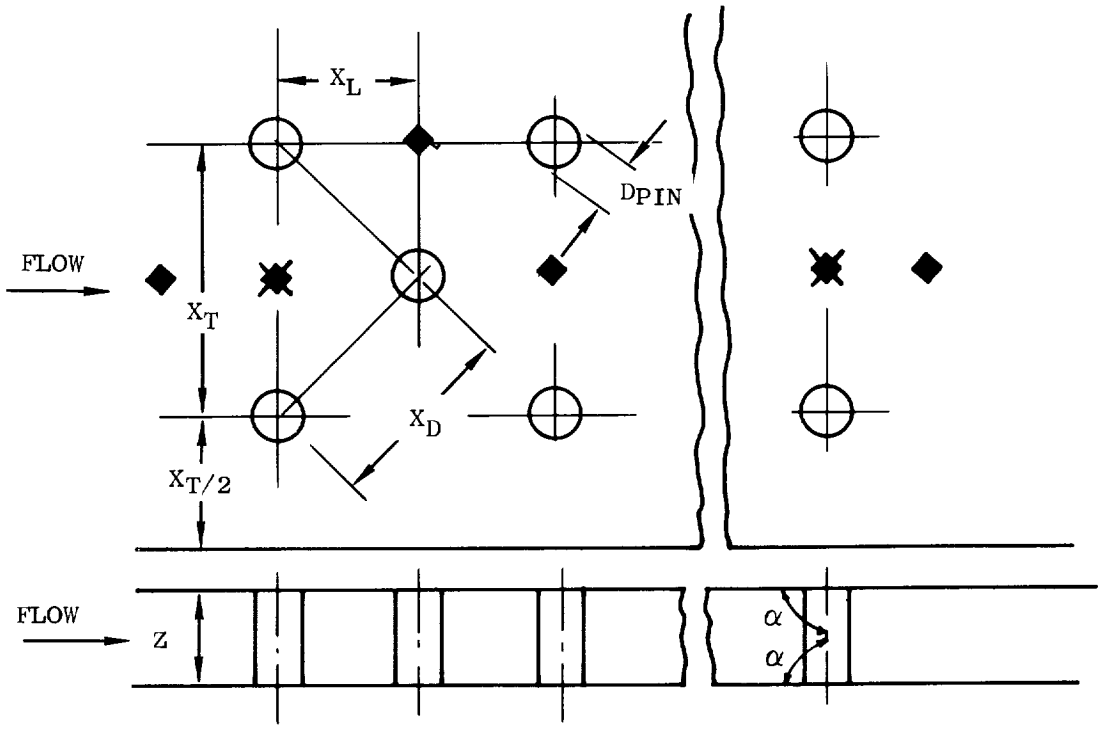

NOTES:
◆ PRESSURE TAPS
✱ PRESSURE TAPS USED IN CORRELATION
20 PINS PER ROW

MODEL	ROWS OF PINS	D_{PIN} IN (CM)	Z/D	ANGLE α DEG. (RAD)	X_D/D	X_t/D	X_L/D
A	10	.020 (.051)	3.75	90 (.7854)	5.0	7.07	3.54
B	10	.100 (.254)	2.0	90 (.7854)	3.0	4.24	2.12
C	10	.100 (.254)	4.0	90 (.7854)	3.0	4.24	2.12
D	10	.100 (.254)	2.0	90 (.7854)	5.0	7.07	3.54
E	10	.100 (.254)	4.0	90 (.7854)	5.0	7.07	3.54
F	5	.100 (.254)	2.3 TO 1.7	.7679	3.0	4.24	2.12

Figure 3 Schematic of Pin Fin Models

NOTES:

1. 20 - 0.125 IN (.318 CM) DIA ORIFICES
2. MODEL LENGTH = 5.0 IN (12.70 CM)
3. ◆ DENOTES PRESSURE TAPS
4. ✱ DENOTES PRESSURE TAP USED IN DATA CORRELATION

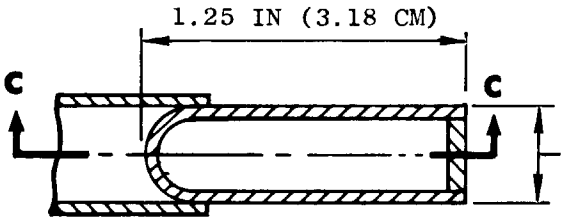

WITH COLLECTOR

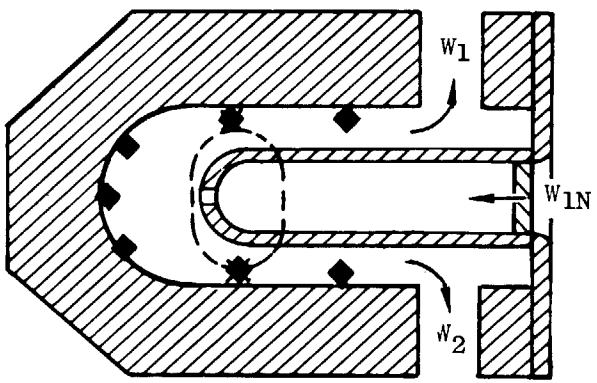

WITH LEADING EDGE COLLECTOR

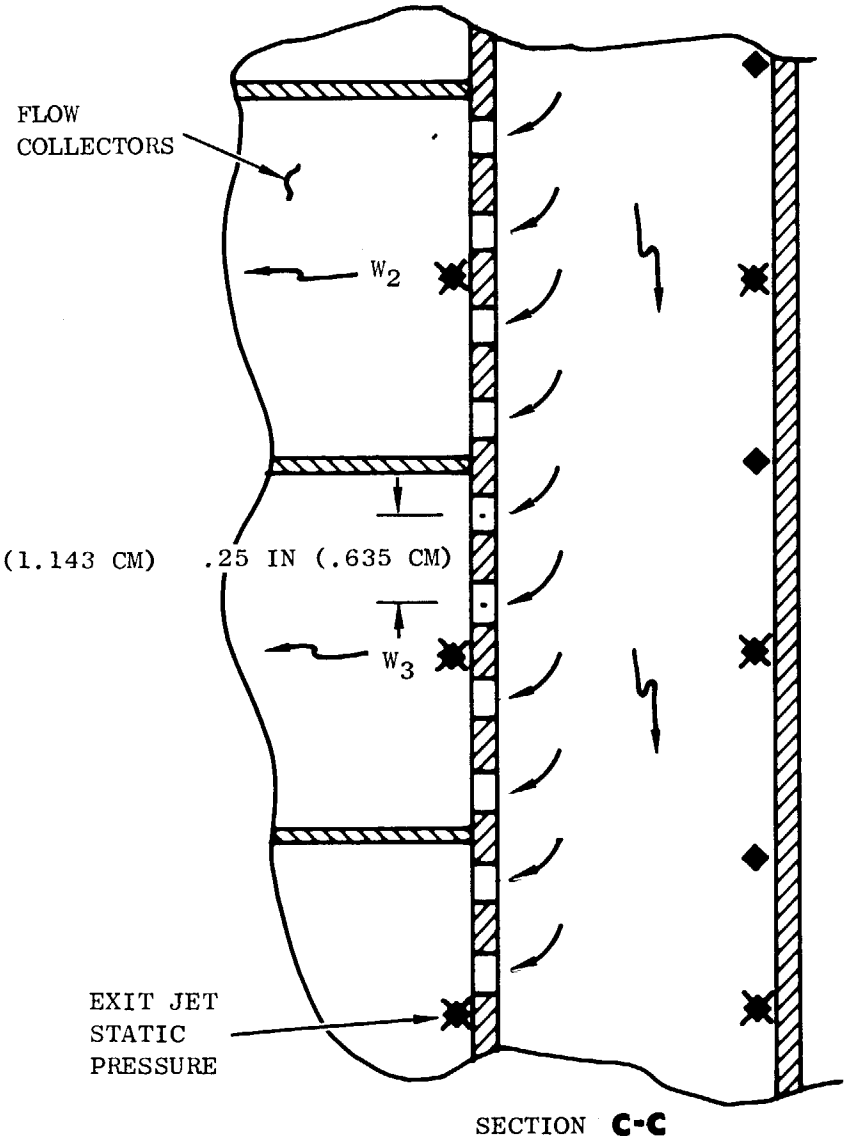

Figure 4 Schematic of Feeder Tube Model

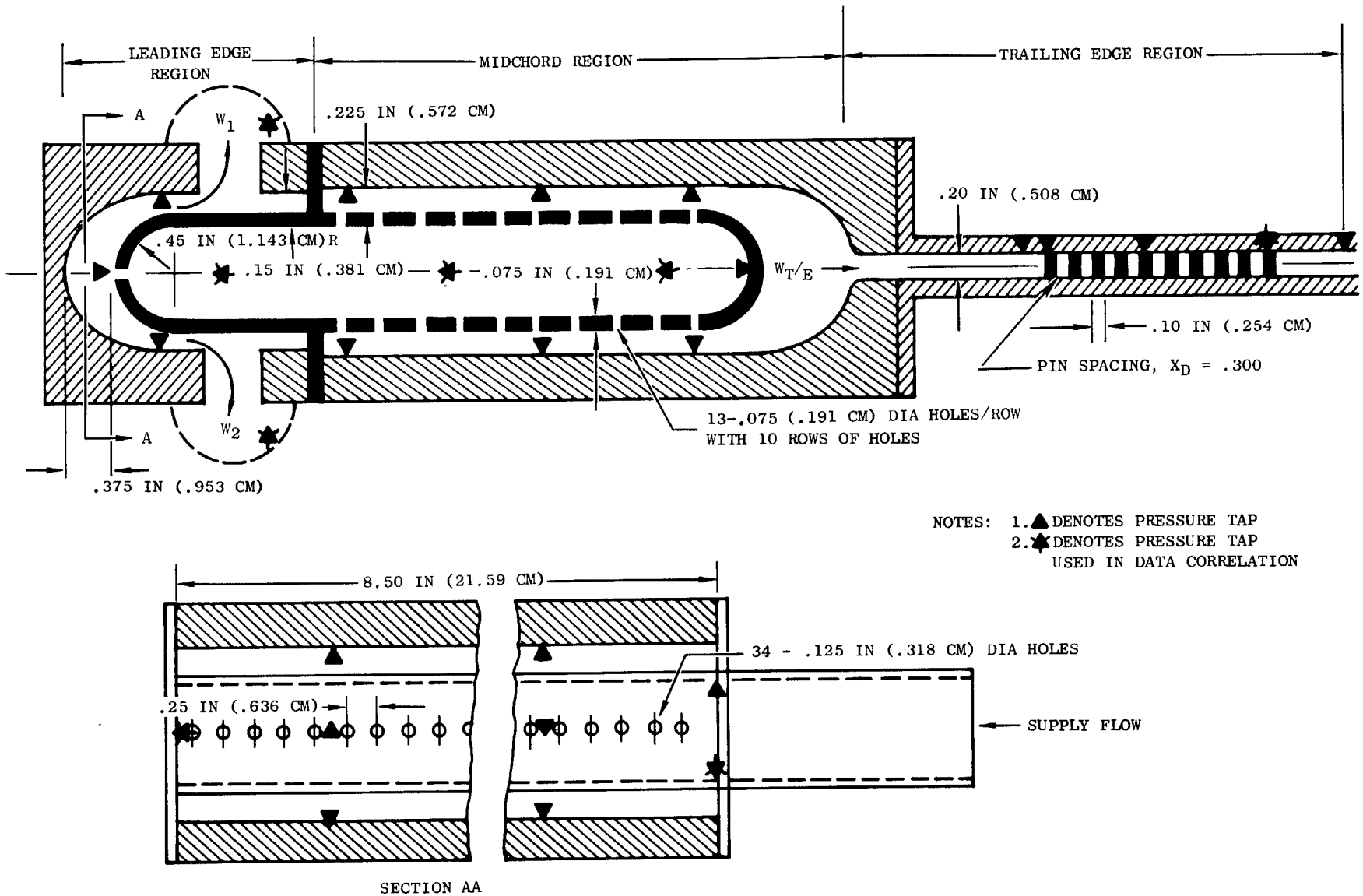

Figure 5 Schematic of Composite Model

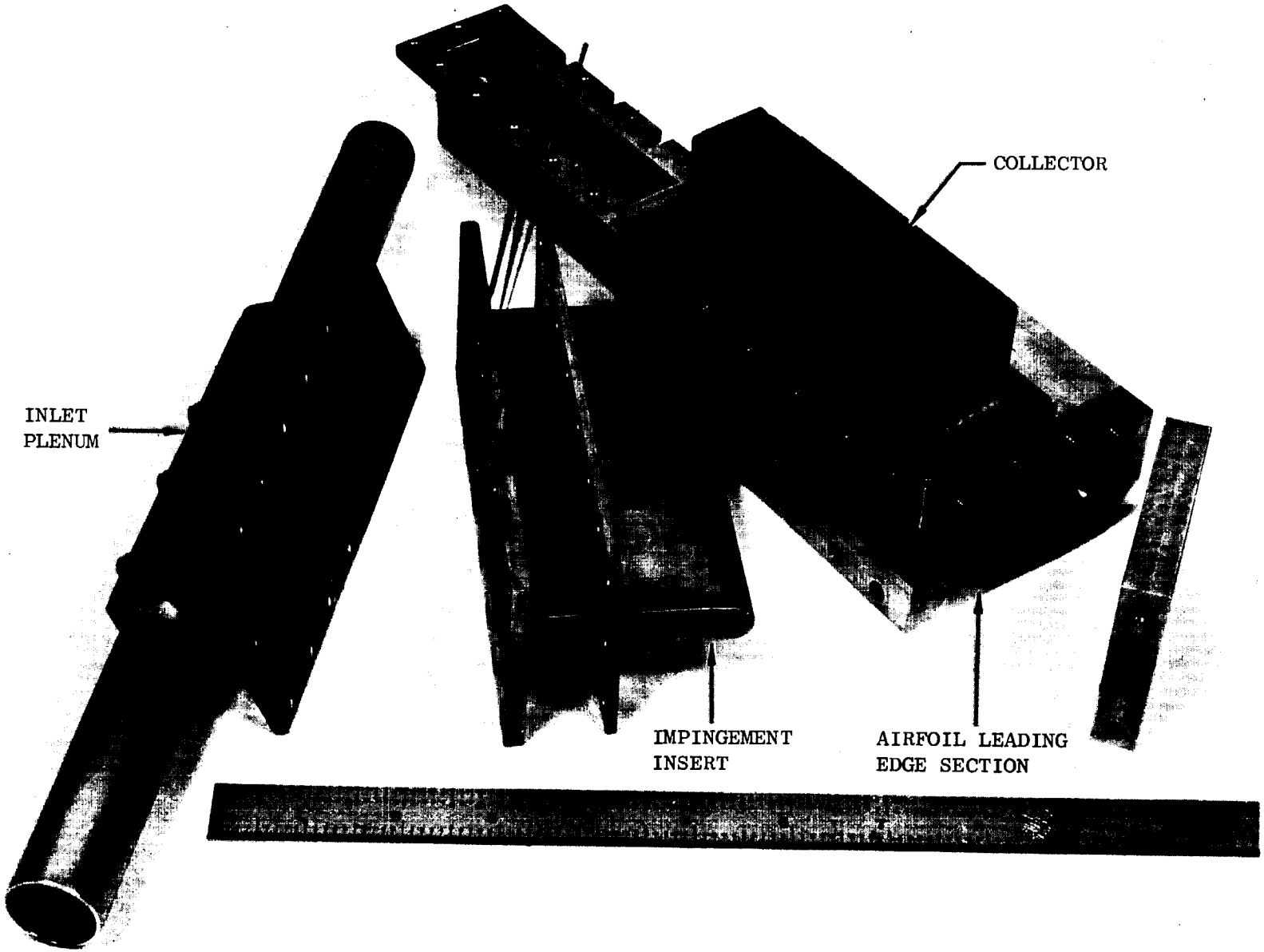

Figure 6 Photograph of Leading Edge Impingement Model

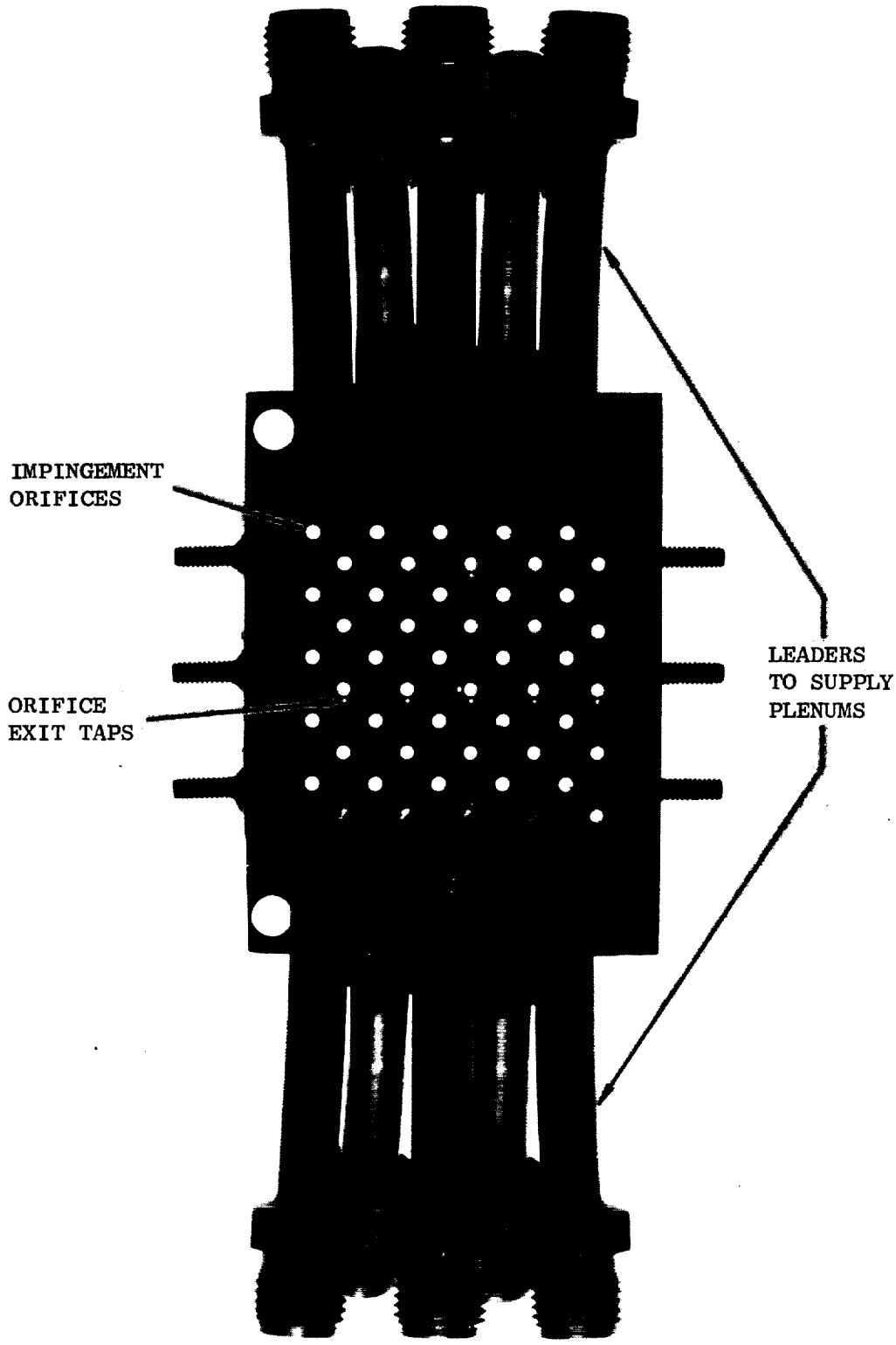

Figure 7 Photograph of Impingement Model 2C

surface that contained the holes, the impinged wall was the surface on which the air jets impinged and the side walls were the two walls normal to the impingement surface. The pressure taps in the impingement plates were located as close to the issuing jet as physically possible. The impinged wall taps were installed opposite the first row of holes in each plenum between hole centerlines and the side wall taps were located in-line and between hole rows in each plenum. The 1X size models were instrumented with plenum and side wall taps only due to space limitations.

Side wall and impinged surfaces, constructed of clear plastic, were also provided for flow visualization studies.

Pin Fin Model

The pin fin turbulence promoter models were investigated in two sizes; a full scale (1X) and a five times full scale (5X). All models contained ten rows of pins in a staggered pin array and a constant duct height, except one 5X size model which had 5 rows of pins in a converging duct. Nominal pin diameters were 0.020 inch (0.051 cm) and 0.100 inch (0.254 cm) for the 1X and 5X size models respectively. Pin spacing-to-diameter ratios (X_D/D) of 3.0 and 5.0 were tested at passage height-to-pin diameter ratios (Z/D) of 2.0 and 4.0 on the 5X size model. Complete airfoil spans were modeled to provide simulation of possible flow resonance phenomena which may influence pressure losses (References 9-11). The details of the model geometries are given in Figure 3 with a photograph of the 5X model shown in Figure 8.

Feeder Tube Model

The feeder tube model had the identical geometry of the leading edge impingement model, except that the air was supplied through a tube in a direction normal to the axis of the hole. Figure 4 illustrates the model tested. The feeder tube had a constant flow area of 0.31 square inch (2.0 cm^2). Eleven pressure taps were equally spaced every 0.5 inch (1.27 cm) along the length of the tube opposite the impingement holes and three pressure taps were located at the exit of the jet. The feeder tube model was tested in two configurations to determine the influence of impingement on a closely spaced surface. In the first configuration the jets were impinged on the concave surface of the leading edge model, while in the second configuration, five flow collector plenums were added to the tube so that the flow from groups of four holes entered the collectors and was measured. Two pressure taps were installed in each collector.

Composite Model

The composite model combined three of the previously tested configurations into an airfoil cooling system. Figures 5 and 9 show a schematic and a photograph of the composite model, respectively. The leading edge region contained thirty-four 0.125 inch (0.3175 cm) diameter equally spaced holes on 0.25 inch (0.635 cm) spacing, while the midchord contained two impingement plates each with 10 rows of 0.075 inch (0.19 cm) diameter holes with 13 holes per row having a diagonal hole spacing of 0.45 inch (1.143 cm). The Z/D ratio was 3.0 for both the leading edge and the midchord region. The flow to the impingement holes was supplied in a direction normal to the axis of the hole by a feeder tube with a 0.9 inch (2.29 cm) passage height, a leading and trailing edge radius of 0.45 inches (1.143 cm) and a flow area of 3.72 square inches (24.0 cm^2). The flow from the midchord region exited through a pin fin trailing edge region which had 0.100 inch (0.254 cm) diameter pins with 20 pins per row and 10 rows of pins with a passage height of 0.20 inch (0.608 cm) and pin spacing, X_D/D, of 3.0. Pressure taps were located as shown on Figure 5 with primary instrumentation of 25% and 75% span.

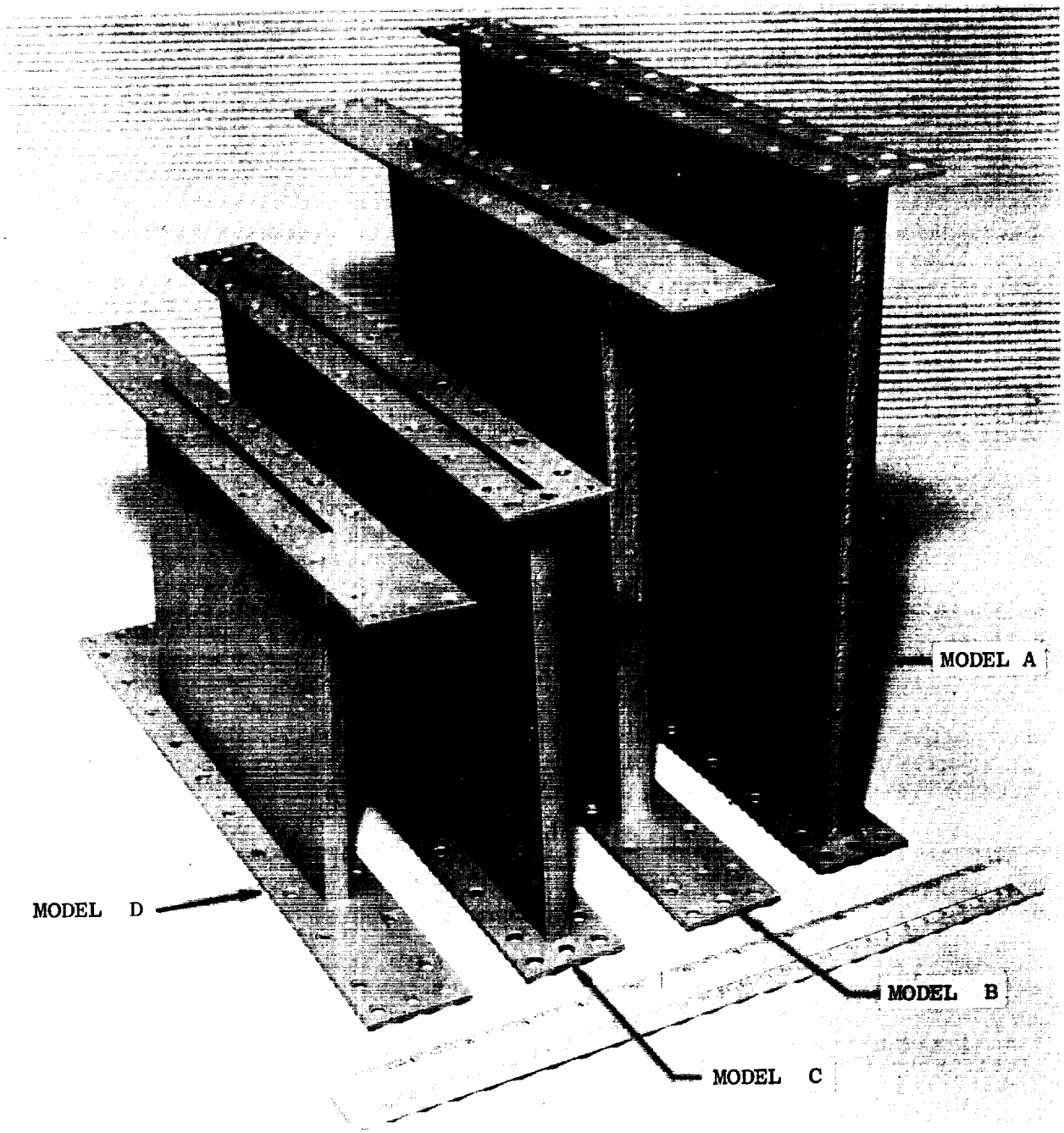

Figure 8 Photograph of 5X Pin Fin Models

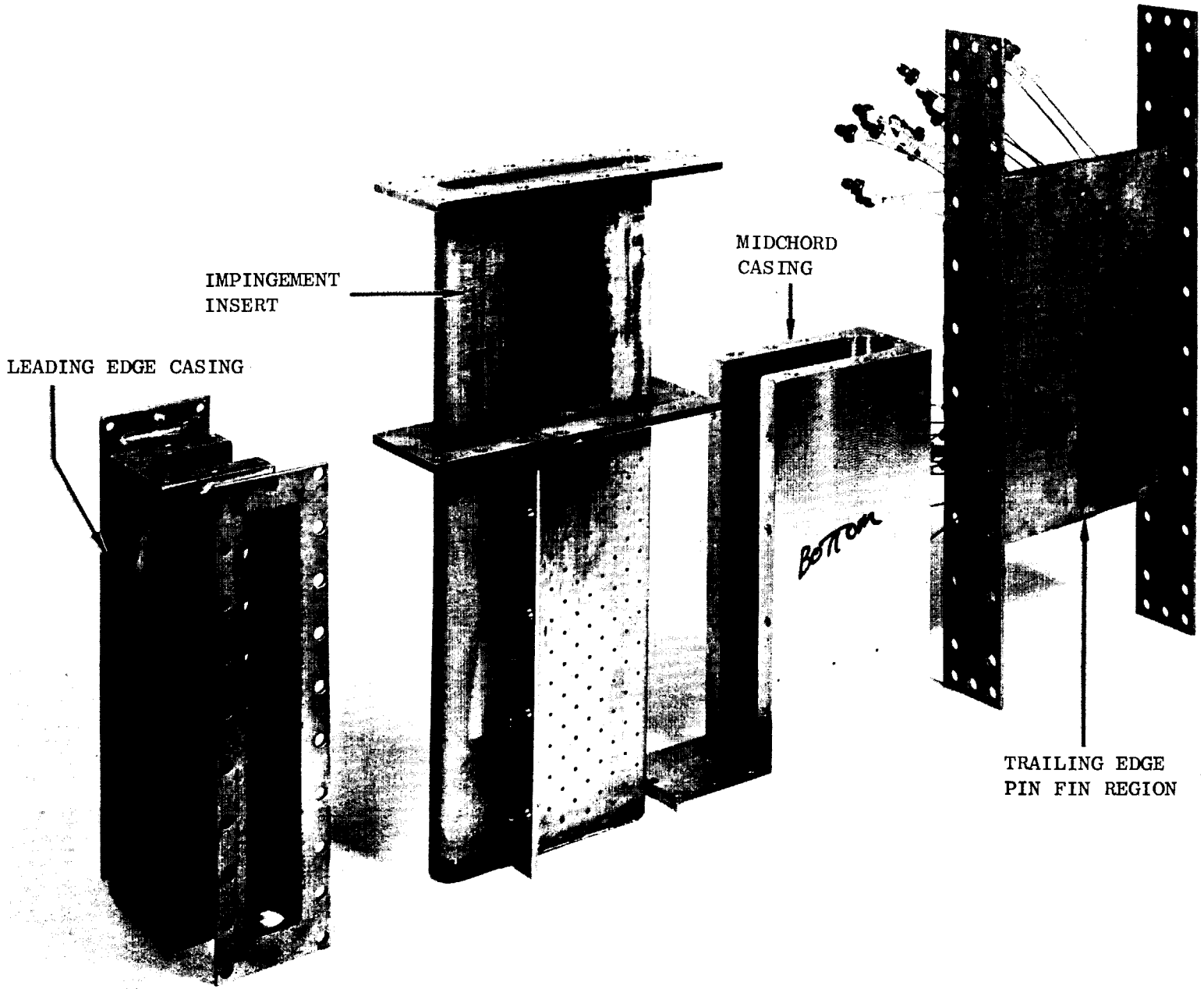

Figure 9 Photograph of Composite Model

EXPERIMENTAL TEST PROCEDURE

The tests were planned so the desired Mach numbers and Reynolds numbers could be obtained at approximately constant pressure levels. The lowest Mach number at a given pressure level was set first and then the flow was increased by opening the downstream valve to obtain the higher Mach number test points. After the highest Mach number was run, the pressure level was changed and the next set of Mach number points was run. On some test points, which are referred to as "ambient tests", the downstream valve was open completely to atmospheric pressure and the upstream pressure was increased in increments of 5 inches of mercury (1.693 N/cm^2). These ambient tests produced simply controlled, continuously changing Mach and Reynolds number points and were used as reference tests for analyzing the data obtained from the tests in which the Mach and Reynolds numbers were specified.

Both the leading edge and pin fin models were tested in the manner described above. Additionally, on the leading edge model, three discharge flow splits were set holding total leading edge flow constant.

For the 5X size crossflow impingement models the pressure and flow, i.e., Mach and Reynolds numbers, were set in the upstream impingement plenum and the pressures in the remaining four plenums were set equal to that of the upstream plenum. All five chambers were maintained at a constant pressure to simulate the impingement plate being fed from one large plenum chamber, but with individual flow measurements possible. The independent crossflow rate was then set as a ratio of the flow in the first plenum. This produced a constant impingement plenum supply pressure with varying crossflow.

The feeder tube tests were run in two configurations. In the first configuration the flow discharged directly into the wall of a common collector and in the second configuration the flow from every group of four holes discharged into individual collectors. The object of testing two configurations was to determine the downstream pressure distribution from the first configuration and then, imposing this distribution upon the second configuration, to determine the flow distribution along the feeder tube. After running the first configuration, the variation in the downstream pressure distribution was found to be small and thus only constant pressure distributions were run on the second configuration for this comparison. The tests on the first configuration were run by setting the Mach and Reynolds numbers in the tube upstream of the holes. The second configuration with individual flow collectors was run by duplicating inlet pressure and the pressure ratios from the first configuration. Additional tests to show the effect of the downstream pressure distribution were run with the downstream pressures adjusted to give an increasing pressure in the direction of the flow in the tube.

The composite model tests were run by setting the midchord impingement hole Mach and Reynolds numbers and adjusting the leading edge and trailing edge flow splits.

Test Conditions

Tests were run over a range of Mach numbers with each Mach number tested at a minimum of three Reynolds numbers. The Reynolds numbers covered approximately a ten-to-one ratio at each Mach number. Pressure levels varied from 30 psia (20.7 N/cm^2) to 2 psia (1.38 N/cm^2) for the 5X size models and from 125 psia (86.2 N/cm^2) to 25 psia (17.3 N/cm^2)

for the full scale models. The flow ranged from 0.0005 lbs/sec. (0.227 g/sec) in the leading edge full scale model to 0.60 lbs/sec. (272 g/sec) for the composite model. For all models the test Mach numbers were based on the actual flow function $W\sqrt{TR/\gamma}/PA$

For the leading edge model, hole Mach numbers of 0.1, 0.3 and 0.5 were tested at Reynolds numbers ranging from 1,300 to 14,000 at $\dot{M}$ = 0.1; from 4,000 to 42,000 at M = 0.3; and from 35,000 to 130,000 at M = 0.5.

The impingement models were run at hole Mach numbers of 0.1, 0.3 and 0.4 or the maximum attainable. The Reynolds number range was 1,000 to 8,700 at M = 0.1; 2,400 to 27,000 at M = 0.3; and 3,000 to 35,000 at M = 0.4.

The pin fin models were tested at four inlet Mach numbers at the first row of pins. The inlet Mach numbers were 0.1, 0.2, 0.3 and 0.4 or the maximum obtainable due to choking at the exit, and the pin Reynolds numbers were 1,000 to 10,000 at M = 0.1; 2,100 to 23,000 at M = 0.2; 3,000 to 34,000 at M = 0.3; and 4,000 to 40,000 at M = 0.4.

The feeder tube model was tested at tube inlet Mach numbers of 0.1, 0.2, 0.25, and 0.3. The Reynolds numbers were 5,000 to 50,000 at M = 0.1; 11,000 to 110,000 at M = 0.2; 13,000 to 135,000 at M = 0.25; and, 15,000 to 150,000 at M = 0.3.

The composite model was tested by setting midchord impingement hole Mach numbers of 0.1, 0.2, 0.3 with corresponding Reynolds number ranges from 800 to 9,000; 2,000 to 20,000 and 2,400 to 28,000 respectively. At each Reynolds number, two leading edge-to-trailing edge flow ratios of 0.5 and 0.33 were tested. Additionally, at the 0.5 trailing edge flow condition, a leading edge flow split of two-to-one was set.

DATA ANALYSIS

During the reduction and analysis of the test data, various equations and assumptions were used. To properly interpret the test results, pertinent definitions, equations and assumptions are listed below.

Leading Edge Impingement Model

The data for the leading edge impingement model has been presented as orifice discharge coefficients and total loss coefficients. The orifice discharge coefficient is defined as the ratio of the actual flow to the ideal flow

$$C_D = w/\rho_j V_j A \tag{1}$$

where the ideal jet velocity and density were determined by the use of the following compressible flow relations:

$$V_j = \sqrt{\frac{2\gamma RT_T}{(\gamma-1)} \left[1 - \left(\frac{p_j}{P}\right)^{(\gamma-1)/\gamma}\right]} \tag{2}$$

$$\rho_j = \frac{p_j}{RT_T} \left(\frac{P}{p_j}\right)^{(\gamma-1)/\gamma} \tag{3}$$

In the calculation of the ideal jet velocity and density, the total pressure used was obtained from a pressure tap located in the supply plenum. Comparison of the plenum pressure and the total pressure calculated from a static pressure tap upstream of the orifice showed insignificant differences due to the relatively large passage area and rounded inlet section to the passage. The static pressure used to calculate the ideal jet velocity was obtained from two pressure taps, one located in the insert near the exit of the jet (jet exit tap) and the other located in the collector side wall. Figure 1 shows the location of the two pressure taps.

The total pressure loss coefficient is defined as the loss in total pressure divided by the dynamic head.

$$K_T = \Delta P / \frac{1}{2} \rho_j V_j^2 \tag{4}$$

where:

$$\Delta P = P_{in} - P_{out} \tag{5}$$

To calculate the downstream total pressure, the collector side wall taps and collector flow rates were used. For the hole Mach number, the following equation taken from Reference 13 was used:

$$\frac{M}{\left[1 + \frac{\gamma-1}{2} M^2\right]^{(\gamma+1)/2(\gamma-1)}} = \frac{w}{AP}\sqrt{\frac{RT_T}{\gamma}} \tag{6}$$

where P is the upstream total pressure, T_T is the total temperature, w the actual flow and A the physical hole area. The Reynolds number has been calculated using the following equation:

$$Re = \frac{w\,D}{A\,\mu} \tag{7}$$

Cross Flow Impingement Model

The discharge coefficients for the impingement models were calculated using equation 1. Total pressures were obtained from pressure taps located in the five supply plenums, while the downstream jet static pressure was evaluated based on the crossflow duct static pressure as measured by the taps located in the side wall of the cross flow passage and in line with the corresponding plenum and also based on the jet exit taps. Comparisons of the measured and calculated static pressure distribution in the cross flow passage were made using the following equation taken from Reference 14. The equation was derived for the case of flow in a rotating passage with injection through a porous wall, but is applicable to passages with increasing flow in the direction of flow.

$$\left[1 - \left(\frac{w}{A}\right)^2 \frac{RT_s}{p^2}\right] \frac{dp}{dx} = \frac{p\,r\,\omega^2}{RT}\cos\theta \tag{8}$$

$$- \frac{2RT_s}{p}\left(\frac{w}{A}\right)\frac{d\left(\frac{w}{A}\right)}{dx} - \left(\frac{w}{A}\right)^2 \frac{R}{p}\left(\frac{4fT}{2D_h} + \frac{dT_s}{dx} + \frac{T_s dA}{A\,dx}\right)$$

For nonrotating, constant area and isothermal flow, the equation reduces to

$$\left[1 - \left(\frac{w}{A}\right)^2 \frac{RT_s}{p^2}\right] \frac{dp}{dx} = -\frac{2RT_s}{p}\left(\frac{w}{A}\right)\frac{d\left(\frac{w}{A}\right)}{dx} - \left(\frac{w}{A}\right)^2 \frac{4R\,f\,T_s}{p\,2\,D_h} \tag{9}$$

From the test data, it was found that the mass velocity in the impingement holes varies linearly with distance along the passage so that d (w/A)/dx was constant. The solution to the first order differential equation was obtained numerically by the use of a Runge-Kutta technique.

Pin Fin Model

Friction factors for the pin fin models were obtained from the following equation which accounts for the friction losses through N rows of pins due to (N-1) expansions and contractions,

$$f = \frac{\Delta P_T\,\rho}{2\,(N-1)\left(\frac{w}{A}_{min}\right)^2} \tag{10}$$

The total pressure loss was calculated from the difference in total pressure in the first and last pin row. Using the pressure in the first and last pin row made the data independent of the configuration upstream and downstream of the pin rows. Therefore, the data can be applied to configurations such as converging, diverging or abrupt exits which are found in engine applications by making pressure loss assumptions consistent with the geometry involved. The N-1 term was used because the first contraction and the last expansion had not been taken into account by using the pressure in the first and last pin rows to obtain the pressure drop. The Reynolds number has been based upon the pin diameter and the minimum flow area as follows:

$$Re = \frac{w\,D}{A_{min}\,\mu} \tag{11}$$

Feeder Tube Model

For the feeder tube model, the discharge coefficients were calculated from equation 1. Average discharge coefficients were based on the upstream static pressure calculated from the average of the pressure taps located along the feeder tube, while the downstream pressure used was the average of the taps in the collectors or plenums. This average coefficient was used to compare the flow characteristics of the feeder tube discharging into the collectors with the case where the flow is impinged on a half cylinder. Individual discharge coefficients were also calculated for the second configuration which had collectors for every four holes. These coefficients were based on the upstream pressure obtained from pressure taps located in the feeder tube opposite the four holes and downstream pressure obtained from the taps in the collectors. Data is provided for coefficients based on both supply static and total pressures, where total pressure is calculated from static pressure, local flow rate and flow area.

To calculate the pressure distribution along the feeder tube, the following equation taken from Reference 15 has been used. The equation was derived for flow ejection from a porous passage which approximates the feeder tube flow.

$$\left[1 - \frac{RT_S}{p^2}\left(\frac{w}{A}\right)^2\right]\frac{dp}{dx} = -\frac{RT_S}{p}\left(\frac{w}{A}\right)\frac{d(w/A)}{dx} - \frac{R}{p}\left(\frac{w}{A}\right)^2\left(\frac{dT_s}{dx} + \frac{4\,fT_S}{2\,D_h}\right) \tag{12}$$

For the feeder tube flow, the temperature and d(w/A)/dx were considered constant and the friction factor was calculated from

$$f = .046/Re^{.2} \tag{13}$$

which was taken from Reference 15. Equation 12 was solved by the same method used for equation 9.

Composite Model

The analysis of the data from the composite model utilized a Compressible Flow Network Analysis computer program developed during this study. The program is discussed in the computer program section of this report. The program incorporates all of the pressure loss and flow coefficient correlations obtained from the previous models and was used to calculate flow and pressure distribution from the measured inlet and exit pressures.

Computer Program

The Compressible Flow Network Analysis (CFNA) computer program (Reference 17) calculates the flow distribution through an arbitrarily connected network of one-dimensional flow passages or branches with prescribed external temperature and pressure boundary conditions. Pressure variations resulting from laminar or turbulent pipe friction, orifice losses, inlet and exit losses, momentum balances, area changes, heat pickup, pumping and pin fin relationships can be included.

The program iterates between local effects in the various branches and overall balances of internal pressures and flow for the network. The program handles local flow reversals and choked conditions automatically. The flow is considered to be one-dimensional within any given flow passage. However, the momentum balance at the junction of two or more branches is computed vectorially.

The program has the capability of calculating geometries with up to 150 flow passages connected by 50 internal passage connections with a maximum of 20 equal divisions or stations assigned to each flow passage. The area, hydraulic diameter and friction coefficient multiplier may be varied from station to station for any flow passage. The program output includes velocity, static pressure, temperature, Mach number and Reynolds number at each station along each flow passage in addition to the inlet pressure, temperature and flow for each flow passage.

RESULTS AND DISCUSSION

Leading Edge Impingement Model

Leading edge scaling test results for the 1X and 5X size leading edge impingement models are shown on Figure 10 as Mach number, calculated from equation 6, versus measured pressure ratio. Good agreement is shown for the two models indicating that scaling should not be a problem when applying leading edge impingement results from larger models to actual turbine blade hardware.

Figure 11 shows the orifice flow coefficient results from the 5X size model as a function of Reynolds number for the three orifice to impinged wall spacing-to-hole diameter ratios tested (Z/D = 2, 3, and 5) and equal flow split between the discharge ports. No discernible effect of Reynolds number is observed at constant Mach number over a 10 to 1 Reynolds number range; however, increasing flow coefficient with increasing Mach number is indicated. Repeatability of the data is shown by the shaded symbols at Z/D = 3.0. Good agreement existed at the two high Mach number points with about a 10% deviation at a Mach number of 0.1 caused by uncertainties in the measurement of the low flow and low pressure drop. The effect of Mach number is observed in Figure 12 for the three spacing ratios with the following final correlation imposed on the data:

$$C_D = .819\,(Z/D)^{.045}\,M^{.057} \tag{14}$$

The flow coefficients on Figures 11 and 12 are based on the static pressure as measured on the collector side walls (see Figure 1). Coefficients were also calculated based on the taps located at the jet exits. These results, plotted on Figure 13, are nearly identical to the collector side wall tap results, i.e., jet exit static pressure is equal to cavity side wall static pressure. On all other figures, except where noted, discharge coefficients are based on the side wall taps.

Correlation of leading edge spacing (Z/D) effects for the three Mach number levels is illustrated on Figure 14. Results are also shown on these plots for test points with ambient pressure in the discharge plenums. These ambient test results were weighted into the final correlation, particularly at low Mach numbers where a considerable scatter was exhibited in the controlled pressure data. At a Z/D of 3.0, flow between the discharge ports was varied up to a ratio of 2 to 1 at a constant orifice Mach number with the results shown on Figure 15. Open and closed symbols indicate static pressure taps on the high and low flow sides were used in the calculation of the respective discharge coefficients with variation between sides of up to 3% indicated at the highest flow split. No significant effect of flow split is indicated by the data.

Correlation of the data in terms of total pressure loss coefficients is shown on Figure 16 as a function of Mach number for the three leading edge spacing ratios. Coefficients were calculated using side wall static tap measurements and calculated discharge total pressure based on this static pressure and average velocity in the collector passage. Total pressure recovery based on these assumptions is seen to decrease with increasing Mach number (loss

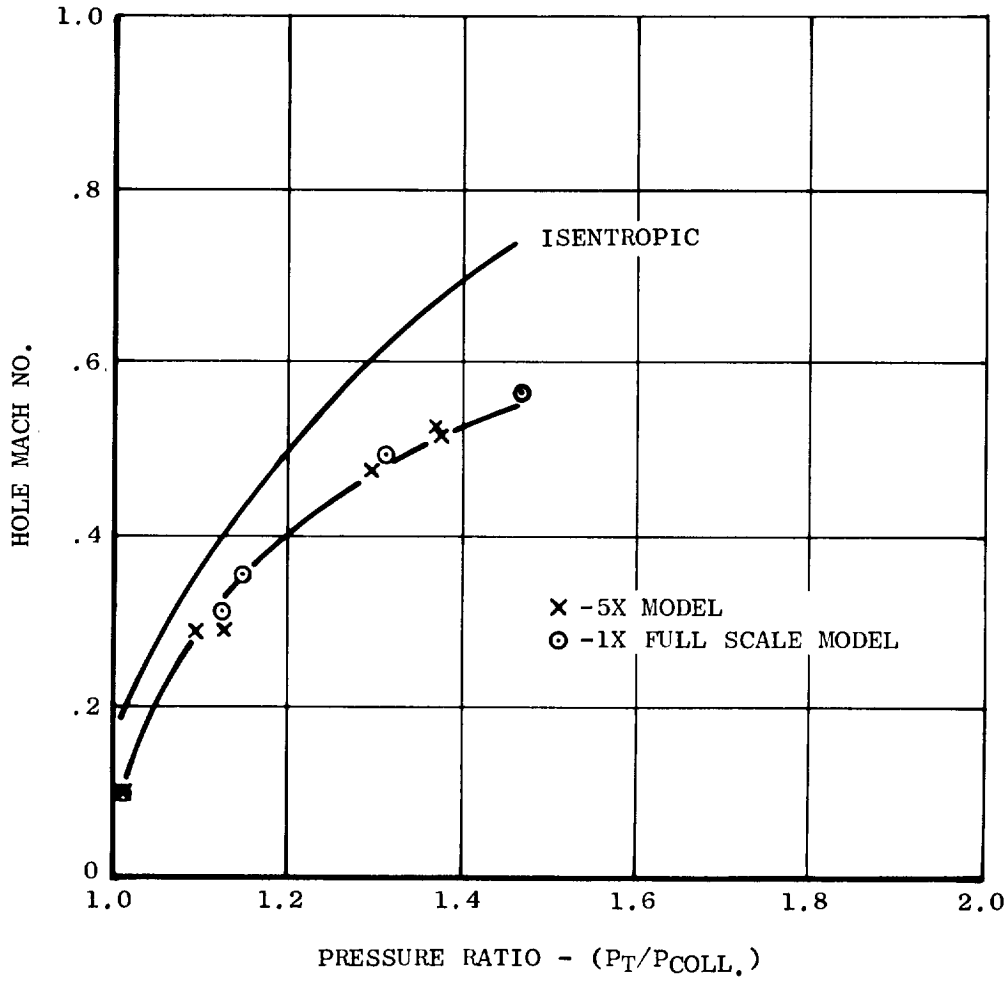

Figure 10 Comparison of Full Scale and 5X Leading Edge Model Results

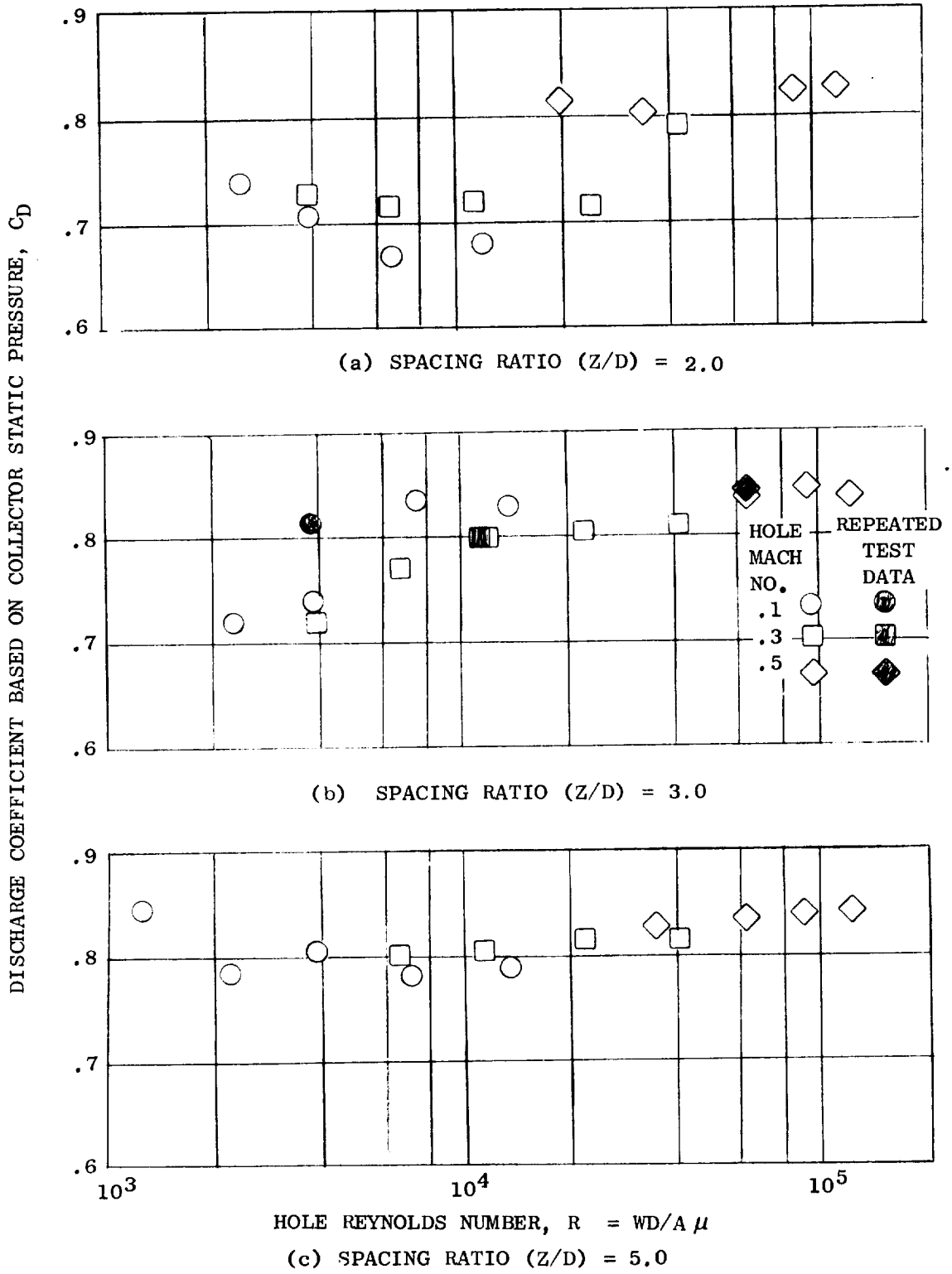

Figure 11 Discharge Coefficient for Leading Edge Model as a Function of Hole Reynolds Number for Various Spacing Ratios and Equal Flow Split

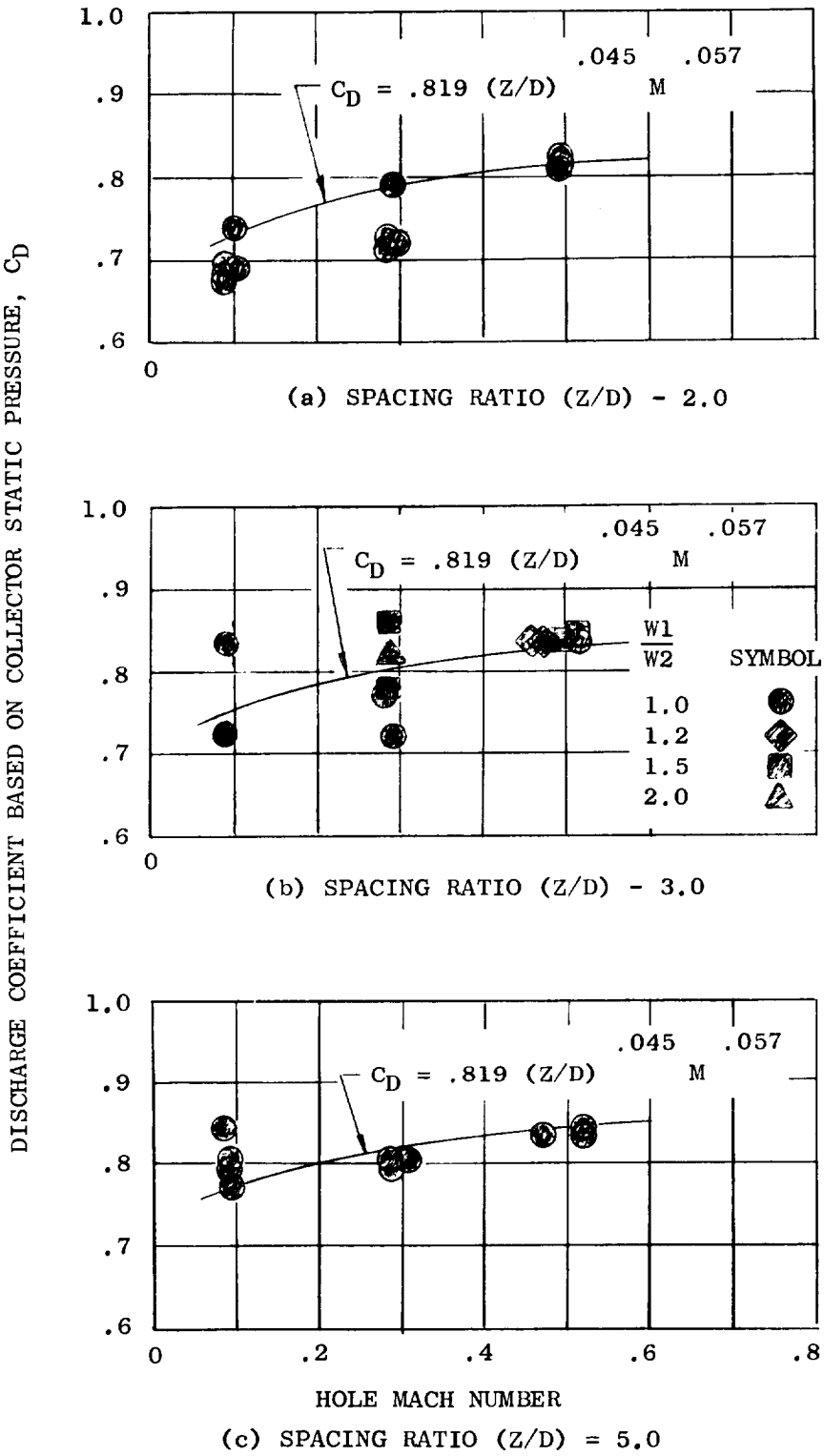

Figure 12 Discharge Coefficient for Leading Edge Model Based on Collector Static Pressure as a Function of Hole Mach Number for Various Spacing Ratios

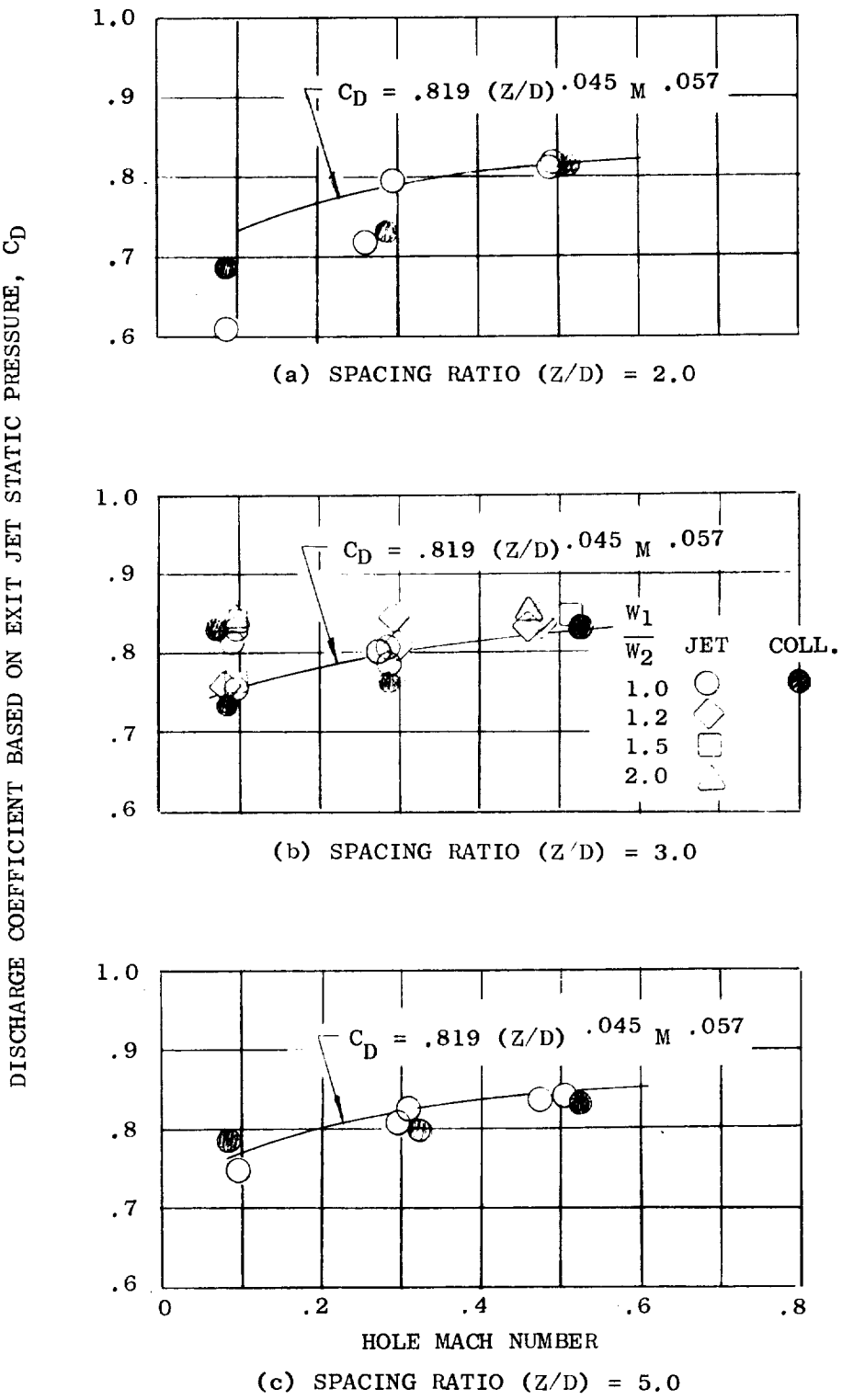

Figure 13 Discharge Coefficient for Leading Edge Model Based on Jet Exit Static Pressure as a Function of Hole Mach No. for Various Spacing Ratios with Comparison to Typical Coefficients Based On Collector Pressure

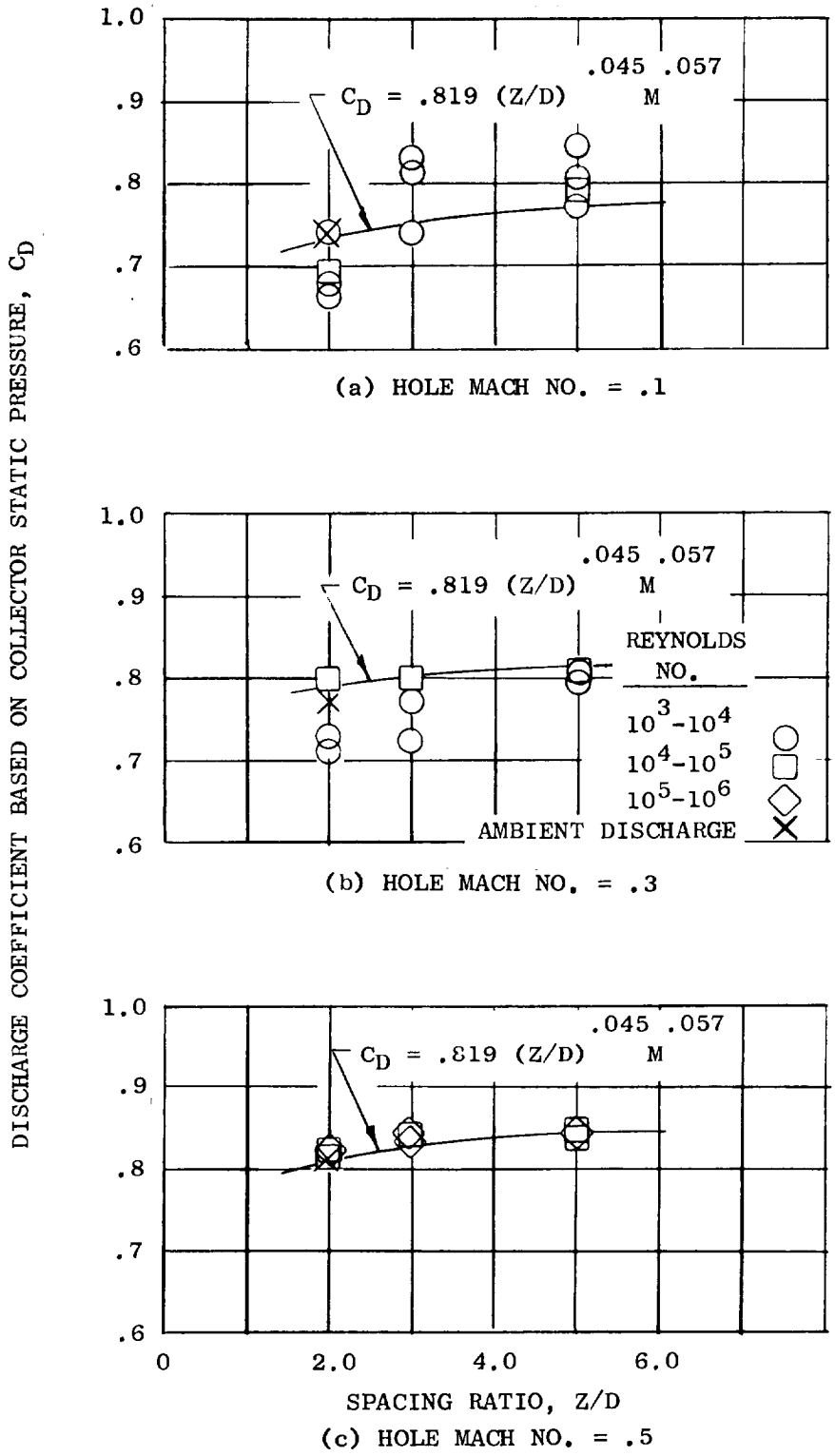

(a) HOLE MACH NO. = .1

(b) HOLE MACH NO. = .3

(c) HOLE MACH NO. = .5

Figure 14 Discharge Coefficient for Leading Edge Model as a Function of Spacing Ratio for Various Mach Nos. with Equal Flow Split

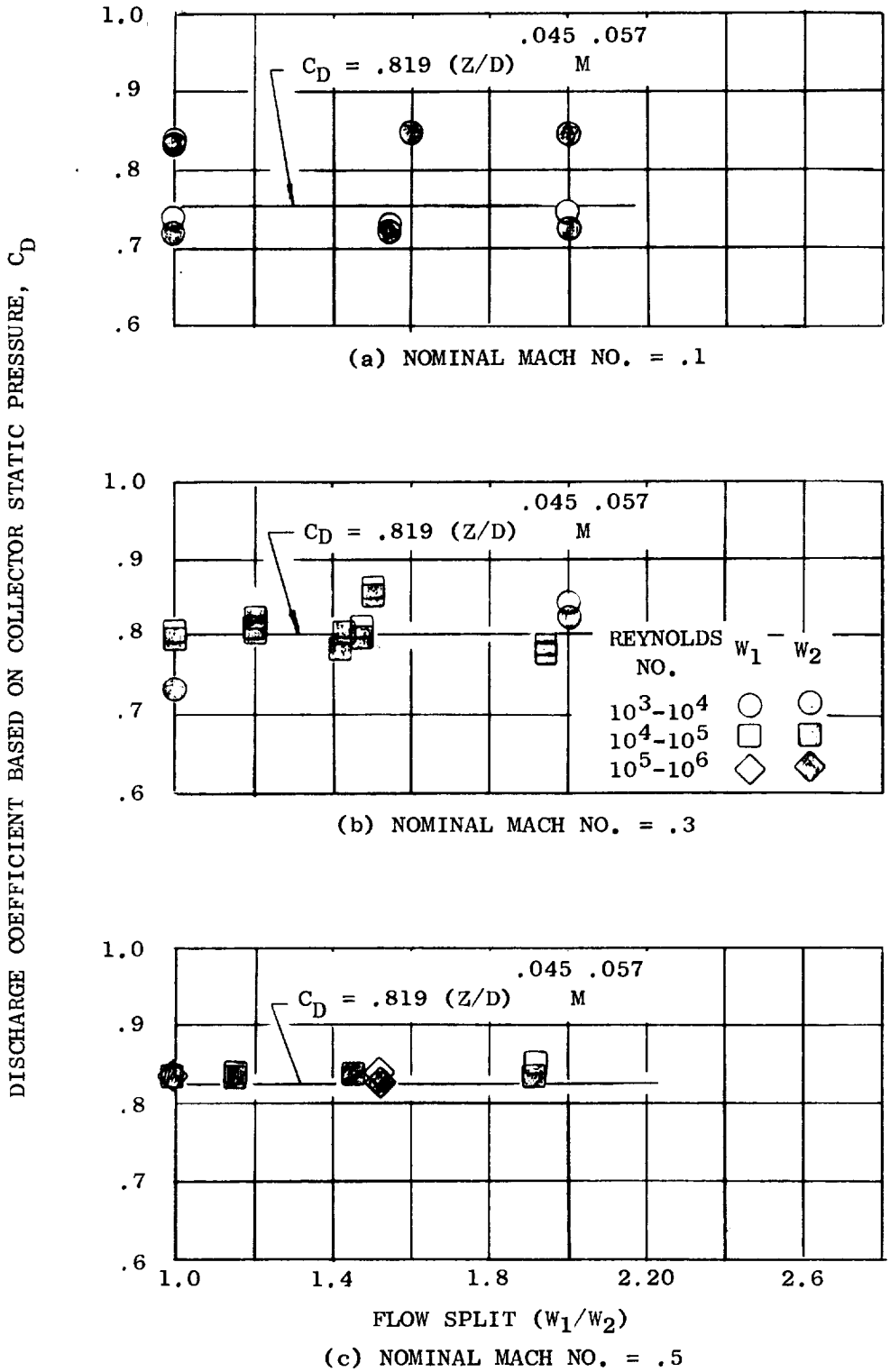

(a) NOMINAL MACH NO. = .1

(b) NOMINAL MACH NO. = .3

(c) NOMINAL MACH NO. = .5

Figure 15 Discharge Coefficient for Leading Edge Model as a Function of Flow Split for Various Mach Numbers.

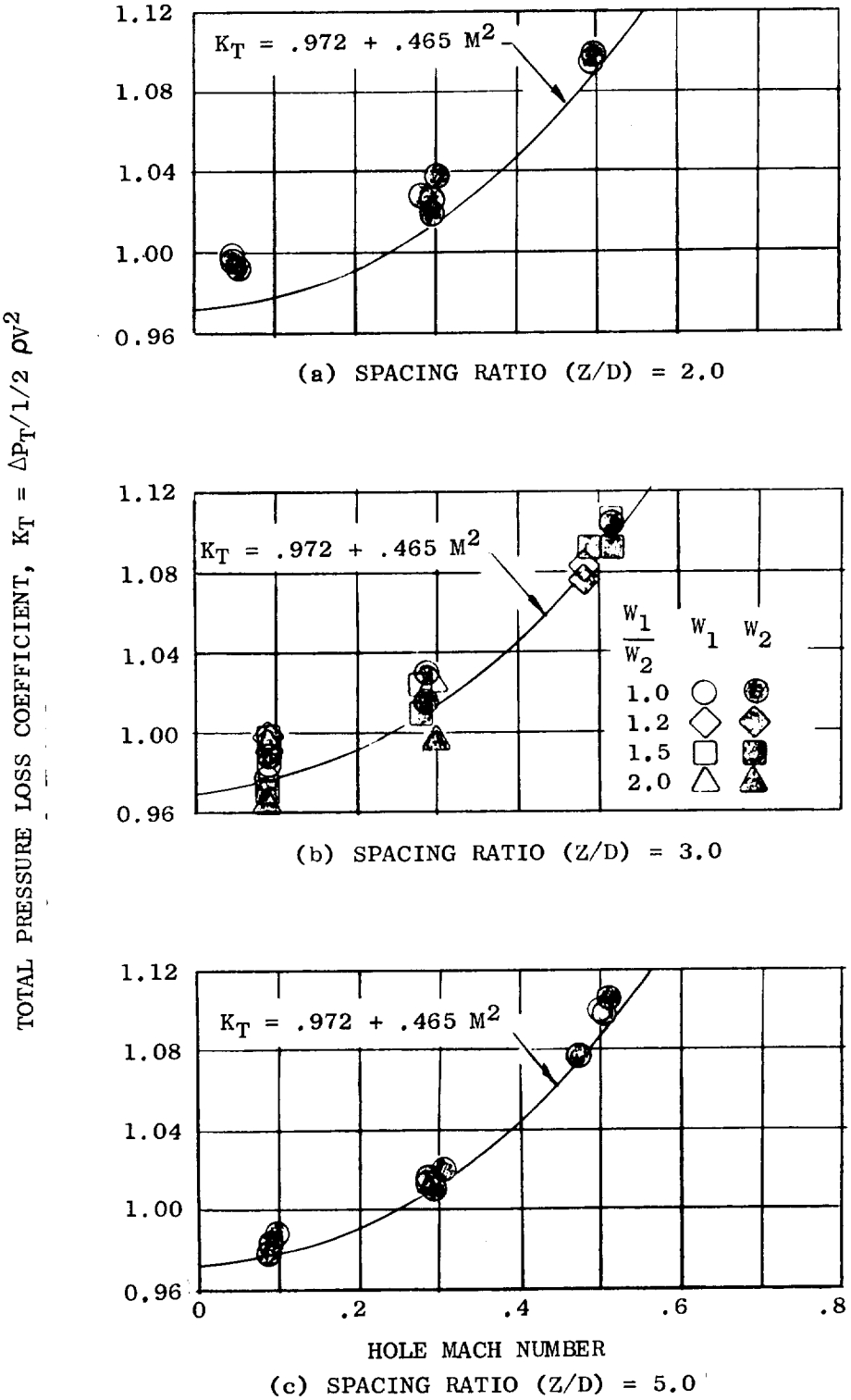

Figure 16 Total Pressure Loss Coefficient for Leading Edge Model as a Function of Hole Mach No. for Various Spacing Ratios

coefficients increase) with little effect of flow split or spacing ratio evidenced. Approximately one velocity head loss is indicated as best correlated by:

$$K_T = .97 + .465M^2 \quad (15)$$

A flow visualization study was made to help understand the complex flow fields present in the leading edge impingement model. The flow visualization study was accomplished by moving a tufted probe in the jet to locate the center line of the jet and the impingement point on the wall. The stream lines could be detected by noting changes in direction of the tuft. When the probe was moved elsewhere in the cavity, regions of low velocity could be detected by a fluttering motion of the tuft. Tests were run at hole Mach numbers of 0.1 and 0.5, spacing ratios of 2 and 5, and flow splits of 1, 1.2, 1.5 and 2. Results of the flow visualization study are shown in Figure 17a where the ratio of the jet deflection distance-to-hole diameter has been plotted as a function of the flow split for two spacing ratios and two Mach numbers. Figure 17a indicates that the deflection of the jet is small and that the spacing ratio has a greater effect than the Mach number or flow split. The results of probing the entire cavity showed that low velocity or recirculating regions existed adjacent to the insert and around the hole and that these regions increased in size on the low flow side of the insert as the Mach number, spacing ratio and flow split increased, resulting in flow recirculating across the jet. This effect is sketched in Figure 17b.

Impingement with Crossflow

To determine if large scale models could be used to get detailed data on impingement with crossflow models, a full scale (engine hardware size) and a five times scale model of two impingement geometries were tested at Z/D of 3.0, nominal Mach numbers of 0.1 and 0.4 and independent crossflow ratio of 0, 1, and 3. Definition of these models, identified as Models 2A, B, C and D, is provided in Figure 2. Results from the full size model 2A were found to be in error and are not reported herein. Data from the full scale model 2B and 5X size model 2D are tabulated on Figure 18. Four pressure taps on the side wall of the crossflow passage, which were common to both models, were used for pressure ratio and flow coefficient calculations. For the 5X size model, coefficients were calculated for every two rows of holes corresponding to individual flow supplies. For the full size model, impingement flow was supplied from one plenum requiring that an assumption of constant flow per row be made. At low Mach number the 5X scale model exhibited flow coefficients 10-25% higher than the full scale model values, while at a Mach number of 0.4 reasonably good agreement is obtained. Based on these data large scale models appear to be representative of engine applications.

The effects of orifice Reynolds number and Mach number on discharge coefficients are shown on Figures 19 and 20 for the first plenum (W_1) of the 5X size models tested. The discharge coefficients are based on side wall pressure tap measurement. In general, discharge coefficients range from 0.7 to 0.8 with no significant effect of orifice Mach number, Reynolds number or independent crossflow ratio. At Z/D of 3.0 model 2C exhibited a discharge coefficient reduction of about 10%; however, model 2D did not exhibit this characteristic. From Figure 20, a data spread of approximately ±7% is indicated. This spread is about three times the error predicted from assumed experimental inaccuracies.

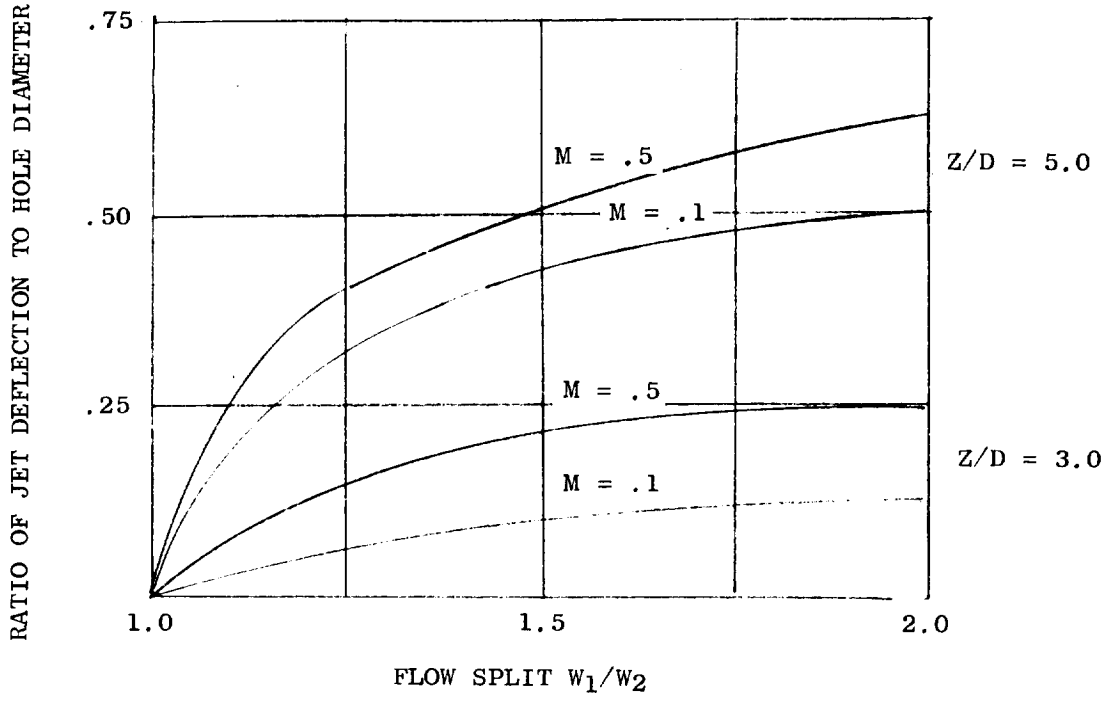

(a) Observed Jet Deflection

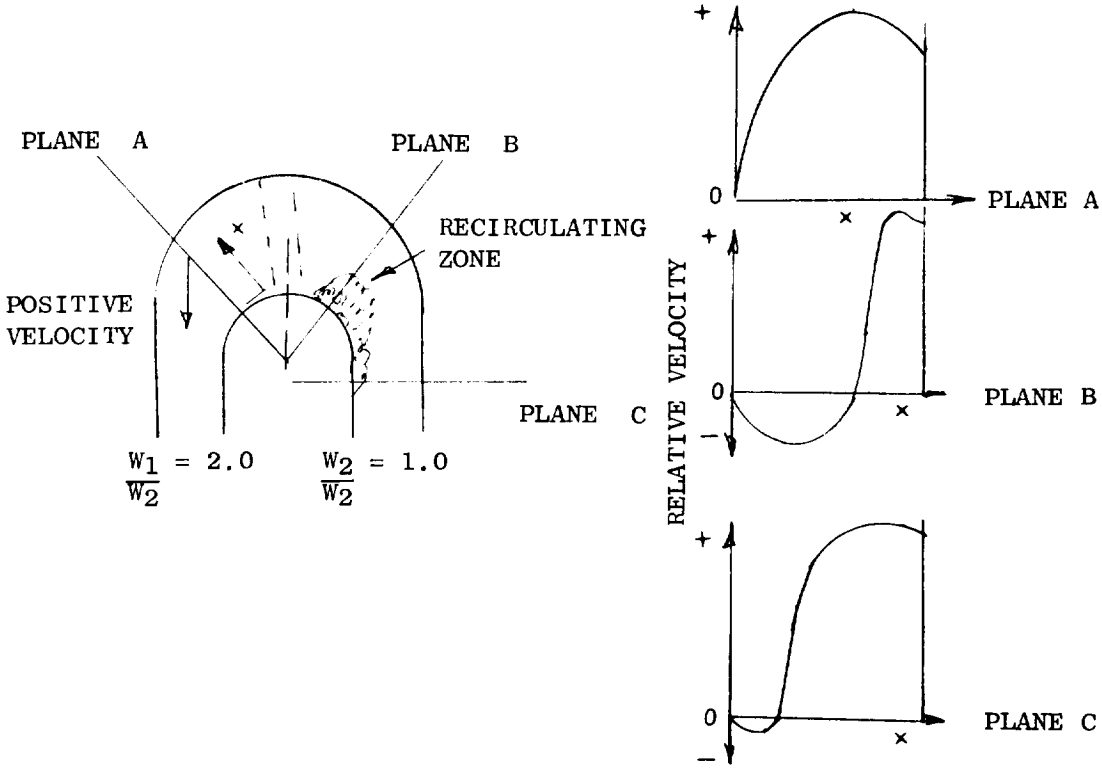

(b) Observed Velocity Profile

Figure 17 Results of Flow Visualization Tests on Leading Edge Impingement Models

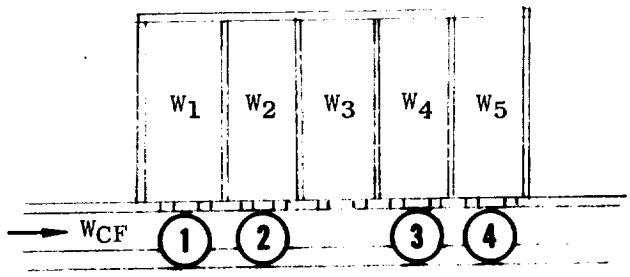

MACH/REYNOLDS	Wcf/Wl	SCALE	PT/PS	CD	PT/PS	CD	PT/PS	CD	PT/PS	CD
			①		②		③		④	
.12/7200	0	1	1.017	.744	1.019	.708	1.019	.712	1.02	.700
		5	1.013	.803	1.013	.811	1.012	.87	1.014	.726
	1	1	1.016	.76	1.018	.711	1.018	.711	1.02	.684
		5	1.012	.835	1.013	.839	1.011	.94	1.013	.85
	3	1	1.014	.801	1.016	.746	1.018	.718	1.019	.685
		5	1.01	.875	1.011	.905	1.013	.925	1.022	.88
.4/23000	0	1	1.247	.768	1.26	.756	1.285	.737	1.316	.725
		5	1.201	.783	1.207	.788	1.202	.81	1.237	.803
	1	1	1.246	.781	1.267	.763	1.291	.746	1.327	.726
		5	1.207	.782	1.216	.784	1.20	.815	1.25	.801
	3	1	1.194	.83	1.201	.819	1.268	.756	1.403	.70
		5	1.187	.806	1.2	.801	1.214	.811	1.25	.817

Figure 18 Scaling Test Comparison for Impingement with Crossflow Models 2B and 2D

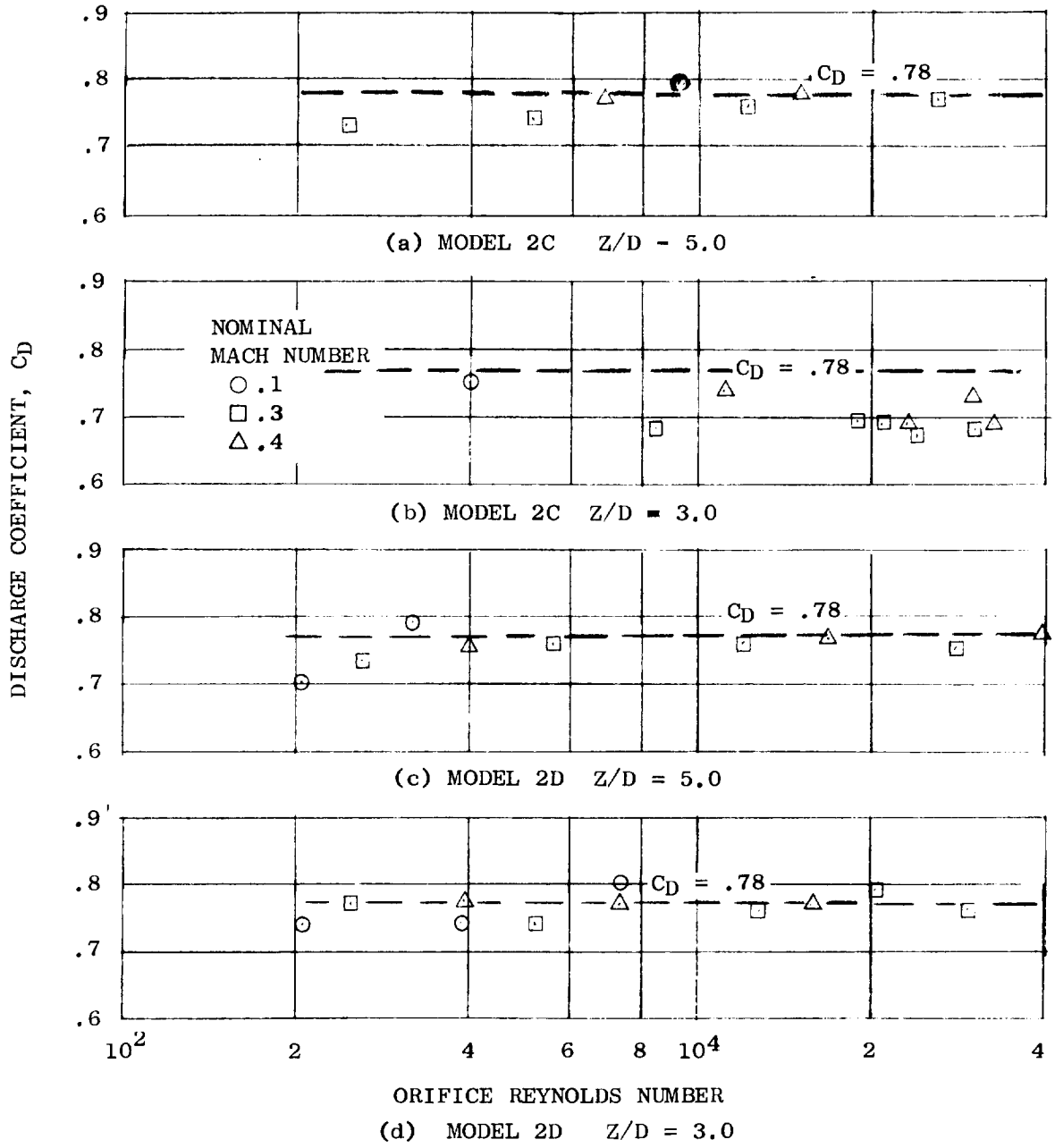

Figure 19 Effect of Orifice Reynolds Number on Discharge Coefficient for First Plenum of Impingement with Crossflow Models with No Independent Crossflow

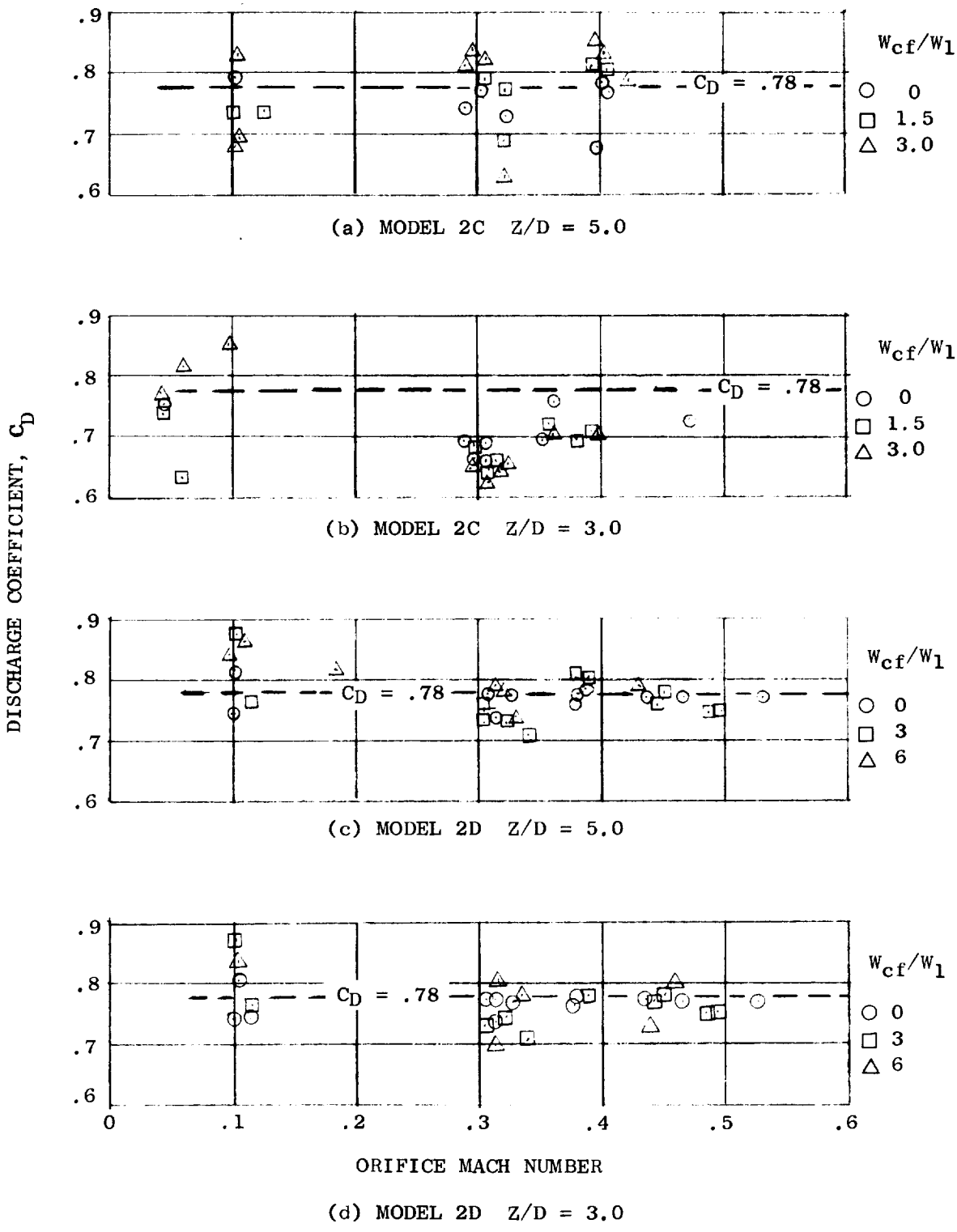

(a) MODEL 2C Z/D = 5.0

(b) MODEL 2C Z/D = 3.0

(c) MODEL 2D Z/D = 5.0

(d) MODEL 2D Z/D = 3.0

Figure 20 Effect of Orifice Mach Number on Discharge Coefficient for First Plenum of Impingement with Crossflow Models

To determine the effect of crossflow velocity, discharge coefficients are shown on Figures 21 to 24 for the individual plenums of each model as a function of the ratio of the jet Mach number to the crossflow Mach number, with symbols identifying the three nominal Mach number levels. Observation of the data from the individual plenums shows no effect of crossflow velocity on discharge coefficient within the range tested; however, a trend of increasing discharge coefficient with downstream plenum location is noted in particular on model 2C at Z/D = 3 and 5. Discharge coefficients are also shown for each plenum based on the measured pressure on the impingement plate (near the jet) for a nominal Mach number of 0.3 and for three crossflow rates. This pressure is lower than that measured by the sidewall taps and results in discharge coefficients of reduced magnitude but nearly constant level. For any plenum the crossflow from upstream jets is approximately constant, therefore variations in Mach number ratios for a particular plenum are due to variations in the independent crossflow rate. It appears that flow from the independent source has a smaller effect on orifice flow characteristics than that from self-generated impingement flow because of differences in the resulting crossflow passage velocity profiles. Complete understanding of this effect cannot be obtained from the limited data available. The recommended discharge coefficient relationship is:

$$C_D = \text{constant} = 0.78 \tag{16}$$

Figure 25 shows typical measured pressure distributions in the crossflow passage as a function of distance along the passage. The three types of pressure tap locations (side wall, impinged wall and impingement plate) show that the side wall and impinged wall taps agree, while the impingement plate taps show a reduced pressure next to the issuing jets as noted previously in describing the discharge coefficient data. The impingement plate pressure taps measured a local low pressure region surrounding the jet which is not representative of the overall pressure distribution in the passage. The momentum balance prediction employing equation 9 is also shown in Figure 12. The momentum balance is shown to have good agreement with the side and impingement wall taps which should represent the static pressure along the passage. It can also be observed that little, if any, total pressure is picked up by the taps on the impinged plate located directly under the jet.

Flow visualization testing was conducted on the 5X size model configurations (using clear plastic side walls and impinged wall) at orifice Mach numbers of 0.1 and 0.4 and three values of independent crossflow. Using a tufted probe to sense flow direction indicated that, with no crossflow on the first row, the jet could be "tracked" to the point of impingement on the impinged wall; however, for all other rows and for the first row when crossflow was introduced, the tuft immediately bent in the direction of crossflow. Typical probe results for model 2C at Z/D = 5.0 are shown in Figure 26.

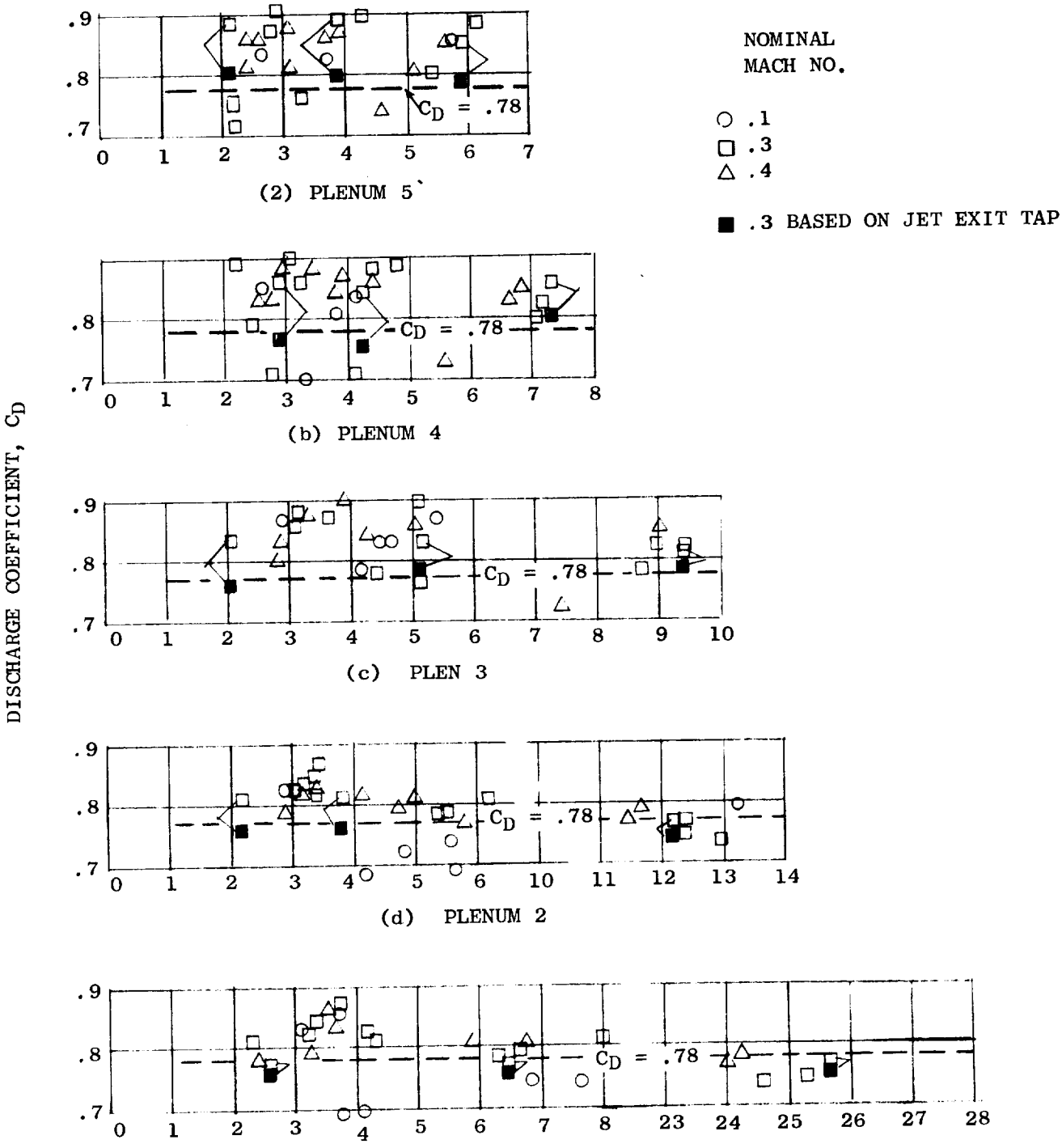

Figure 21 Effect of Crossflow Velocity on Discharge Coefficient for Model 2C $Z/D = 5.0$

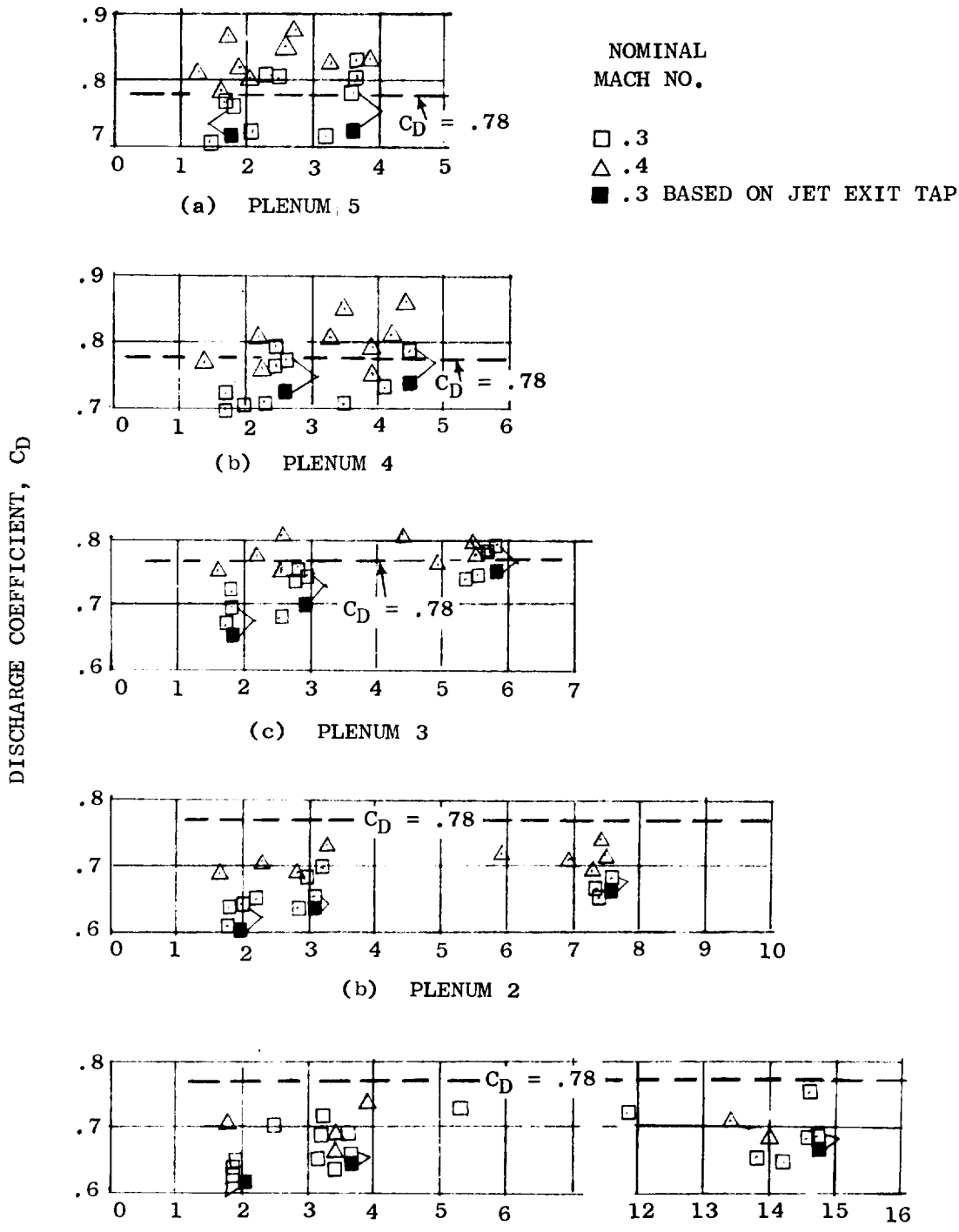

Figure 22 Effect of Crossflow Velocity on Discharge Coefficient for Model 2C Z/D = 3.0

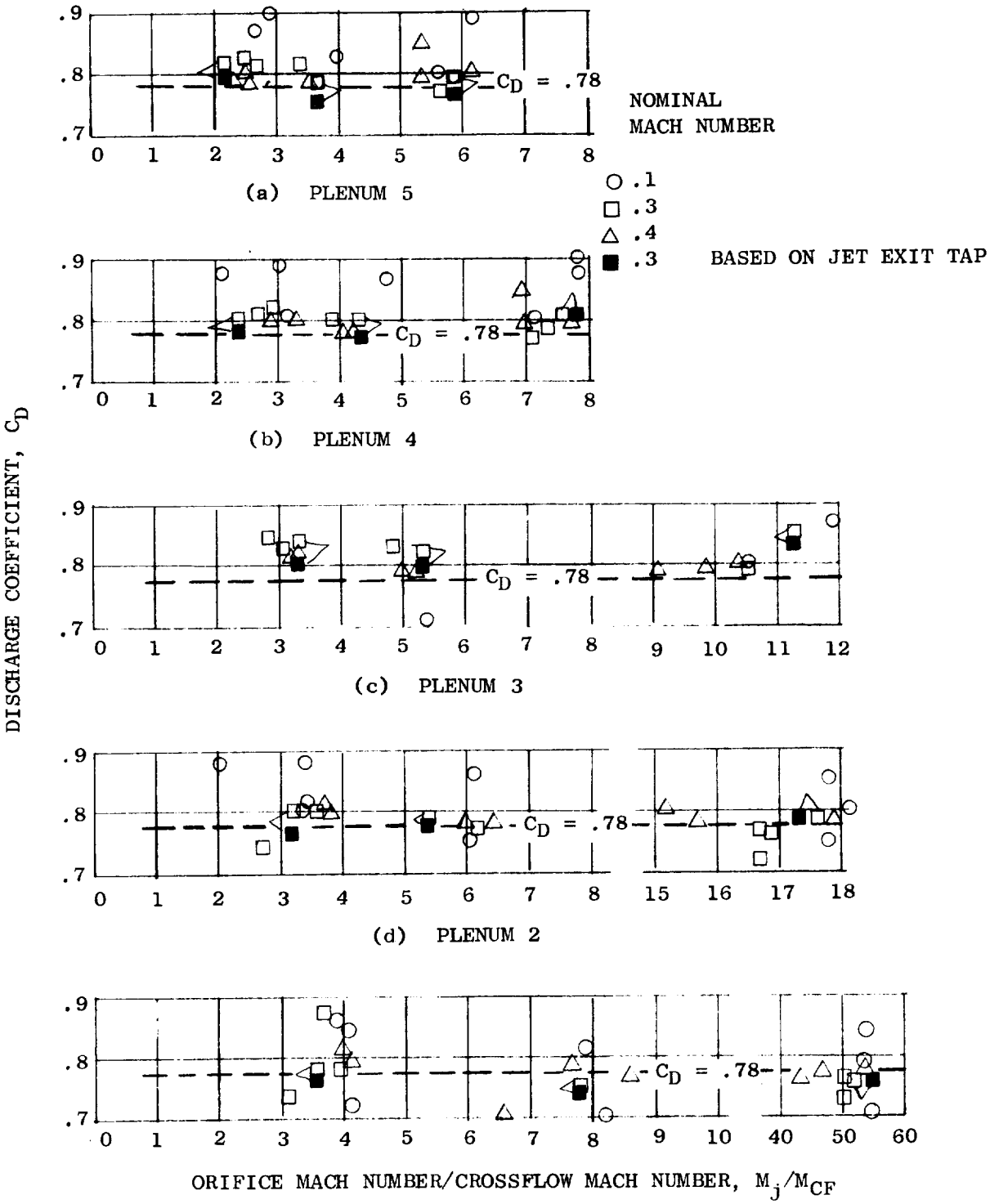

Figure 23 Effect of Crossflow Velocity on Discharge Coefficient for Model 2D Z/D = 5.0

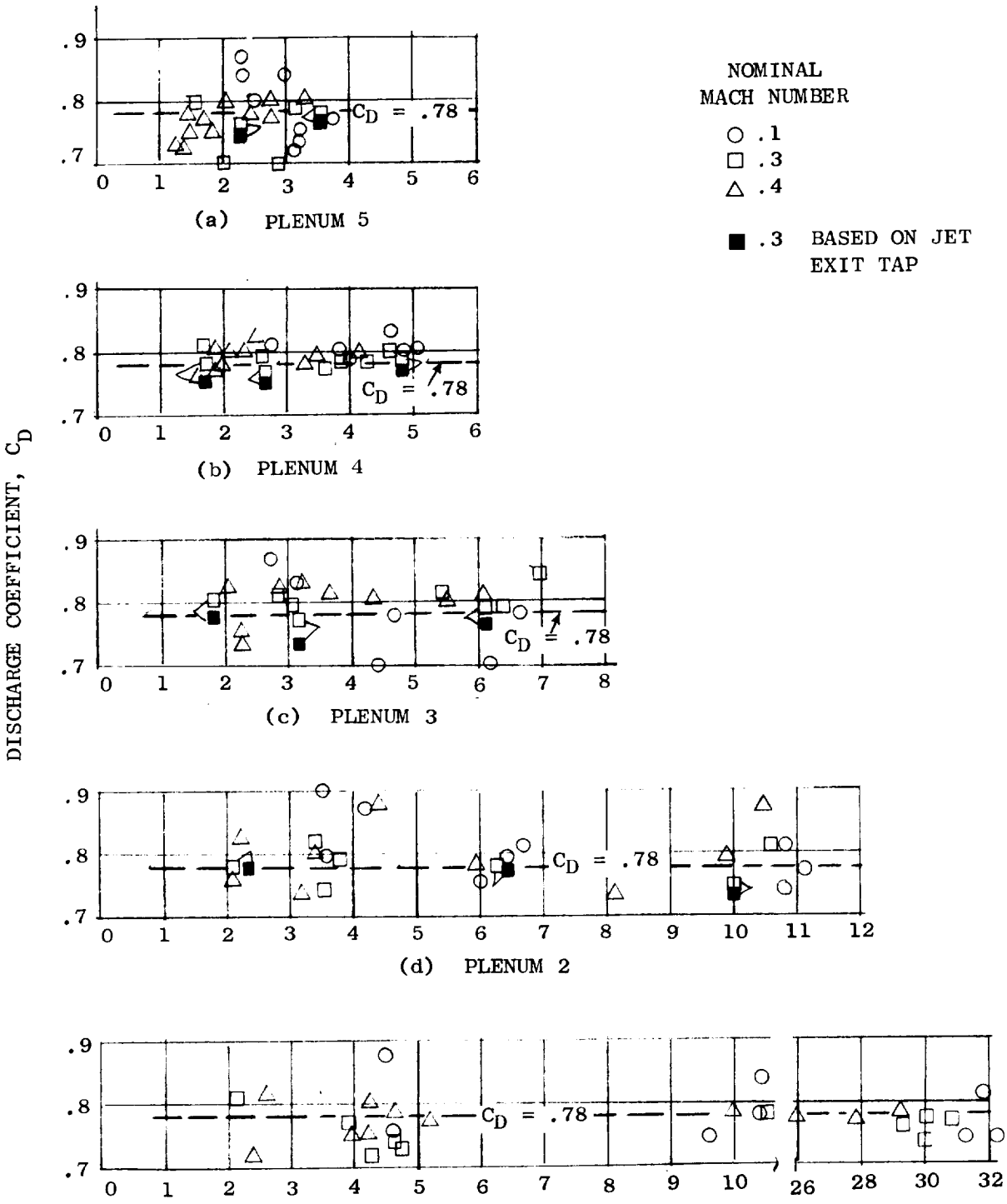

Figure 24 Effect of Crossflow Velocity on Discharge Coefficient for Model 2D Z/D = 3.0

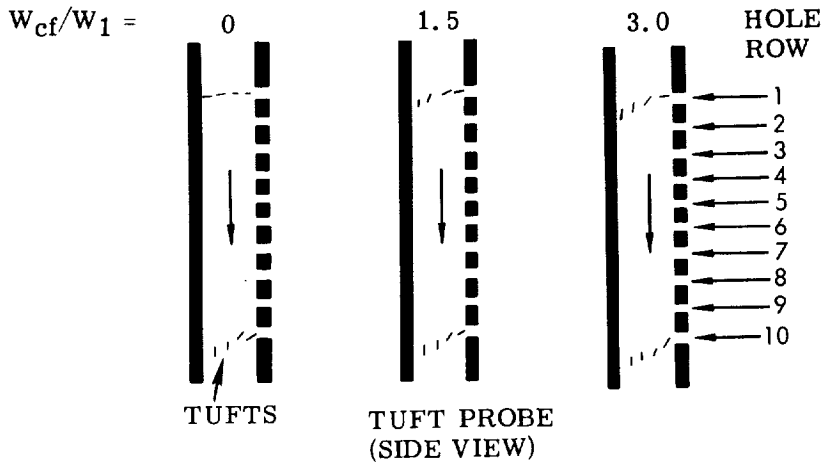

Figure 26 Typical Impingement with Crossflow Flow Visualization Results

All models showed the same general pattern which indicated jet bending is dependent on cross-flow-to-jet mass velocity ratio. To obtain more detailed probing requires a model of larger size.

Pin Fin

Six (6) pin fin models, defined in Figure 3 and identified as models 3A, B, C, D, E and F, were tested. Results from the pin fin models have been presented in the form of friction factor versus Reynolds number based on pin diameter and minimum flow area between pins, where the friction factor is the average for (N-1) pin rows. Models 3A and 3E correspond to the full scale (engine size) and five times full scale size configurations, respectively, with results shown on Figure 27(a). Generally good agreement is shown for the two models, indicating scaled model results should be valid. This figure and the figures for the other pin fin models show two friction factor relationships. One is the correlation of Grimison's data by Jakob (Reference 5).

$$f = \left[.25 + \frac{.1175}{\left[\frac{X_t}{D} - 1\right]^{1.08}}\right] Re^{-.16} \tag{17}$$

the other is the relationship which best correlated these data

$$f = \left[2.06 \left(\frac{X_t}{D}\right)^{-1.1}\right] Re^{-.16} \tag{18}$$

Flagged symbols on these plots denote flow points where the models were discharging to ambient pressure.

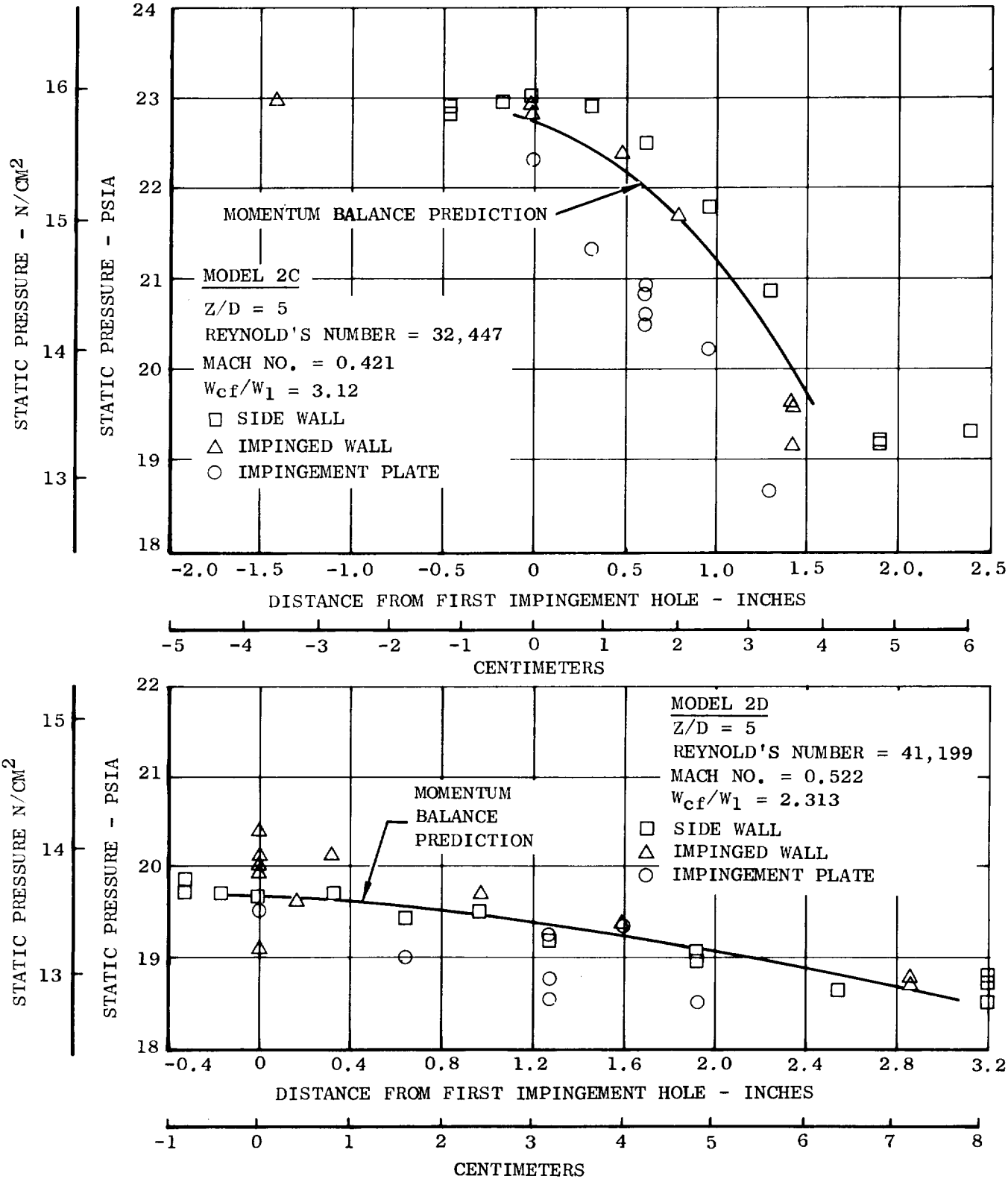

Figure 25 Typical Static Pressure Distribution in the Cross-Flow Passage for Models 2C and 2D Compared to Prediction

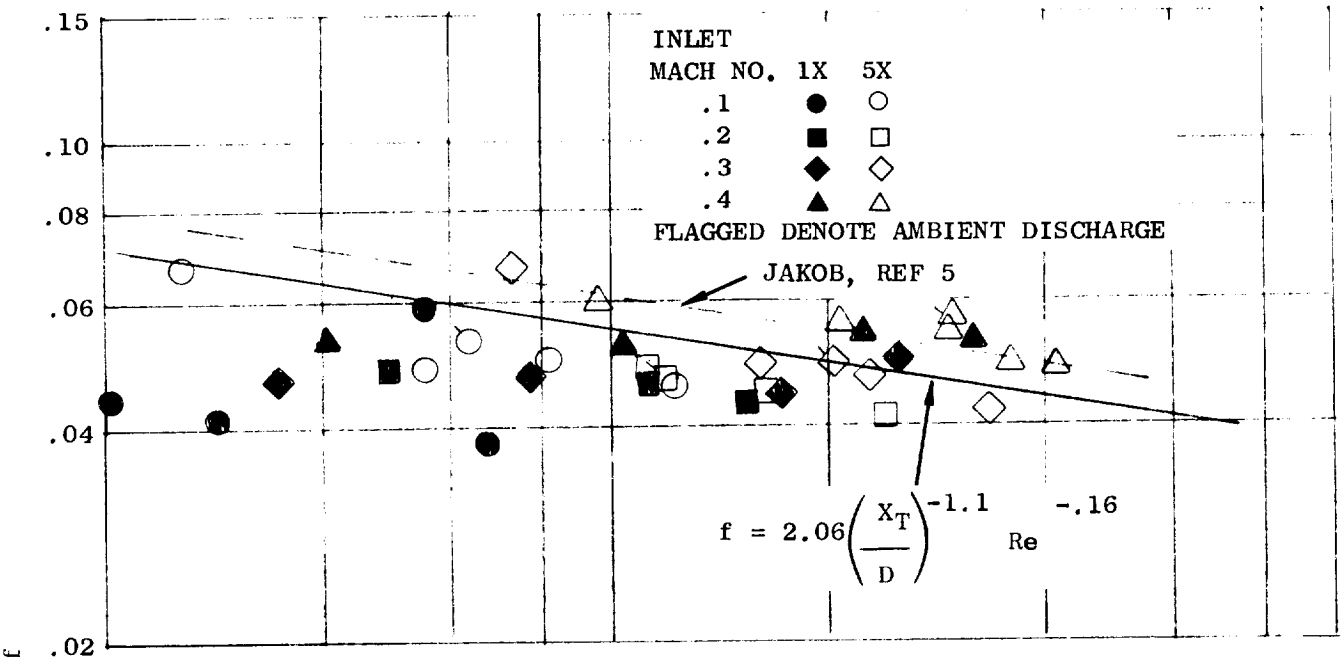

(a) COMPARISON OF DATA FROM 1X MODEL (3A) 5X MODEL (3E) AT Z/D = 4.0

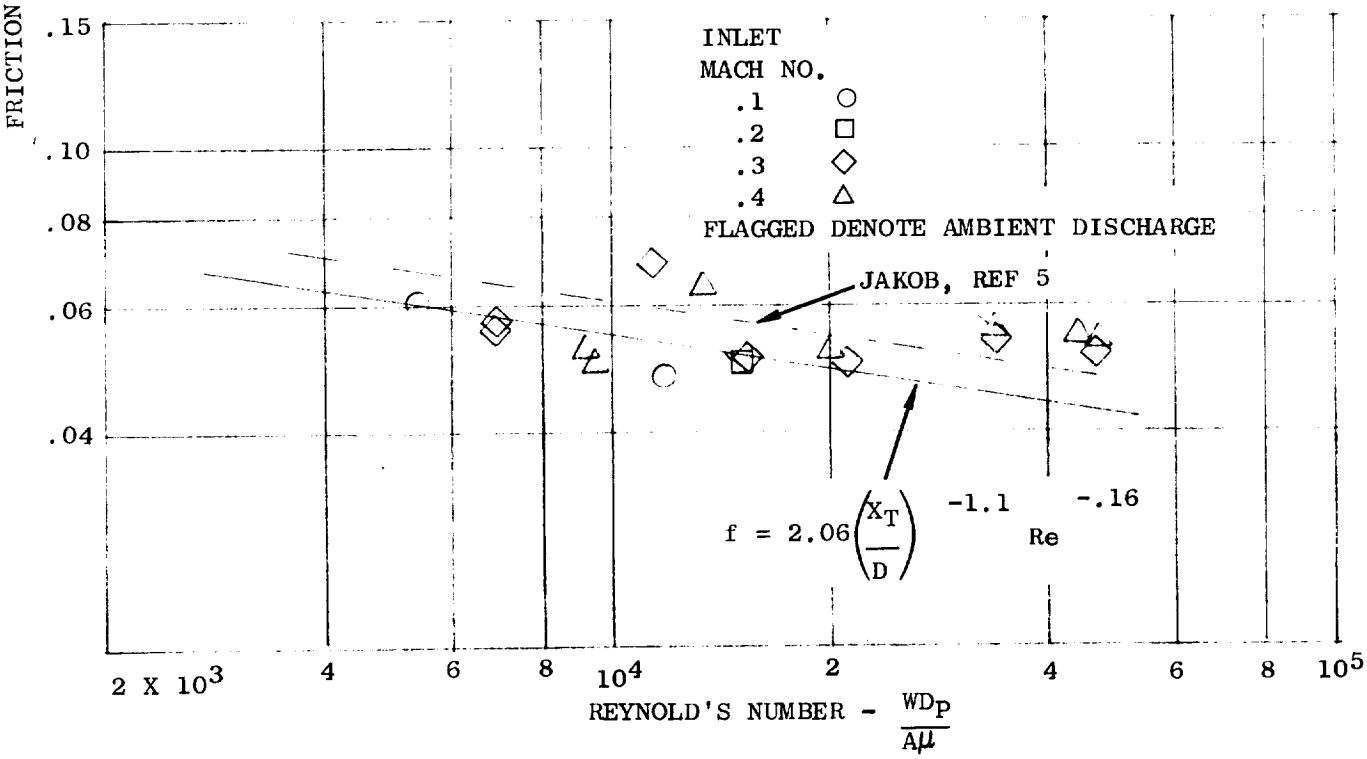

(b) DATA FROM MODEL 3D AT Z/D = 2.0

Figure 27 Pin Fin Friction Factor as a Function of Pin Reynolds Number at $X_D/D = 5.0$

From Figures 27(a) and (b) a comparison of results of models 3E and 3D, which have wide pin spacing ($X_D/D = 5.0$) and passage heights (Z/D) of 4.0 and 2.0, respectively, can be made. No effect of passage height is evident in this data, nor does there appear to be a consistent effect of Mach number.

Figures 28(a) and (b) show the results for models 3C and 3B with close pin spacing, $X_D/D = 3.0$, and varying passage height, $Z/D = 4.0$ and 2.0, respectively. Again no passage height or Mach number effects are seen, but, by comparing to Figure 27, a distinct pin spacing effect is noted and results in an increase in friction factor of about 75% at the close spacing which has been accounted for in the data correlation. Comparison of these results with Jakob's correlation for staggered pins (equation 17) shows good agreement at wide pin spacing, but poor agreement at close spacing. This disagreement with equation 17 is not unexpected since the range of pin spacing correlated by Jakob was limited to $X_t/D<3.0$ compared to the closest spacing in this test of 4.24, however the better agreement would be expected at the closer spacing. Additionally, no axial spacing effect was correlated by Jakob although the curves of Grimison (Reference 6) indicate an effect. Data presented in Reference 7 for in-line tube arrays, where both transverse and lateral spacings were varied from one to six, confirm the trends from this test, i.e., decreasing friction factor with increasing axial spacing, although the levels are about 30% of the values for these tests.

Figure 29 shows the results for model 3F compared to the correlation and data from model 3B. This model has the same average passage height and the same pin spacing as model 3B, but has only five rows of pins in a convergent passage. At low Mach numbers the convergent passage friction factors were lower indicating a possible effect of convergence or number of pin rows. Good agreement is shown at higher Mach numbers.

To determine if an effect of pin rows exists, Mach numbers and friction factor are plotted on Figure 30 for each pin row of model 3B for constant Reynolds number and four values of inlet Mach number. Below a Mach number of 0.36 friction factor remains constant through the array while above 0.36, an increase in friction factor with increasing Mach number is shown.

In summary, the data obtained from the pin fin model tests are best correlated by equation (18), which shows an effect of Reynolds number and pin spacing on pin fin friction factor. Mach number and passage height produced no consistently significant effect on pin fin friction factor.

Feeder Tube Results

The feeder tube tests were run in two configurations (see Figure 4). In the first configuration, the flow discharged directly onto the wall of a common collector, simulating leading edge impingement. In the second configuration, the flow from every group of four holes discharged into individual collectors to provide local flow measurements. By comparing the total flow characteristics of the configurations, the influence on the orifice flow of the direct jet impingement on a surface could be determined.

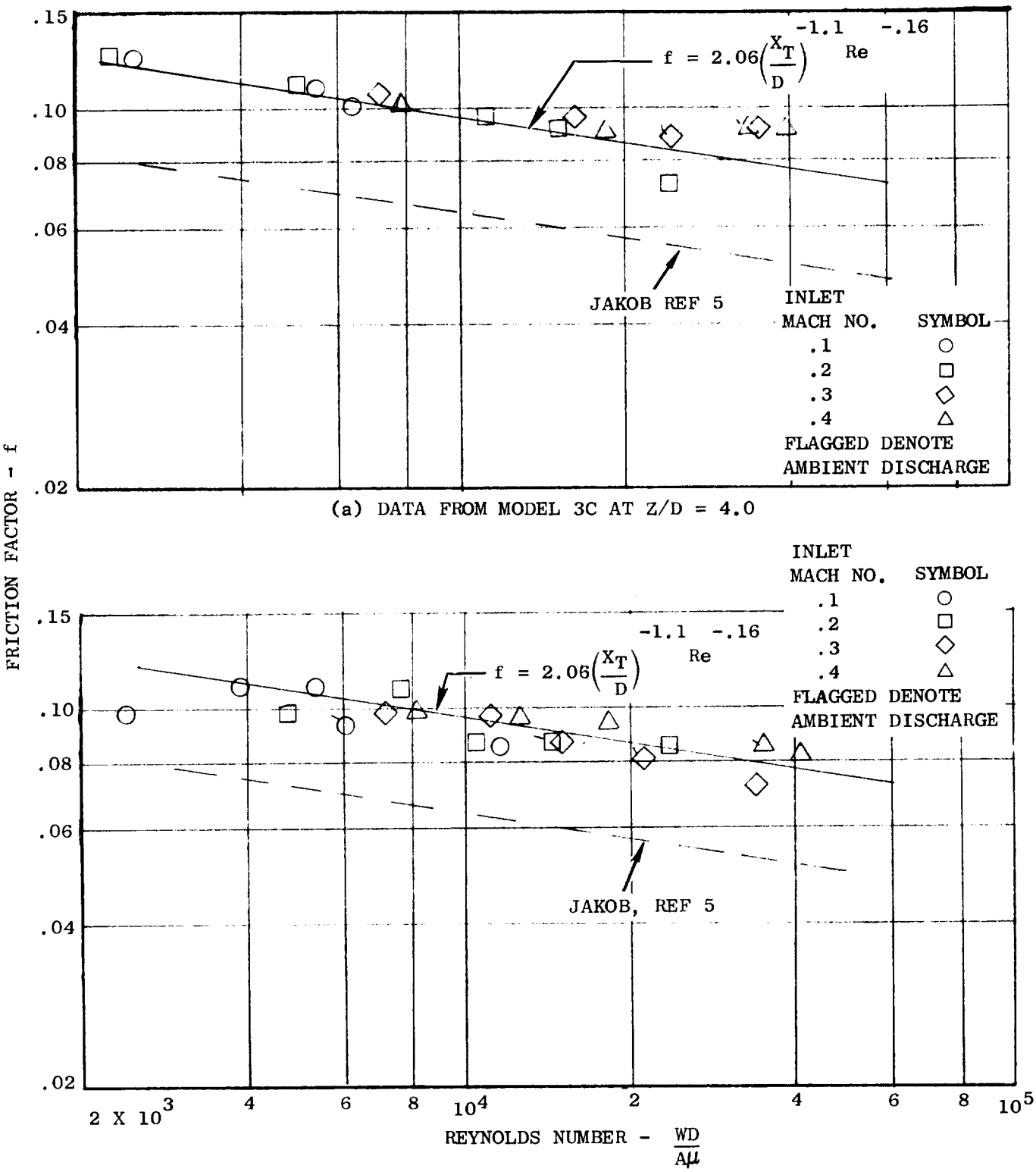

(a) DATA FROM MODEL 3C AT Z/D = 4.0

(b) DATA FROM MODEL 3B AT Z/D = 2.0

Figure 28 Pin Fin Friction Factor as a Function of Pin Reynold's Number at $X_D/D = 3.0$

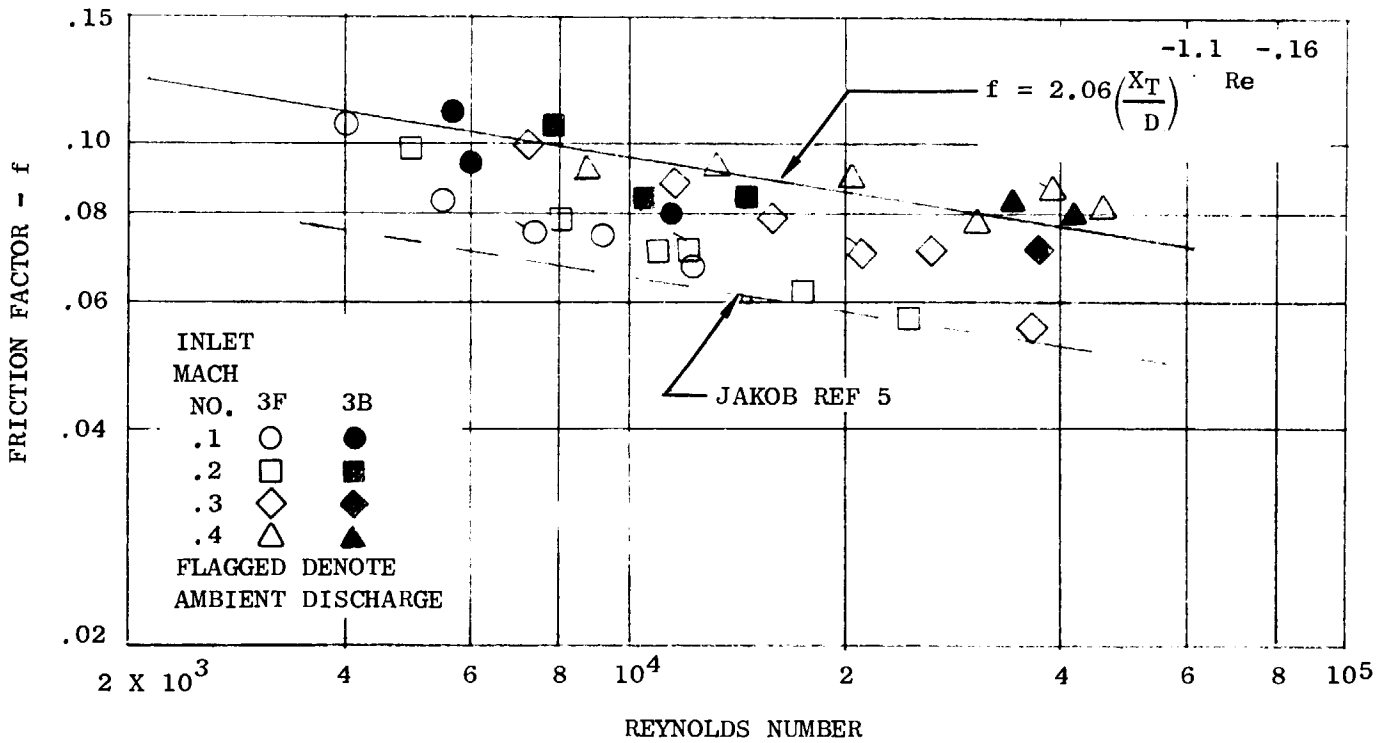

Figure 29 Pin Fin Friction Factor as a Function of Pin Reynolds Number for Model 3F at $X_D/D = 3.0$, $Z/D = 2.0$

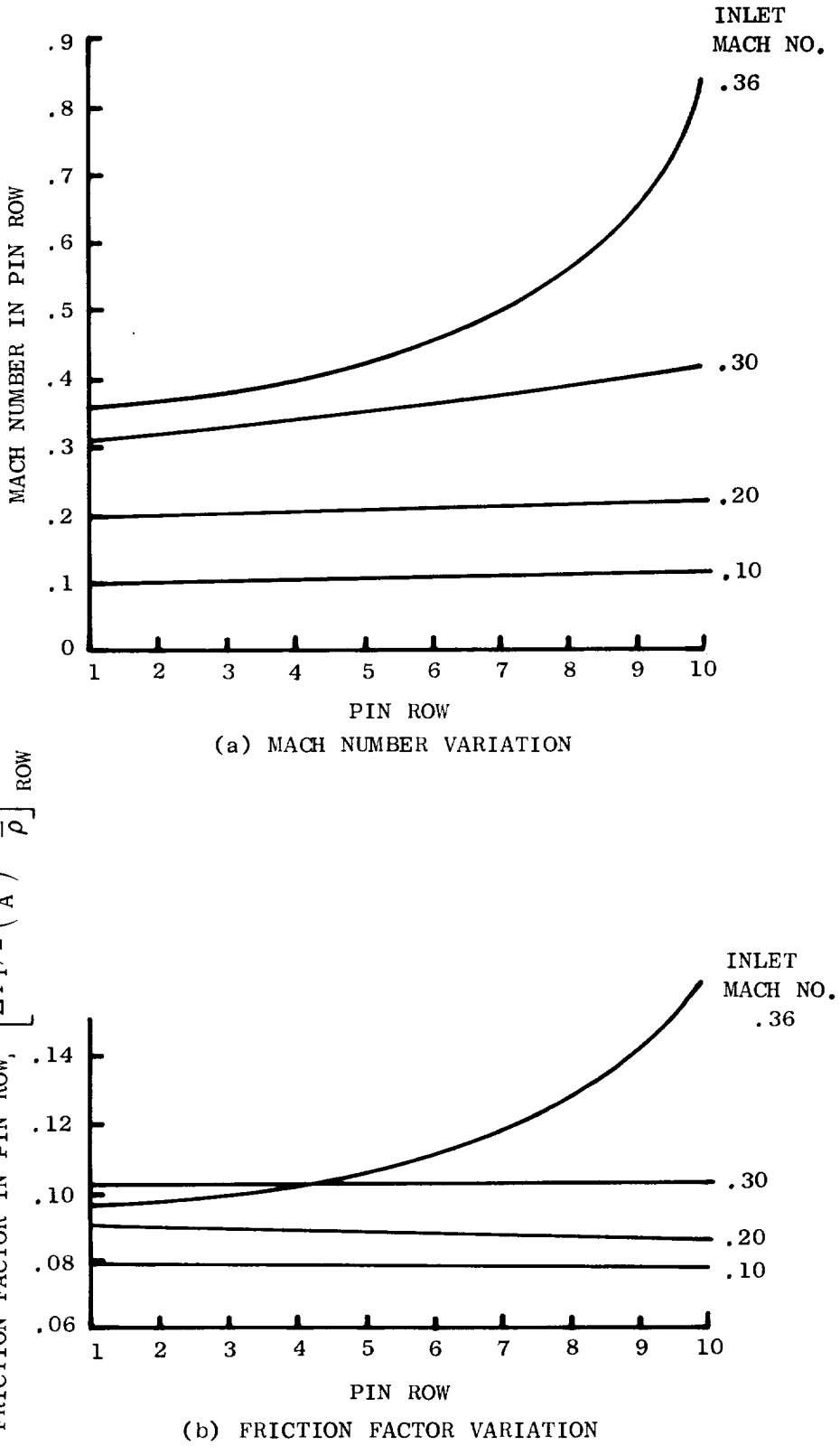

Figure 30 Variation of Mach Number and Friction Factor Through Model 3B, $X_D/D = 3.0$, $Z/D = 2.0$

Figures 31(a), (b) and (c) show the effect of flow split, spacing ratio and the two feeder tube configurations upon average discharge coefficient as a function of the inlet Mach number in the feeder tube. By comparing the solid and open symbols in Figure 31(a), the effect of the ratio of the exhaust flows is seen to be negligible. Figure 31(b) shows that the effect of the ratio of orifice to impinged wall spacing-to-hole diameter (Z/D) is small for the two ratios tested (Z/D = 3.0 and 5.0). On the leading edge impingement model a small effect due to spacing was noted which would have an effect of about 3% on the feeder tube configuration and could not be detected. Figure 31(c) compares the feeder tube with and without the individual flow collectors. Similar average discharge coefficients were calculated and it was concluded that removing the impingement wall and adding individual collector plenums did not change the orifice flow characteristics.

To compare the feeder tube discharge coefficients with those of the leading edge model, the average discharge coefficient based on inlet static pressure has been plotted and correlated as a function of average orifice Mach number on Figure 32. This figure also shows the correlation for the leading edge model at Z/D = 5.0. The Mach number effect is seen to be similar to that of the leading edge model with a level reduction of about 20% due to the back-side velocity.

$$C_D = .69\ M^{.057} \tag{19}$$

The feeder tube discharge coefficients shown on the previous figures were calculated using the upstream static pressure as the total pressure in equations 2 and 3, which is the usual procedure when the flow is normal to the axis of the hole. However, to compare the feeder tube data to the results presented in Reference 3, discharge coefficients were calculated using the total pressure obtained from the local measured static pressure flow rate and area. Reference 3 presented data for flow perpendicular to the axis of a single orifice. By using the data for model 1 of Reference 3, which had a wall thickness-to-orifice diameter ratio (t/D) of 0.51, comparisons were made for the feeder tube model with a t/D = 0.66. Figures 33(a) and (b) show the discharge coefficient as a function of velocity head ratio, which is the ratio of total-to-static pressure difference across the hole to the total-to-static pressure difference in the feeder tube upstream of the hole, for constant and variable collector pressure, respectively. Data for the five collector plenums and two feeder tube inlet Mach numbers, along with the single hole data taken from Reference 3, have the same trend. This trend can be seen by comparing the open and closed symbols with the curves of Reference 3 for related duct Mach numbers. Because the feeder tube Mach number is decreasing along the passage, the higher Mach number data shown moved toward the lower Mach number data as the collector number increased. The above agreement gives some assurance that single orifice data can be used in multiple orifice configurations.

For the variable pressure distribution, good agreement was obtained for the first three collectors; however, the fourth and fifth collectors exhibited large scatter because of the low flow rates and pressure drops and is not believed to be valid.

Figures 34 and 35 show typical pressure distributions from the feeder tube tests. These results were obtained from the second feeder tube configuration which had the individual flow collectors for every four holes. Figure 34 is for a feeder tube Mach number of 0.10, while Figure 35 is for a higher Mach number of 0.28. Both pressure distributions were similar, with equation 12 predicting a slightly higher static pressure rise. The flow was lowest in the first plenum, increased in the second plenum and remained constant in the last three plenums, reflecting the static pressure shown. Feeder tube downstream static pressures below that predicted could be due to poor diffusion and increased friction, however, this has little effect on orifice flow since these losses are small compared to the overall pressure drop.

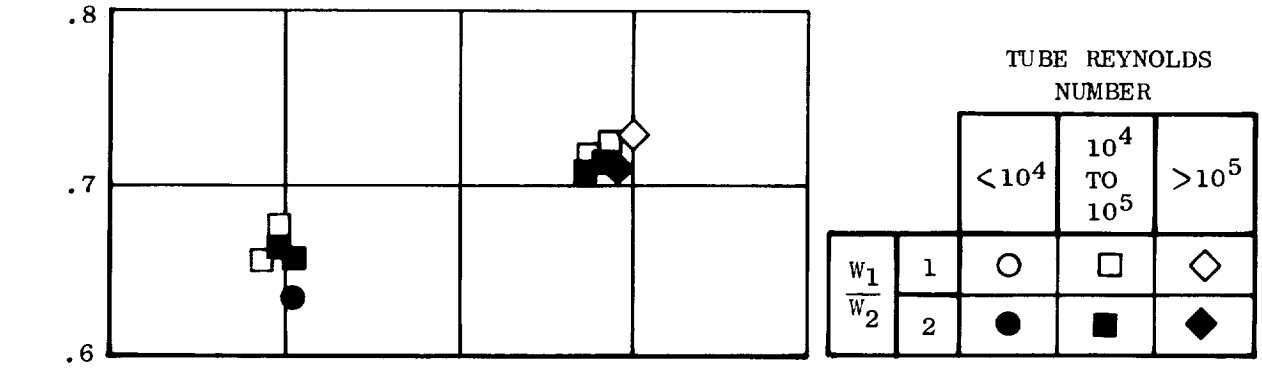

(a) EFFECT OF FLOW SPLIT AT Z/D = 5.0

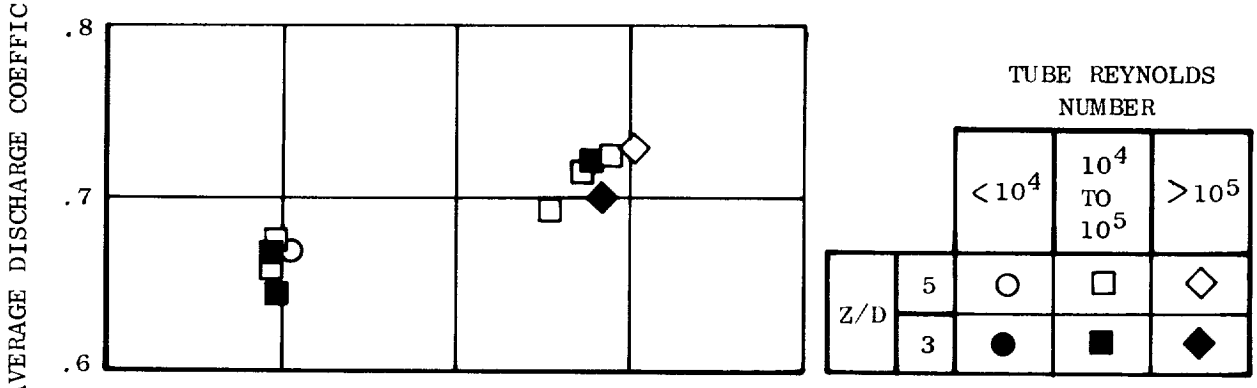

(b) EFFECT OF LEADING EDGE SPACING (Z/D) AT $W_1/W_2 = 2.0$

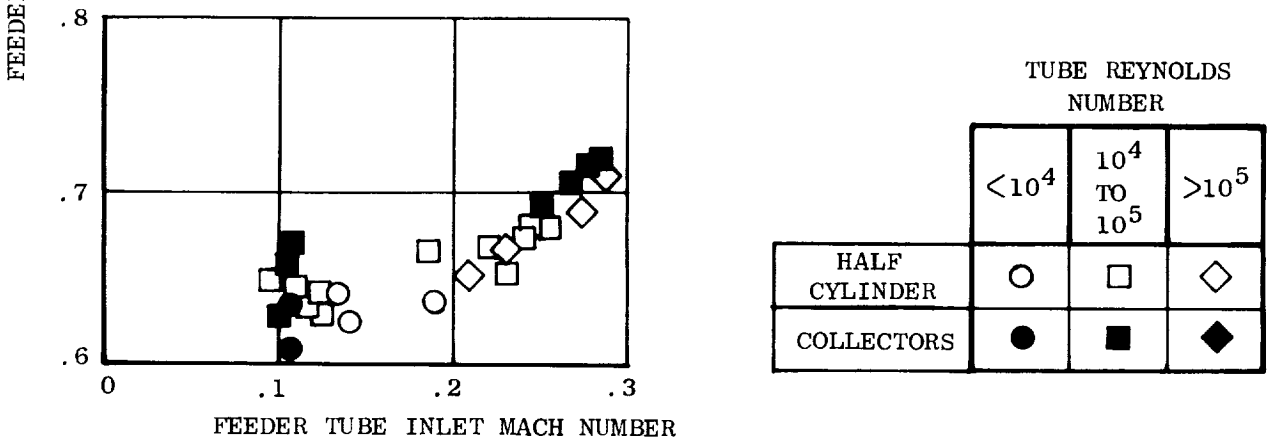

(c) DISCHARGE INTO A HALF-CYLINDER COMPARED TO DISCHARGE INTO COLLECTORS

Figure 31 Effect of Downstream Conditions on Feeder Tube Average Discharge Coefficient

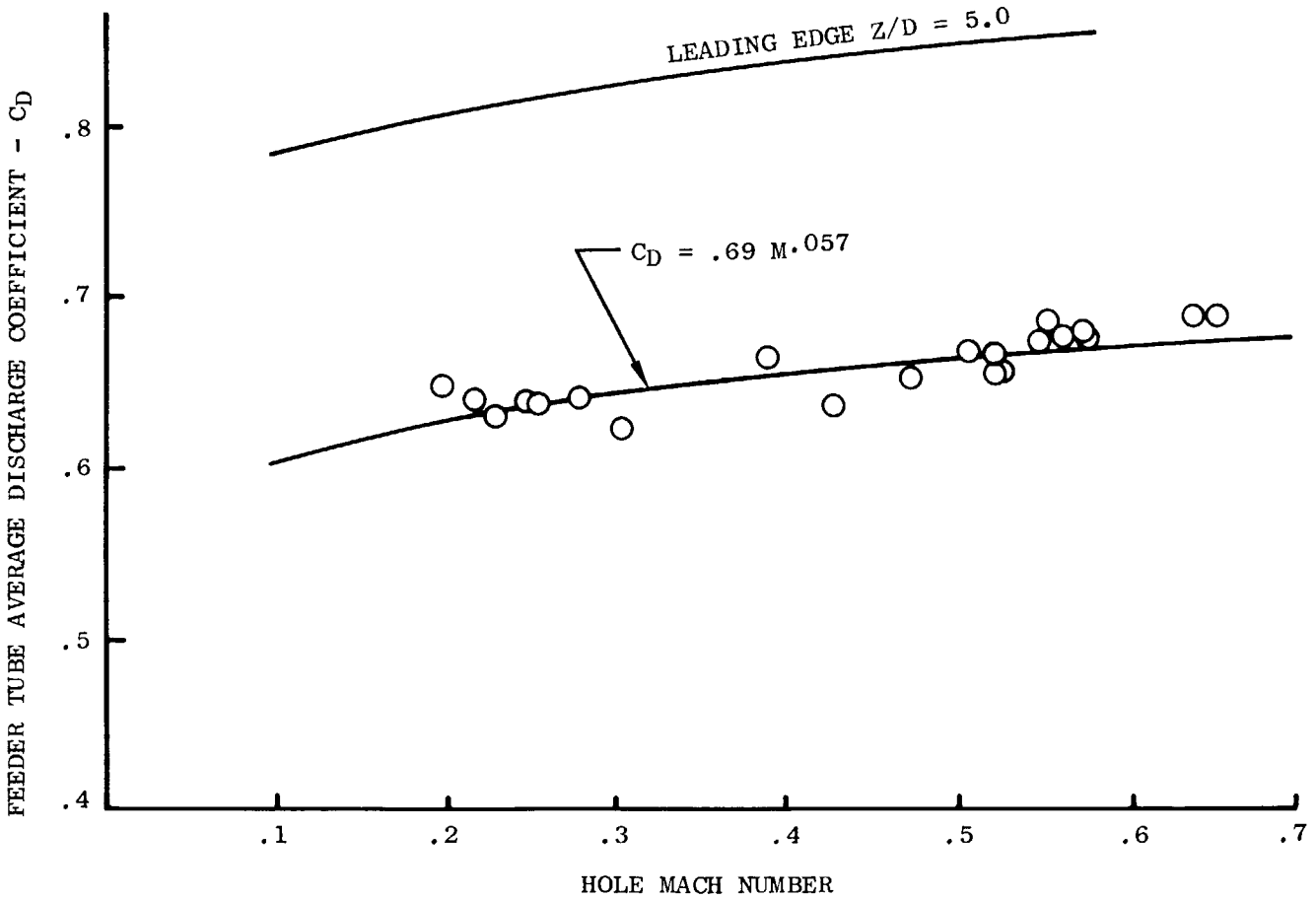

Figure 32 Feeder Tube Average Discharge Coefficient as a Function of Hole Mach Number with Constant Discharge Pressure

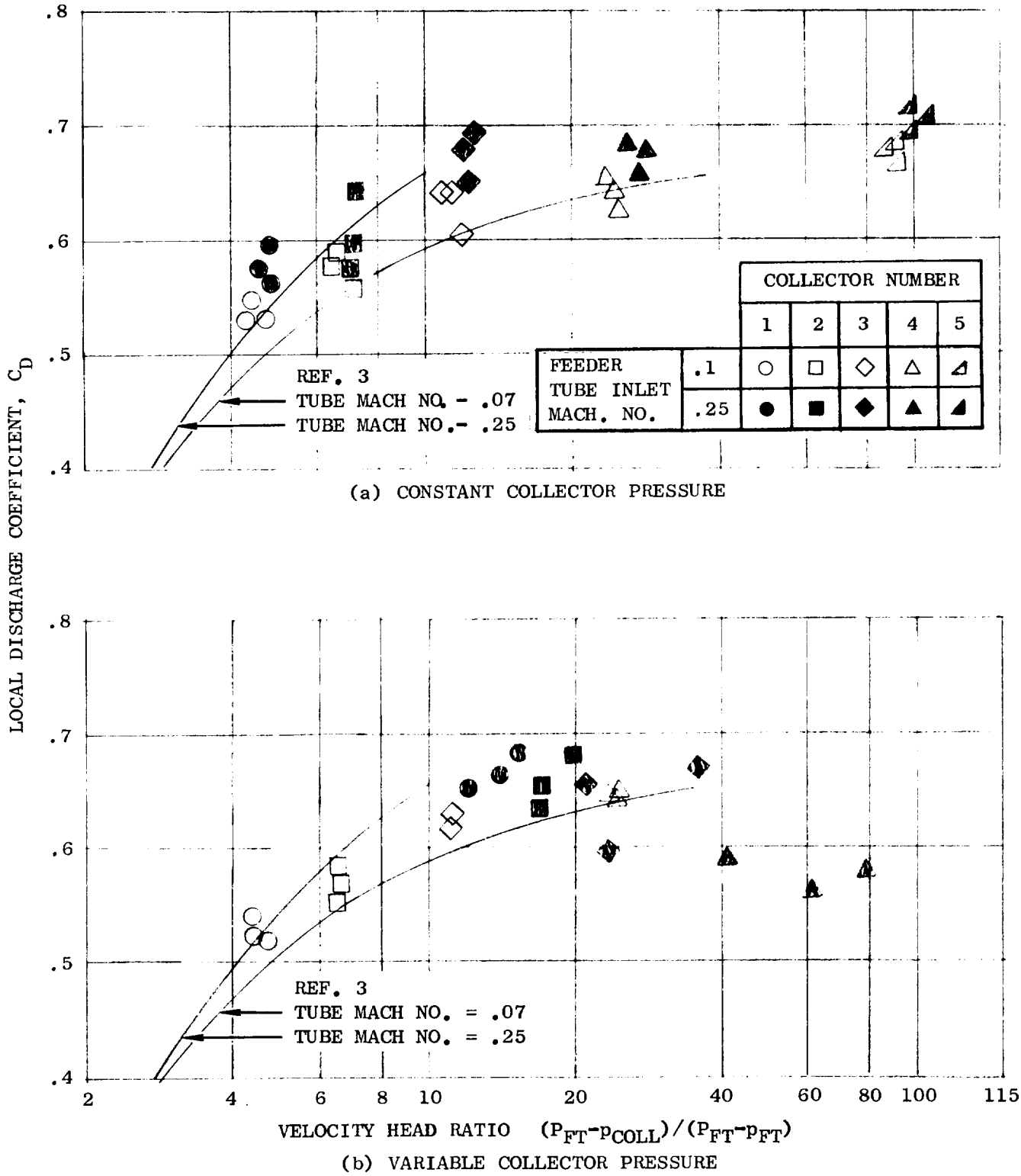

Figure 33 Effect of Velocity Head Ratio and Feeder Tube Mach Number on Orifice Discharge Coefficient For Individual Collectors

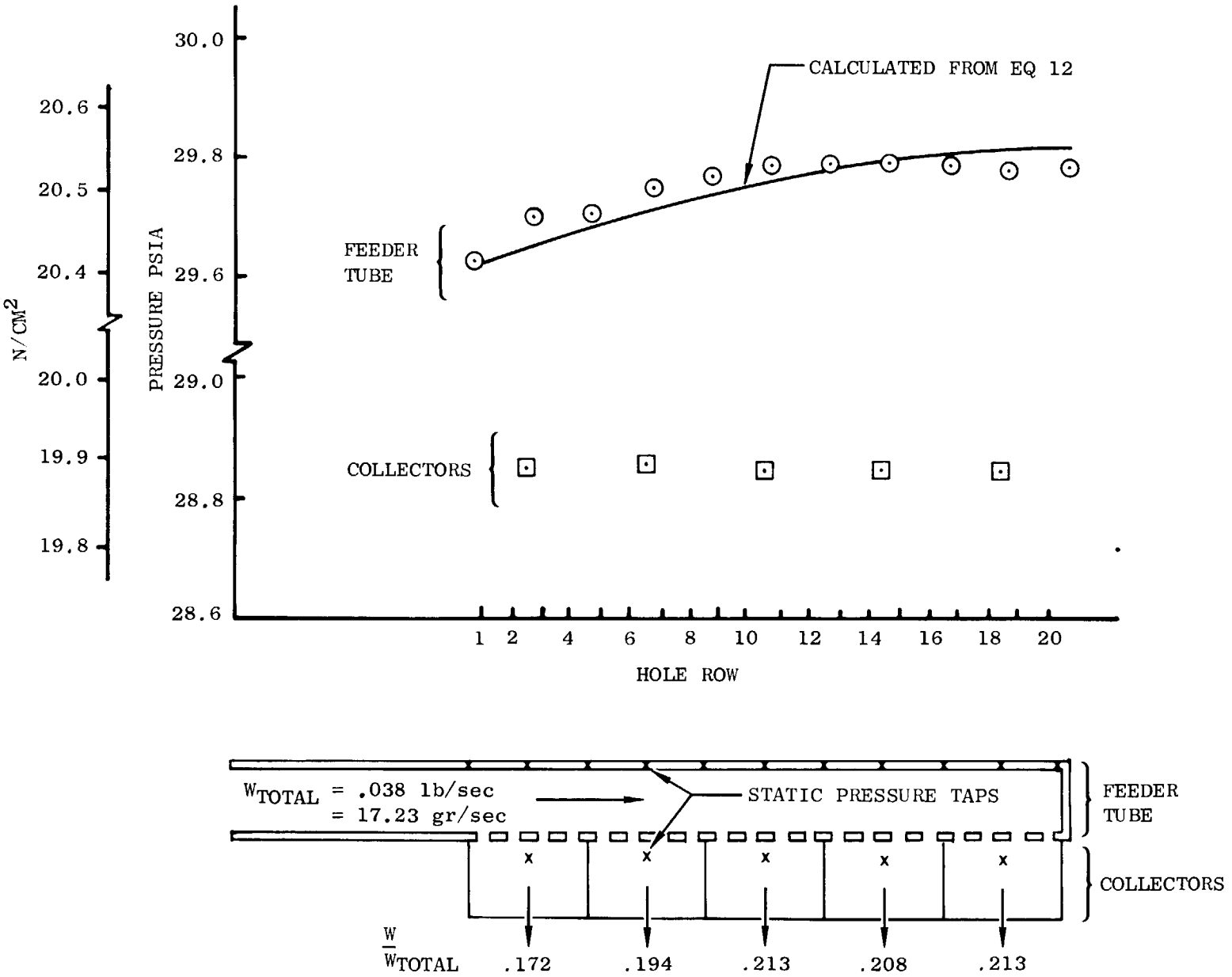

Figure 34 Pressure Distribution Along Feeder Tube Compared to Prediction for Inlet Mach Number of 0.1

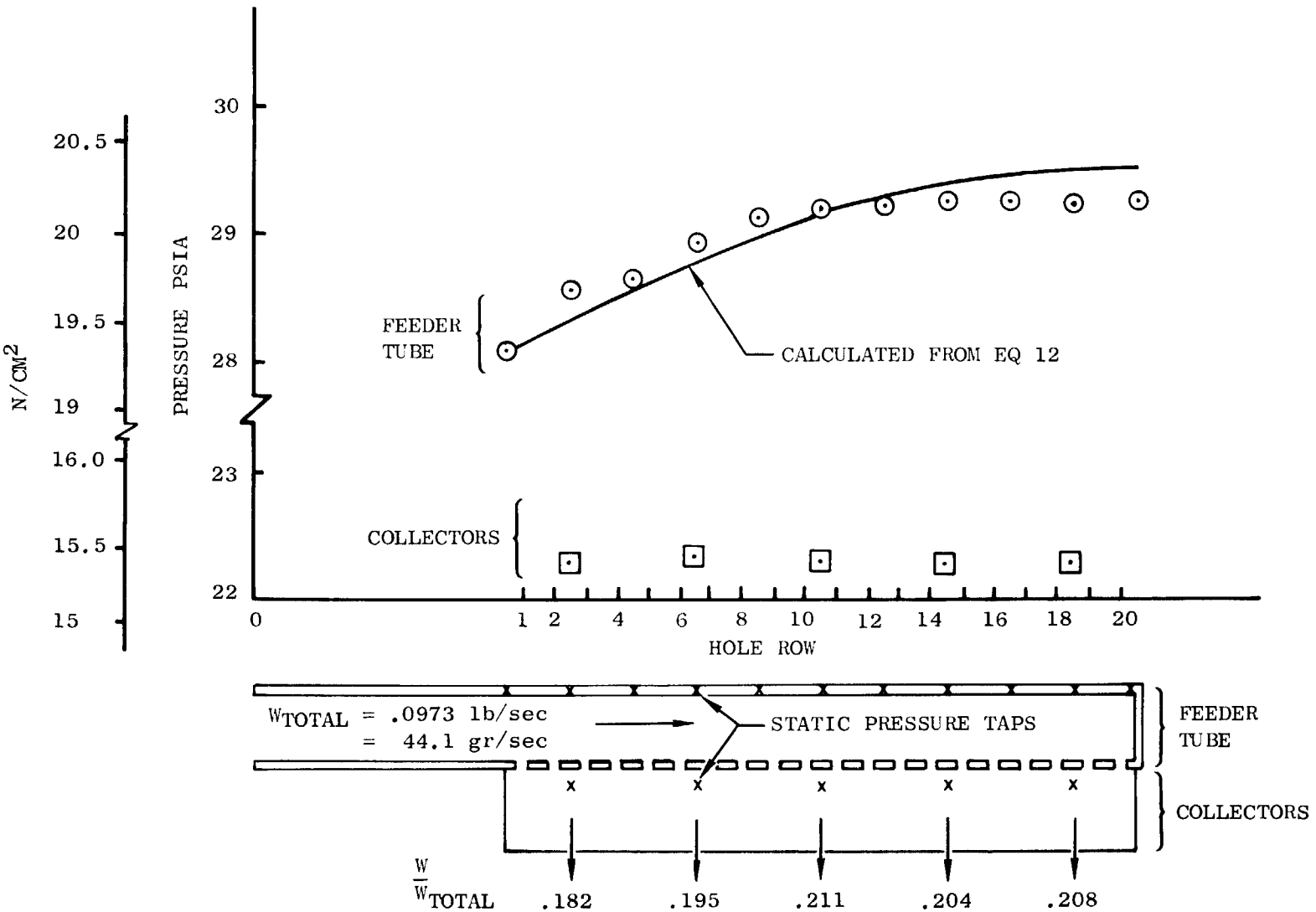

Figure 35 Pressure Distribution Along Feeder Tube Compared to Prediction for Inlet Mach Number of .25

Composite Model Results

The composite model test data have been used to compare measured and calculated flows obtained from a flow network computer program using the correlations previously obtained.

Table I shows the results from the 27 test points of the composite model. Figure 36 indicates static pressure tap locations on the model to be used in conjunction with Table I. A one-dimensional flow model, simulating the composite model, was used to compare the first two test points (points 3 and 9) shown in Table I. The two pressure distributions are similar with small chordwise pressure distribution in the feeder tube and with the trailing edge having a larger pressure drop than the midchord region. For these tests the leading edge flow was set at 50% of the trailing edge flow.

The flow model consisted of one external source pressure, simulating the feeder tube supply pressure, and three external sink pressures, which were the two leading edge and the one trailing edge pressures. Intermediate internal pressures were located along the impingement cross flow passage and through the pin fin passage. The flow model was run on the Compressible Flow Network Analysis (CFNA) computer program using external pressures obtained from the test data. The external pressures were the spanwise and chordwise average of the pressure taps located within the model supply and discharge plenums. Figure 36(b) shows the computer program representation.

The computer program calculated the flow and internal pressures using the leading edge correlation (Equation 14), a midchord discharge coefficient of 0.78 (Equation 16) and the pin fin correlation (Equation 18).

For the low Mach number case (see point 3 of Table I), the calculated trailing edge flow is 6% lower than measured, while the calculated leading edge flow is 17% higher. For the higher Mach number case (see point 9 of Table I), the calculated trailing edge flow is 7% higher than measured and the calculated leading edge flow is 13% higher. Calculated flows reflect both the adequacy of the computer program and the data correlations. No attempt has been made to separate these effects.

Concluding Remarks

This investigation of flow distribution characteristics of turbine airfoil cooling systems has led to the following general conclusions:

1. Leading edge impingement discharge coefficients are influenced by orifice Mach number and by orifice to impinged wall spacing-to-hole diameter, but not by Reynolds number or flow split.

2. Orifice discharge coefficients for the impingement with crossflow model were found to be constant, i.e., independent of impinged wall to jet spacing, Reynolds number and crossflow rate. Pressure drop in the crossflow passage is reasonably predicted by a simple one-dimensional momentum balance.

3. Feeder tube orifice discharge coefficients are correlated as a function of the orifice velocity-to-feeder tube velocity. Pressure drop in the feeder tube is reasonably predicted by a simple one-dimensional momentum balance.

4. Pin fin friction factors were found to be a function of pin Reynolds number and pin spacing and to be independent of passage height and Mach number.

5. Using the results of component pressure loss tests in the Compressible Flow Network Analysis Computer Program permits prediction of the flow characteristics of complex airfoil cooling systems which incorporate the components tested.

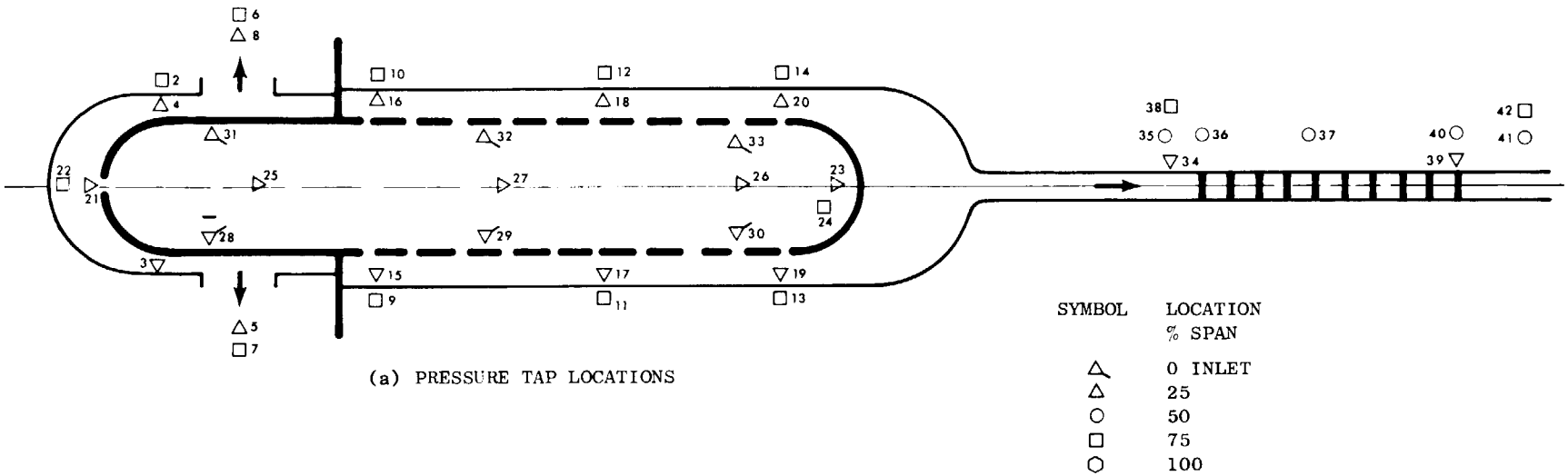

(a) PRESSURE TAP LOCATIONS

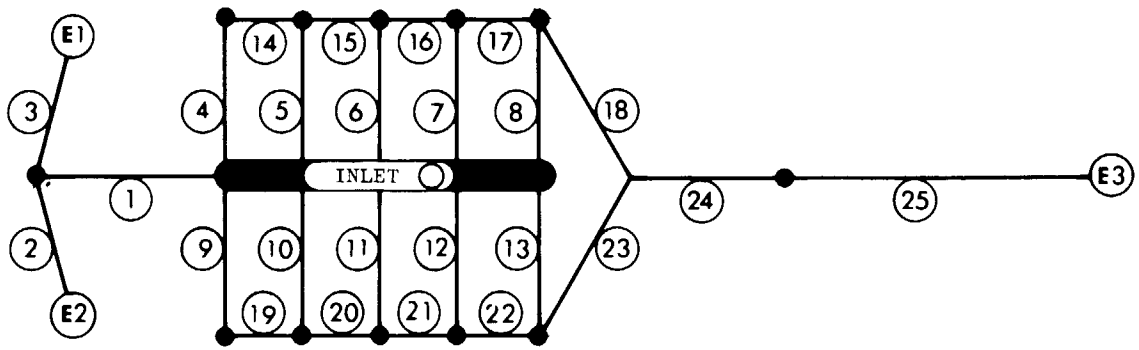

(b) COMPUTER PROGRAM BRANCH NETWORK

Figure 36 Composite Model Pressure Tap Locations to be Used in Conjunction With Table I and Computer Program Branch Network

TABLE I

COMPOSITE MODEL - PRESSURE RATIOS RELATIVE TO INLET (29)
(Figure 36 Gives Pressure Tap Locations)
(Calculated Values in Parenthesis)

TEST POINT

3. TR EG FLOW (LBS/SEC) = 0.15549 (.1465) M. C. MACH NO. = 0.108
TR EG FLOW (GR/SEC) = 70.53 (66.45) M. C. REY. NO. = 9858.6
INLET PRESS (PSIA) = 31.640 FLOW SPLIT (L. E.) = 0.972 (1.0)
INLET PRESS (N/CM^2) = 21.82 FLOW SPLIT (L. E./T. E.) = .452

TAP							
No. 1 =	1.030	1.030	1.030 (1.031)	1.030 (1.031)	1.031	1.031	1.031
No. 8 =	1.031	-----	-----	1.015	1.016	1.016	1.016
No. 15 =	1.015 (1.0123)	1.015 (1.0123)	1.008 (1.0126)	1.012 (1.0126)	1.012 (1.0133)	1.015 (1.0133)	1.031
No. 22 =	1.030	0.999	0.999	0.998	0.998	0.998	0.960
No. 29 =	1.000	1.000	1.000	1.001	1.001	1.022 (1.0199)	1.020
No. 36 =	1.024	1.032	1.021	1.042 (1.041)	1.040	1.039	1.040

9. TR EG FLOW (LBS/SEC) = 0.43210 (.454) M. C. MACH NO. = 0.302
TR EG FLOW (GR/SEC) = 196 (205.5) M. C. REY. NO. = 26720.1
INLET PRESS (PSIA) = 31.751 FLOW SPLIT (L. E.) = 0.988 (1.0)
INLET PRESS (N/CM^2) = 21.89 FLOW SPLIT (L. E./T. E.) = .470 (.469)

TAP							
No. 1 =	1.406	1.405	1.409 (1.414)	1.400 (1.414)	1.423	1.423	1.423
No. 8 =	1.425	-----	-----	1.190	1.192	1.201	1.201
No. 15 =	1.177 (1.151)	1.182 (1.151)	1.101 (1.156)	1.147 (1.156)	1.166 (1.160)	1.193 (1.160)	1.422
No. 22 =	1.420	0.993	0.992	0.989	0.986	0.986	0.678
No. 29 =	1.000	0.998	1.002	1.005	1.002	1.281	1.257
No. 36 =	1.318	1.533	1.269	2.212 (2.303)	2.254	2.235	2.27

1. TR EG FLOW (LBS/SEC) = 0.01179 M. C. MACH NO. = 0.118
TR EG FLOW (GR/SEC) = 5.35 M. C. REY. NO. = 736.4
INLET PRESS (PSIA) = 2.225 FLOW SPLIT (L. E.) = 0.859
INLET PRESS (N/CM^2) = 1.53 FLOW SPLIT (L. E./T. E.) = 0.784

TAP							
No. 1 =	1.027	1.028	1.027	1.027	1.027	1.030	1.028
No. 8 =	1.028	-----	-----	1.035	1.035	1.037	1.037
No. 15 =	1.035	1.039	1.032	1.035	1.030	1.040	1.022
No. 22 =	1.020	1.003	0.997	0.998	0.998	0.998	0.498
No. 29 =	1.000	1.000	1.000	1.000	1.000	1.040	1.042
No. 36 =	1.042	1.055	1.039	1.071	1.075	1.084	1.084

TABLE I (Cont.)

TEST POINT

2. TR EG FLOW (LBS/SEC) = 0.07464 — M. C. MACH NO. = 0.115
TR EG FLOW (GR/SEC) = 33.85 — M. C. REY. NO. = 4666.8
INLET PRESS (PSIA) = 14.400 — FLOW SPLIT (L. E.) = 1.027
INLET PRESS (N/MC^2) = 9.93 — FLOW SPLIT (L. E./T. E.) = .427

TAP							
No. 1 =	1.026	1.026	1.026	1.026	1.026	1.026	1.026
No. 8 =	1.027	-----	-----	1.019	1.019	1.020	1.020
No. 15 =	1.018	1.018	1.008	1.016	1.013	1.020	1.027
No. 22 =	1.026	0.999	0.998	0.998	0.998	0.998	0.956
No. 29 =	1.000	0.999	0.999	1.000	0.999	1.025	1.024
No. 36 =	1.028	1.037	1.025	1.049	1.049	1.049	1.050

2R. TR EG FLOW (LBS/SEC) = 0.06702 — M. C. MACH NO. = 0.103
TR EG FLOW (GR/SEC) = 30.4 — M. C. REY. NO. = 4213.6
INLET PRESS (PSIA) = 14.338 — FLOW SPLIT (L. E.) = 1.000
INLET PRESS (N/CM^2) = 9.89 — FLOW SPLIT (L. E./T. E.) = .414

TAP							
No. 1 =	1.018	1.018	1.018	1.019	1.019	1.019	1.019
No. 8 =	1.019	-----	-----	1.015	1.015	1.016	1.016
No. 15 =	1.014	1.014	1.007	1.012	1.011	1.015	1.019
No. 22 =	1.019	0.999	0.999	0.998	0.998	0.998	0.968
No. 29 =	1.000	1.000	1.000	1.000	1.000	1.020	1.019
No. 36 =	1.022	1.029	1.019	1.038	1.039	1.037	1.038

4. TR EG FLOW (LBS/SEC) = 0.03096 — M. C. MACH NO. = 0.325
TR EG FLOW (GE/SEC) = 14.04 — M. C. REY. NO. = 1932.9
INLET PRESS (PSIA) = 2.097 — FLOW SPLIT (L. E.) = 0.846
INLET PRESS (N/CM^2) = 1.45 — FLOW SPLIT (L. E./T. E.) = .294

TAP							
No. 1 =	1.007	1.009	1.007	1.009	1.007	1.010	1.007
No. 8 =	1.010	-----	-----	1.181	1.176	1.188	1.190
No. 15 =	1.171	1.169	1.092	1.150	1.128	1.183	1.012
No. 22 =	1.012	0.995	0.993	0.993	0.991	0.993	0.475
No. 29 =	1.000	0.998	0.998	1.002	1.002	1.271	1.252
No. 36 =	1.296	1.500	1.265	1.872	1.860	1.854	1.866

5. TR EG FLOW (LBS/SEC) = 0.13050 — M. C. MACH NO. = 0.202
TR EG FLOW (GR/SEC) = 59.2 — M. C. REY. NO. = 8204.7
INLET PRESS (PSIA) = 14.219 — FLOW SPLIT (L. E.) = 0.895
INLET PRESS (N/CM^2) = 9.81 — FLOW SPLIT (L. E./T. E.) = .417

TAP							
No. 1 =	1.089	1.090	1.090	1.090	1.093	1.094	1.092
No. 8 =	1.094	-----	-----	1.059	1.060	1.062	1.062
No. 15 =	1.056	1.057	1.025	1.046	1.046	1.063	1.094
No. 22 =	1.093	0.996	0.993	0.992	0.992	0.992	0.962
No. 29 =	1.000	0.999	0.999	1.000	0.999	1.082	1.079
No. 36 =	1.093	1.141	1.078	1.187	1.194	1.184	1.188

TABLE I (Cont.)

TEST POINT

5R. TR EG FLOW (LBS/SEC) = 0.13585
TR EG FLOW (GR/SEC) = 61.62
INLET PRESS (PSIA) = 14.292
INLET PRESS (N/CM^2) = 9.85
M. C. MACH NO. = 0.209
M. C. REY. NO. = 8588.9
FLOW SPLIT (L. E.) = 0.993
FLOW SPLIT (L. E./T. E.) = .449

TAP							
No. 1 =	1.109	1.109	1.109	1.094	1.118	1.114	1.118
No. 8 =	1.113	-----	-----	1.069	1.072	1.075	1.074
No. 15 =	1.067	1.068	1.031	1.055	1.059	1.072	1.113
No. 22 =	1.111	0.997	0.996	0.994	0.994	0.994	0.951
No. 29 =	1.000	0.999	1.000	1.001	1.000	1.095	1.090
No. 36 =	1.107	1.153	1.094	1.216	1.220	1.222	1.220

6. TR EG FLOW (LBS/SEC) = 0.29696
TR EG FLOW (GR/SEC) = 134.7
INLET PRESS (PSIA) = 31.48
INLET PRESS (N/CM^2) = 21.71
M. C. MACH NO. = 0.210
M. C. REY. NO. = 18388.6
FLOW SPLIT (L. E.) = 0.997
FLOW SPLIT (L. E./T. E.) = .476

TAP							
No. 1 =	1.139	1.139	1.140	1.138	1.143	1.143	1.143
No. 8 =	1.143	-----	-----	1.073	1.073	1.076	1.074
No. 15 =	1.067	1.069	1.040	1.060	1.065	1.073	1.143
No. 22 =	1.142	0.998	0.996	0.994	0.994	0.994	0.677
No. 29 =	1.000	0.999	1.002	1.003	1.002	1.095	1.089
No. 36 =	1.104	1.150	1.095	1.206	1.212	1.206	1.208

7. TR EG FLOW (LBS/SEC) = 0.04041
TR EG FLOW (GR/SEC) = 18.32
INLET PRESS (PSIA) = 3.467
INLET PRESS (N/CM^2) = 2.39
M. C. MACH NO. = 0.257
M. C. REY. NO. = 2523.2
FLOW SPLIT (L. E.) = 0.320
FLOW SPLIT (L. E./T. E.) = .442

TAP							
No. 1 =	1.062	1.069	1.062	1.068	1.061	1.076	1.062
No. 8 =	1.076	-----	-----	1.110	1.108	1.115	1.116
No. 15 =	1.104	1.106	1.055	1.089	1.078	1.112	1.071
No. 22 =	1.070	1.000	0.999	0.994	0.991	0.992	0.606
No. 29 =	1.000	0.999	0.999	1.001	1.000	1.152	1.147
No. 36 =	1.172	1.258	1.155	1.396	1.404	1.398	1.402

7R. TR EG FLOW (LBS/SEC) = 0.04254
TR EG FLOW (GR/SEC) = 19.3
INLET PRESS (PSIA) = 3.097
INLET PRESS (N/CM^2) = 2.135
M. C. MACH NO. = 0.299
M. C. REY. NO. = 2712.3
FLOW SPLIT (L. E.) = 1.014
FLOW SPLIT (L. E./T. E.) = .442

TAP							
No. 1 =	1.294	1.302	1.302	1.297	1.311	1.311	1.302
No. 8 =	1.316	-----	-----	1.166	1.159	1.174	1.170
No. 15 =	1.153	1.149	1.090	1.124	1.118	1.166	1.302
No. 22 =	1.302	0.995	0.995	0.988	0.988	0.988	0.171
No. 29 =	1.000	0.995	1.000	1.000	1.000	1.239	1.227
No. 36 =	1.263	1.442	1.234	1.856	1.884	1.901	1.924

TABLE I (Cont.)

TEST POINT

8. TR EG FLOW (LBS/SEC) = 0.19406
TR EG FLOW (GR/SEC) = 88.0
INLET PRESS (PSIA) = 13.696
INLET PRESS (N/CM^2) = 9.44
M. C. MACH NO. = 0.306
M. C. REY. NO. = 12481.2
FLOW SPLIT (L. E.) = 1.054
FLOW SPLIT (L. E./T. E.) = .455

TAP							
No. 1 =	1.444	1.440	1.447	1.436	1.462	1.455	1.455
No. 8 =	1.455	-----	-----	1.194	1.194	1.204	1.202
No. 15 =	1.179	1.179	1.179	1.152	1.157	1.199	1.455
No. 22 =	1.447	0.988	0.986	0.981	0.979	0.981	0.478
No. 29 =	1.000	0.998	1.037	1.004	1.000	1.287	1.264
No. 36 =	1.337	1.605	1.282	3.079	3.503	4.092	4.286

10. TR EG FLOW (LBS/SEC) = 0.01092
TR EG FLOW (GR/SEC) = 4.95
INLET PRESS (PSIA) = 2.140
INLET PRESS (N/CM^2) = 1.475
M. C. MACH NO. = 0.113
M. C. REY. NO. = 682.0
FLOW SPLIT (L. E.) = 1.460
FLOW SPLIT (L. E./T. E.) = .900

TAP							
No. 1 =	1.051	1.051	1.051	1.051	1.053	1.049	1.049
No. 8 =	1.049	-----	-----	1.031	1.031	1.033	1.033
No. 15 =	1.029	1.035	1.028	1.029	1.022	1.033	1.037
No. 22 =	1.035	1.000	0.998	0.998	0.997	0.997	0.484
No. 29 =	1.000	1.000	0.998	0.998	0.998	1.031	1.031
No. 36 =	1.033	1.042	1.029	1.057	1.059	1.074	1.074

11. TR EG FLOW (LBS/SEC) = 0.07252
TR EG FLOW (GR/SEC) = 32.9
INLET PRESS (PSIA) = 14.396
INLET PRESS (N/CM^2) = 9.93
M. C. MACH NO. = 0.112
M. C. REY. NO. = 4515.2
FLOW SPLIT (L. E.) = 1.696
FLOW SPLIT (L. E./T. E.) = .458

TAP							
No. 1 =	1.028	1.028	1.029	1.028	1.029	1.028	1.030
No. 8 =	1.028	-----	-----	1.018	1.018	1.019	1.019
No. 15 =	1.017	1.017	1.008	1.015	1.013	1.019	1.029
No. 22 =	1.029	0.999	0.998	0.998	0.998	0.998	0.955
No. 29 =	1.000	0.999	0.999	1.000	1.000	1.025	1.023
No. 36 =	1.027	1.036	1.024	1.046	1.046	1.046	1.046

12. TR EG FLOW (LBS/SEC) = 0.15505
TR EG FLOW (GR/SEC) = 70.33
INLET PRESS (PSIA) = 31.860
INLET PRESS (N/MC^2) = 21.97
M. C. MACH NO. = 0.107
M. C. REY. NO. = 9830.5
FLOW SPLIT (L. E.) = 1.697
FLOW SPLIT (L. E./T. E.) = .470

TAP							
No. 1 =	1.029	1.029	1.029	1.029	1.031	1.029	1.031
No. 8 =	1.029	-----	-----	1.015	1.015	1.016	1.016
No. 15 =	1.015	1.015	1.007	1.012	1.012	1.015	1.031
No. 22 =	1.030	0.999	0.998	0.997	0.997	0.997	0.959
No. 29 =	1.000	0.999	1.000	1.000	1.000	1.021	1.020
No. 36 =	1.023	1.032	1.020	1.041	1.040	1.038	1.039

TABLE I (Cont.)

TEST POINT

13. TR EG FLOW (LBS/SEC) = 0.02595
TR EG FLOW (GR/SEC) = 11.77
INLET PRESS (PSIA) = 2.242
INLET PRESS (N/CM^2) = 1.55
M. C. MACH NO. = 0.256
M. C. REY. NO. = 1620.2
FLOW SPLIT (L. E.) = 0.444
FLOW SPLIT (L. E./T. E.) = .538

TAP							
No. 1 =	1.056	1.063	1.056	1.063	1.056	1.072	1.060
No. 8 =	1.072	-----	-----	1.105	1.103	1.111	1.111
No. 15 =	1.099	1.103	1.058	1.091	1.074	1.113	1.069
No. 22 =	1.067	0.997	0.994	0.990	0.990	0.990	0.497
No. 29 =	1.000	0.998	0.998	1.000	0.998	1.143	1.139
No. 36 =	1.158	1.247	1.146	1.370	1.367	1.373	1.376

14. TR EG FLOW (LBS/SEC) = 0.13586
TR EG FLOW (GR/SEC) = 61.63
INLET PRESS (PSIA) = 14.201
INLET PRESS (N/CM^2) = 9.79
M. C. MACH NO. = 0.210
M. C. REY. NO. = 8577.9
FLOW SPLIT (L. E.) = 1.995
FLOW SPLIT (L. E./T. E.) = .450

TAP							
No. 1 =	1.112	1.107	1.112	1.106	1.117	1.109	1.116
No. 8 =	1.109	-----	-----	1.067	1.070	1.072	1.072
No. 15 =	1.064	1.065	1.028	1.053	1.057	1.071	1.113
No. 22 =	1.111	0.995	0.993	0.991	0.991	0.991	0.949
No. 29 =	1.000	0.998	0.999	1.000	0.998	1.091	1.087
No. 36 =	1.103	1.148	1.091	1.209	1.215	1.211	1.213

15. TR EG FLOW (LBS/SEC) = 0.29854
TR EG FLOW (GR/SEC) = 135.4
INLET PRESS (PSIA) = 31.457
INLET PRESS (N/CM^2) = 21.69
M. C. MACH NO. = 0.211
M. C. REY. NO. = 18486.4
FLOW SPLIT (L. E.) = 2.124
FLOW SPLIT (L. E./T. E.) = .476

TAP							
No. 1 =	1.136	1.130	1.136	1.130	1.143	1.132	1.142
No. 8 =	1.132	-----	-----	1.068	1.069	1.072	1.071
No. 15 =	1.063	1.065	1.035	1.055	1.059	1.069	1.138
No. 22 =	1.137	0.993	0.992	0.991	0.991	0.992	0.675
No. 29 =	1.000	0.999	1.000	1.001	0.998	1.092	1.086
No. 36 =	1.105	1.148	1.093	1.200	1.203	1.199	1.200

16. TR EG FLOW (LBS/SEC) = 0.04292
TR EG FLOW (GR/SEC) = 19.5
INLET PRESS (PSIA) = 3.136
INLET PRESS (N/CM^2) = 2.16
M. C. MACH NO. = 0.298
M. C. REY. NO. = 2732.6
FLOW SPLIT (L. E.) = 2.377
FLOW SPLIT (L. E./T. E.) = .433

TAP							
No. 1 =	1.298	1.279	1.305	1.285	1.324	1.285	1.316
No. 8 =	1.298	-----	-----	1.163	1.157	1.172	1.168
No. 15 =	1.149	1.147	1.088	1.127	1.123	1.157	1.305
No. 22 =	1.298	0.995	0.995	0.988	0.985	0.985	0.173
No. 29 =	1.000	0.995	1.003	1.003	1.003	1.247	1.235
No. 36 =	1.279	1.444	1.223	1.863	1.863	1.837	1.863

TABLE I (Cont.)

TEST POINT

17. TR EG FLOW (LBS/SEC) = 0.19513 — M. C. MACH NO. = 0.309
TR EG FLOW (GR/SEC) = 88.51 — M. C. REY. NO. = 12514.0
INLET PRESS (PSIA) = 13.647 — FLOW SPLIT (L. E.) = 2.351
INLET PRESS (N/CM^2) = 9.411 — FLOW SPLIT (L. E./T. E.) = .459

TAP							
No. 1 =	1.395	1.371	1.395	1.368	1.422	1.371	1.416
No. 8 =	1.373	-----	-----	1.192	1.190	1.203	1.200
No. 15 =	1.177	1.177	1.084	1.151	1.155	1.192	1.395
No. 22 =	1.388	0.986	0.984	0.981	0.979	0.979	0.477
No. 29 =	1.000	0.998	1.000	1.002	0.998	1.286	1.263
No. 36 =	1.335	1.599	1.277	3.085	3.526	4.108	4.331

18. TR EG FLOW (LBS/SEC) = 0.43452 — M. C. MACH NO. = 0.304
TR EG FLOW (GR/SEC) = 197.1 — M. C. REY. NO. = 26906.3
INLET PRESS (PSIA) = 31.653 — FLOW SPLIT (L. E.) = 1.894
INLET PRESS (N/CM^2) = 21.83 — FLOW SPLIT (L. E./T. E.) = .466

TAP							
No. 1 =	1.567	1.533	1.567	1.528	1.610	1.544	1.610
No. 8 =	1.544	-----	-----	1.172	1.173	1.180	1.179
No. 15 =	1.156	1.161	1.098	1.134	1.151	1.172	1.569
No. 22 =	1.561	0.992	0.990	0.986	0.986	0.986	0.677
No. 29 =	1.000	0.998	1.002	1.005	1.002	1.249	1.230
No. 36 =	1.277	1.456	1.241	1.813	1.857	1.818	1.836

19. TR EG FLOW (LBS/SEC) = 0.00778 — M. C. MACH NO. = 0.088
TR EG FLOW (GR/SEC) = 3.53 — M. C. REY. NO. = 485.9
INLET PRESS (PSIA) = 1.972 — FLOW SPLIT (L. E.) = 0.980
INLET PRESS (N/CM^2) = 1.36 — FLOW SPLIT (L. E./T. E.) = 1.256

TAP							
No. 1 =	0.986	0.987	0.986	0.987	0.984	0.989	0.987
No. 8 =	0.989	-----	-----	1.002	1.002	1.004	1.004
No. 15 =	1.000	0.998	0.996	1.000	0.996	1.007	1.000
No. 22 =	1.000	0.987	0.991	0.991	0.993	0.993	0.450
No. 29 =	1.000	1.000	1.000	1.000	1.000	1.040	1.038
No. 36 =	1.046	1.060	1.044	1.079	1.081	1.083	1.083

20. TR EG FLOW (LBS/SEC) = 0.06898 — M. C. MACH NO. = 0.106
TR EG FLOW (GR/SEC) = 31.3 — M. C. REY. NO. = 4306.8
INLET PRESS (PSIA) = 14.400 — FLOW SPLIT (L. E.) = 0.968
INLET PRESS (N/CM^2) = 9.93 — FLOW SPLIT (L. E./T. E.) = .368

TAP							
No. 1 =	1.015	1.015	1.016	1.015	1.016	1.016	1.016
No. 8 =	1.016	-----	-----	1.016	1.016	1.017	1.017
No. 15 =	1.016	1.016	1.008	1.013	1.011	1.017	1.016
No. 22 =	1.015	0.999	0.999	0.999	0.999	0.999	0.956
No. 29 =	1.000	1.000	1.000	1.000	1.000	1.021	1.021
No. 36 =	1.024	1.031	1.021	1.039	1.040	1.041	1.041

TABLE I (Cont.)

TEST POINT

21. TR EG FLOW (LBS/SEC) = 0.14978
TR EG FLOW (GR/SEC) = 68.04
INLET PRESS (PSIA) = 31.923
INLET PRESS (N/CM^2) = 22.01
M. C. MACH NO. = 0.103
M. C. REY. NO. = 9470.2
FLOW SPLIT (L. E.) = 1.018
FLOW SPLIT (L. E./T. E.) = .347

TAP							
No. 1 =	1.015	1.015	1.015	1.015	1.015	1.015	1.015
No. 8 =	1.015	-----	-----	1.014	1.015	1.015	1.015
No. 15 =	1.014	1.014	1.007	1.012	1.011	1.014	1.016
No. 22 =	1.016	0.999	0.999	0.998	0.998	0.998	0.960
No. 29 =	1.000	1.000	1.000	1.001	1.000	1.019	1.019
No. 36 =	1.022	1.029	1.019	1.038	1.037	1.036	1.037

22. TR EG FLOW (LBS/SEC) = 0.02029
TR EG FLOW (GR/SEC) = 9.20
INLET PRESS (PSIA) = 2.091
INLET PRESS (N/CM^2) = 1.44
M. C. MACH NO. = 0.215
M. C. REY. NO. = 1266.5
FLOW SPLIT (L. E.) = 0.764
FLOW SPLIT (L. E./T. E.) = .465

TAP							
No. 1 =	1.019	1.021	1.019	1.021	1.019	1.025	1.019
No. 8 =	1.025	-----	-----	1.076	1.076	1.082	1.082
No. 15 =	1.076	1.076	1.055	1.076	1.056	1.084	1.025
No. 22 =	1.023	0.993	0.993	0.993	0.991	0.991	0.474
No. 29 =	1.000	0.998	0.997	0.998	0.997	1.111	1.107
No. 36 =	1.124	1.176	1.111	1.255	1.258	1.253	1.255

23. TR EG FLOW (LBS/SEC) = 0.13369
TR EG FLOW (GR/SEC) = 60.64
INLET PRESS (PSIA) = 14.254
INLET PRESS (N/CM^2) = 9.83
M. C. MACH NO. = 0.206
M. C. REY. NO. = 8429.1
FLOW SPLIT (L. E.) = 1.001
FLOW SPLIT (L. E./T. E.) = .312

TAP							
No. 1 =	1.046	1.046	1.046	1.046	1.051	1.049	1.049
No. 8 =	1.049	-----	-----	1.065	1.067	1.069	1.069
No. 15 =	1.063	1.063	1.028	1.052	1.055	1.068	1.048
No. 22 =	1.047	0.997	0.996	0.994	0.994	0.994	0.951
No. 29 =	1.000	0.998	0.998	1.000	0.999	1.091	1.087
No. 36 =	1.101	1.150	1.086	1.206	1.211	1.202	1.205

24. TR EG FLOW (LBS/SEC) = 0.29570
TR EG FLOW (GR/SEC) = 134.1
INLET PRESS (PSIA) = 31.873
INLET PRESS (N/CM^2) = 21.98
M. C. MACH NO. = 0.207
M. C. REY. NO. = 18310.1
FLOW SPLIT (L. E.) = 1.044
FLOW SPLIT (L. E./T. E.) = .314

TAP							
No. 1 =	1.053	1.053	1.053	1.053	1.055	1.055	1.055
No. 8 =	1.055	-----	-----	1.071	1.072	1.072	1.072
No. 15 =	1.065	1.068	1.036	1.057	1.061	1.071	1.057
No. 22 =	1.055	0.999	0.998	0.997	0.995	0.995	0.680
No. 29 =	1.000	0.999	1.000	1.002	1.001	1.096	1.091
No. 36 =	1.108	1.149	1.092	1.204	1.210	1.198	1.202

TABLE I (Cont.)

TEST
POINT

25. TR EG FLOW (LBS/SEC) = 0.03928
TR EG FLOW (GR/SEC) = 17.82
INLET PRESS (PSIA) = 3.029
INLET PRESS (N/CM^2) = 2.09
M. C. MACH NO. = 0.282
M. C. REY. NO. = 2501.2
FLOW SPLIT (L. E.) = 1.168
FLOW SPLIT (L. E./T. E.) = .285

TAP							
No. 1 =	1.094	1.088	1.094	1.094	1.099	1.098	1.098
No. 8 =	1.094	-----	-----	1.148	1.144	1.164	1.159
No. 15 =	1.138	1.138	1.088	1.128	1.117	1.148	1.088
No. 22 =	1.088	1.000	1.000	0.995	0.992	0.992	0.168
No. 29 =	1.000	1.000	1.000	1.005	1.005	1.216	1.216
No. 36 =	1.240	1.394	1.209	1.678	1.710	1.691	1.691

26. TR EG FLOW (LBS/SEC) = 0.19967
TR EG FLOW (GR/SEC) = 90.6
INLET PRESS (PSIA) = 14.087
INLET PRESS (N/CM^2) = 9.71
M. C. MACH NO. = 0.307
M. C. REY. NO. = 12786.5
FLOW SPLIT (L. E.) = 0.970
FLOW SPLIT (L. E./T. E.) = .297

TAP							
No. 1 =	1.112	1.112	1.112	1.110	1.114	1.116	1.114
No. 8 =	1.115	-----	-----	1.200	1.200	1.205	1.208
No. 15 =	1.183	1.188	1.085	1.154	1.164	1.200	1.116
No. 22 =	1.114	0.995	0.991	0.990	0.988	0.990	0.486
No. 29 =	1.000	1.000	1.004	1.003	1.003	1.295	1.272
No. 36 =	1.346	1.609	1.289	3.099	3.515	4.179	4.369

27. TR EG FLOW (LBS/SEC) = 0.43180
TR EG FLOW (GR/SEC) = 195.9
INLET PRESS (PSIA) = 31.555
INLET PRESS (N/CM^2) = 21.76
M. C. MACH NO. = 0.303
M. C. REY. NO. = 26738.3
FLOW SPLIT (L. E.) = 0.963
FLOW SPLIT (L. E./T. E.) = .318

TAP							
No. 1 =	1.137	1.136	1.138	1.135	1.141	1.141	1.140
No. 8 =	1.141	-----	-----	1.188	1.190	1.197	1.196
No. 15 =	1.172	1.176	1.102	1.146	1.167	1.190	1.142
No. 22 =	1.140	0.996	0.994	0.992	0.990	0.991	0.677
No. 29 =	1.000	0.999	1.002	1.005	1.003	1.276	1.255
No. 36 =	1.312	1.520	1.266	2.098	2.161	2.115	2.150

APPENDIX A

SYMBOLS

The following symbols, with consistent units, are used:

A	cross-sectional area of flow passage
C_D	discharge coefficient
D	diameter of flow passage or pin diameter
f	friction factor
K_T	total pressure loss coefficient
L	length of passage, model width
M	Mach number
M. C.	midchord
N	number of rows of pin fins
P	total pressure
p	static pressure
R	gas constant
Re	Reynolds number
r	radius to element measured in plane of rotation
S	spacing between impingement orifices
TR. EG.	trailing edge
T	temperature
t	plate thickness
V	velocity
w	flow rate
x	distance from passage inlet
X_L	axial pin spacing
X_t	pin spacing transverse to flow direction

X_D	diagonal pin spacing
Z	orifice to impinged plate spacing, pin fin passage height
β	angle between velocity vector
μ	viscosity
ρ	density
ω	angular velocity

Subscripts:

COLL	collector
FT	feeder tube
h	hydraulic diameter
in	inlet
le	leading edge
mc	midchord
min	minimum
out	outlet
s	static
te, TE	trailing edge
T	Total
j	jet
cf	independent crossflow
CF	total crossflow
1	impingement plenum locations (numbered upstream to downstream)
1, 2	leading edge impingement discharge plenum

REFERENCES

1. Kercher, D.M., Heat Transfer by a Multiple Array of Round Air Jets Impinging Perpendicular to a Flat Surface Including the Effects of Spent Air, Journal of Engineering for Power, January 1970.

2. Kolodzie, P.A. and Van Winkle, W., Discharge Coefficients Through Perforated Plates, AI Ch E Journal, Vol. 3, No. 3, 1957.

3. Rohde, John E., Richards, Hadley T.; and Metger, George W., Discharge Coefficients for Thick Plate Orifices with Approach Flow Perpendicular and Inclined to the Orifice Axis, NASA TN D-5467, 1969.

4. Theoclitus, G., Heat-Transfer and Flow-Friction Characteristics of Nine Pin-Fin Surfaces, J. Heat Transfer, Vol. 88, No. 4, Nov. 1966, pp. 383-390.

5. Jakob, Max, Heat Transfer and Flow Resistance in Cross Flow of Gases Over Tube Banks - Discussion, Trans. ASME, Vol. 60, No. 4, May 1938, pp. 384-386.

6. Grimson, E.C., Correlation and Utilization of New Data on Flow Resistance and Heat Transfer for Crossflow of Gases Over Tube Banks, Trans. ASME, Vol. 59, October 1937.

7. Gram, A.J., Markey, C.O., and Monrie, E.S., Convection Heat Transfer and Pressure Drop of Air Flowing Across In-Line Tube Banks, Trans. of the ASME, January, 1958.

8. Kays, W., and A.I. London, Compact Heat Exchangers, 2nd Edition, McGraw Hill Company, 1958.

9. Grotz, B.J., Arnold, F.R., Flow Induced Vibrations in Heat Exchangers, Stanford Technical Report Number 31, Department of Mechanical Engineering, Stanford University, Stanford, California, August, 1956.

10. Putnam, A.A., Flow Induced Noise in Heat Exchangers, Trans. of the ASME Journal of Engineering Power, pp. 417, 422, October, 1959.

11. Putnam, A.A., Flow Induced Noise and Vibration in Heat Exchangers, ASME Paper Number 4-WA/HT-21, 1964.

12. Kline, S.J. and McClintock, F.A., Describing Uncertainties in Single-Sample Experiments, ASME Mech. Eng., January 1953.

13. Shapiro, Ascher H., The Dynamics and Thermodynamics of Compressible Fluid Flow, Ronald Press Co., 1956.

14. Eckert, E.R.G.; Livingood, John N.B.; and Prasse, Ernst I., One-Dimensional Calculation of Flow in a Rotating Passage with Ejection Through a Porous Wall, NACA TN 3408, 1955.

15. Clark, John S.; Richards, Poferl, David J.; Livingood, John N.B., Coolant Pressure and Flow Distribution Through an Air-Cooled Vane for a High-Temperature Gas Turbine, NASA TM X-2028, 1970.

16. McAdams, William H., Heat Transmission, Third Ed., McGraw-Hill Book Co., Inc., 1954.

17. Wilton, M.E. and Murtaugh, J.P., Compressible Flow Network Analysis, GE Report Number R71AEG322, 1971.

Distribution List for
NAS3-13499 (GE)
CR-120883

(1) NASA-Lewis Research Center
21000 Brookpark Road
Cleveland, Ohio 44135
Attn:

	M. S.	Copies
Report Control Office	5-5	1
Technology Utilization Office	3-19	1
Library	60-3	2
Dr. B. Lubarsky	3-3	1
Contract Sec A/Tech Proc Branch	500-206	1
Jack B. Esgar	60-4	1
Louis Russell	77-2	1
John E. Rohde	77-2	15
Herman H. Ellerbrock	77-2	1
David J. Poferl	77-2	1
Robert O. Hickel	77-2	1
Daniel Gauntner	77-2	1
Fluid System Components Division	5-3	1
John Acurio	500-317	1

(2) NASA Scientific & Technical Information Facility — 10
P. O. Box 33
College Park, Maryland 20740
Attn: NASA Representative RQT-2448
(Include all six copies of the Document Release Authorization)

(3) NASA-Headquarters
600 Independence Avenue, S.W.
Washington, D. C. 20546
Attn: N. F. Rekos (RLC) — 1

(4) Wright-Patterson Air Force Base, Ohio 45433
Attn: Mr. J. Richens (APTC) — 1
Mr. John H. Miller (APRT) — 1

(5) Department of the Army
U. S. Army Aviation Material Laboratory
Attn: Mr. Gene Easterling — 1
Mr. John White — 1
Fort Eustis, Virginia 23604

	Copies
(6) Air Force Office of Scientific Research Propulsion Research Division USAF Washington, D. C. 20025	1
(7) Department of the Navy Bureau of Ships Washington, D. C. 20360 Attn: G. L. Graves	1
(8) Department of the Navy Bureau of Naval Weapons Washington, D. C. 20025 Attn: Robert Bronn, RAPP14	1
(9) NASA-Langley Research Center Langley Station Technical Library Hampton, Virginia 23365 Attn: Mark R. Nichols John V. Becker	1 1
(10) United Aircraft Corporation Pratt & Whitney Aircraft Division Florida Research & Development Center P. O. Box 2691 West Palm Beach, Florida 33402 Attn: R. A. Schmidtke	1
(11) United Aircraft Corporation Pratt & Whitney Aircraft Division East Hartford, Connecticut 06108 Attn: M. Suo	1
(12) AiResearch Manufacturing Company 9851-9951 Sepulveda Blvd. Los Angeles, California 90009 Attn: Fred Faulkner	1
(13) Curtiss-Wright Corporation Wright Aeronautical Division Wood-Ridge, New Jersey 07075 Attn: Seymour Moskowitz	1

		Copies
(14)	Northern Research & Engineering Corporation 219 Vassar Street Cambridge, Massachusetts 02139 Attn: K. Ginwals	1
(15)	AVCO Corporation Lycoming Division 550 South Main Street Stratford, Connecticut 06497 Attn: C. W. Bolton	1
(16)	Teledyne-CAE 1330 Laskey Road Toledo, Ohio 43697 Attn: Eli H. Benstein Fred Warrell	1 1
(17)	International Harvester Company, Solar 2200 Pacific Highway San Diego, California 92112 Attn: P. A. Pitt	1
(18)	Commander, Naval Air Systems Command Attn: Air-330 Washington, D. C. 20360	1
(19)	The Boeing Company Commercial Airplane Division P. O. Box 3707 Seattle, Washington Attn: G. J. Schott, M.S. 80-66	1
(20)	Douglas Aircraft Company 3855 Lakewood Blvd. Long Beach, California 90801 Attn: J. E. Merriman	1
(21)	Detroit Diesel Allison Division General Motors Corporation P. O. Box 894 Indianapolis, Indiana 46206 Attn: H. E. Helms Ralph Fox	1 1

	Copies
(22) Westinghouse Electric Corporation Small Steam and Gas Turbines Engineering B-4 Lester Branch P. O. Box 9175 Philadelphia, Pennsylvania 19113 Attn: J. J. Watt	1
(23) McDonnell Aircraft Company Dept. 353, Building 33, Level 6 St. Louis, Missouri 63166 Attn: R. E. Mattes	1
(24) U. S. Air Force Research and Technology Division Aero Propulsion Laboratory Wright-Patterson Air Force Base, Ohio 45433 Attn: Mr. Alan E. Zengel, AFPL Mr. J. Richens, AFAPL (APTC)	1 1
(25) U. S. Naval Air Engineering Center Aeronautical Engine Laboratory Philadelphia, Pennsylvania 19112 Attn: Mr. J. E. Picktelberger	1
(26) Williams Research Corporation 2280 W. Maple Road Walled Lake, Michigan 48088 Attn: W. Schimmel	1